

UNCLASSIFIED

AD NUMBER
AD912391
NEW LIMITATION CHANGE
TO Approved for public release, distribution unlimited
FROM Distribution authorized to U.S. Gov't. agencies only; Test and Evaluation; AUG 1973. Other requests shall be referred to Frankford Arsenal, Philadelphia, PA.
AUTHORITY
FA D/A ltr, 12 Feb 1974

THIS PAGE IS UNCLASSIFIED

UNCLASSIFIED

AD 912 391

LAW LASER RANGEFINDER DESIGN
STUDY AND DEMONSTRATION MODEL

FINAL REPORT

BR- 7628

August 1973

Contract No. DAAA25-73-C-0173

Prepared for

U. S. Army Frankford Arsenal (SMUFA-L3300)
Tacony and Bridge Streets
Philadelphia, Pa. 19137

Distribution limited to personnel involved in
Test and Evaluation; 18 AUG 1973. Other requests
for this document must be referred to

Prepared by

RAYTHEON COMPANY
Missile Systems Division
Hartwell Road
Bedford, Ma. 01730

UNCLASSIFIED

LAW LASER RANGEFINDER DESIGN
STUDY AND DEMONSTRATION MODEL
FINAL REPORT

BR- 7628

August 1973

Contract No. DAAA25-73-C-0173

Prepared for

U. S. Army Frankford Arsenal (SMUFA-L3300)
Tacony and Bridge Streets
Philadelphia, Pa. 19137

Distribution limited to
Test and Evaluation; 13 AUG 1973.
for this document must be referred to

Prepared by

RAYTHEON COMPANY
Missile Systems Division
Hartwell Road
Bedford, Ma. 01730

UNCLASSIFIED

TABLE OF CONTENTS

	<u>Page</u>
1. INTRODUCTION	1-1
2. PERFORMANCE REQUIREMENTS	2-1
2.1 Transmitter Considerations	2-1
2.2 Receiver Considerations	2-3
2.2.1 Signal	2-3
2.2.2 Noise	2-4
2.2.3 Signal to Noise Ratio	2-7
2.3 Signal Integration and Detection	2-9
3. DEMONSTRATION RANGEFINDER	3-1
3.1 Receiver	3-4
3.1.1 Preamplifier and Postamplifier	3-4
3.1.2 Pulse Integrator	3-9
3.1.3 Detection Comparator and Sensitivity Time Control	3-13
3.1.4 Indicator and Driver	3-18
3.1.5 Clock Generator	3-18
3.1.6 Gating Pulse Generator	3-21
3.2 Transmitter	3-23
3.2.1 Laser Pulse Modulator	3-23
3.2.2 DC-DC Converter	3-28
3.3 Battery and Power Regulators	3-28
3.4 System Calibration Demonstration Model	3-32

UNCLASSIFIED

TABLE OF CONTENTS (continued)

	<u>Page</u>
3.5 Demonstration Model Optical System	3-32
3.6 Test Results Demonstration Model	3-38
3.7 Advanced Model Design Description	3-38
3.7.1 Dual Gate Signal Processor	3-38
3.7.2 Sweep, Timing and Display	3-49
3.7.3 Receiver AGC	3-52
3.7.4 System Calibration	3-52
4. DESIGN REQUIREMENTS	4-1
4.1 Optical Design	4-1
4.1.1 Baseline Optical Configuration	4-2
4.1.2 Optical Component Material Selection	4-4
4.1.3 Receiver Optics	4-8
4.1.4 Transmitter Optics	4-17
4.1.5 Viewfinder Optics	4-23
4.1.6 Superelevation Considerations	4-26
4.2 Mechanical Considerations	4-30
4.2.1 Structural Materials	4-30
4.2.2 Fabrication Techniques	4-33
4.3 Electronics Packaging Considerations	4-38
4.4 Cost Considerations	4-40
4.5 Reliability Analysis	4-42

UNCLASSIFIED

TABLE OF CONTENTS (Cont.)

	<u>Page</u>
5. HAZARD LEVEL DOCUMENTATION	5-1
5.1 Eye Hazard Documentation	5-1
5.1.1 Eye Damage Mechanisms	5-2
5.1.2 Exposure Criteria	5-4
5.1.3 Caution and Hazard Viewing Distances	5-11
5.1.4 Recommendations	5-12
5.2 Electrical Shock Hazard Evaluation	5-13
6. SUMMARY AND CONCLUSIONS	6-1
7. REFERENCES	7-1

UNCLASSIFIED

1. Introduction

This document is the final report on contract DAAA25-73-C-0173 for the LAW Laser Rangefinder Design Tradeoff Study. During the early stages of this study effort, the Frankford Arsenal Program Office requested that a demonstration model of a Laser Rangefinder be designed and fabricated. The design of this demonstration device is based on initial analytical results obtained during the study phase. A documentation of the device is also included within this report.

Section 2 contains an analysis leading to the performance requirements of the system. These consist of a set of optical and electronic criteria which the rangefinder must satisfy in order to exhibit ranging capability to 500 meters from the types of targets considered. Basically, the analysis consists of a general signal and noise study in conjunction with the resultant detection probability and time to detection considerations. The optical parameters involved are transmitted power, beam collimation, collecting area, target reflectivity, optical bandpass and atmospheric attenuation. The electronic parameters of interest are detector sensitivity, PRF, preamplifier design, filter design and integration time. The net result is that the interaction of these parameters is defined enabling advantageous tradeoffs to be realized while maintaining system ranging capability.

The major part of Section 3 is concerned with a description and documentation of the demonstration rangefinder fabricated under this contract. In addition to the optical aspects of the rangefinder, a thorough description of the various electronic functions is presented. These include bandpass characteristics of the receiver, transmitter pulse modulator characteristics, DC-DC converter, clock pulse generator, pulse integration and detection, and range gate timing. A discussion of the system power supply and electronic test procedures are also included in this section, as well as a description of the dual range gate --

UNCLASSIFIED

range interpolation processor, automatic gate sweep, and digital range readout. These latter features were incorporated as the result of a change in scope regarding the degree of sophistication of the demonstration hardware. Test data are presented, indicating that the ranging capability of the system is in agreement with the performance requirements generated in Section 2 of this report.

The design requirements of a low cost, lightweight rangefinder are developed in Section 4. These consist of a set of weight and cost considerations which must be satisfied by the rangefinder while simultaneously satisfying the performance criteria developed in Section 2. Generally, this aspect of the study has concentrated on the consideration of alternate materials and the resultant tradeoffs for both the optical and mechanical components from the point of view of weight reduction and potential cost reduction when high volume production techniques are utilized. In particular, the viability of plastic optical components has been considered along with the resultant performance over the operational temperature range specified for the rangefinder. In a similar fashion, the use of high impact plastics in the fabrication of mechanical parts has been considered. Also included in Section 4 is a discussion of potential tradeoffs which can be realized yielding reduced size and weight of the system electronics through the use of technology compatible with high volume production. A reliability and maintainability prediction is also included.

The eye hazard level represented by the demonstration rangefinder is investigated and documented in Section 5. Maximum permissible retinal and corneal irradiances used in this documentation are obtained from the literature. In particular, the safety standards proposed by the American National Standards Institute have been used for evaluating long-term intra-beam viewing of the transmitted radiation. The maximum corneal irradiance for this case is essentially identical to the revised

UNCLASSIFIED

value proposed by TB MED 279 (1969), U. S. Department of Army. In addition, Section 5 also contains an analysis of potential high voltage hazards and preventive measures.

UNCLASSIFIED

2. Performance Requirements

The rangefinder for the LAW weapon must operate at ranges to 500 meters and provide superelevation information to an accuracy of ± 0.5 milliradians. From an examination of the ballistic flight profile of this missile, it has been determined that this superelevation accuracy implies a range determination accuracy of ± 10 meters. Since the rangefinder is essentially a pulsed optical radar, operation under extremes of background illumination must be considered. On the low end sufficient ambient light is required for the operator to see the target. On the high end, direct sunlight against highly reflecting backgrounds such as snow or white sand may be expected. For this condition we assume a surface irradiance from direct overhead sunlight of 6×10^{-6} watts/cm²/Å in the spectral region about 0.9μ. While target reflectivity may be made very low, dirt and dust under battlefield conditions will increase target reflectivity. For the purposes of this study, we assume a target reflectivity of 0.1.

2.1 Transmitter Considerations

In order to assume that a major fraction of the transmitted laser energy falls onto the target, the beam divergence must be made small. We estimate that if the beam divergence is less than about .01 radians, we can illuminate a medium sized tank at 500 meters such that about 75% of the beam falls on the tank. Currently small GaAs laser diodes having peak powers up to 40 watts are available with maximum diode dimensions under .01 inches. The beam divergence from the diodes is such that they must be operated with an optical system no slower than F/1.40 for

UNCLASSIFIED

efficient collection of the radiation. A one inch diameter F/1.25 lens will give the required beam divergence with decreasing system speed decreasing the beam divergence.

The received optical power density from a target which is directly illuminated by the transmitting laser may be obtained from

$$P_D = \frac{P_L \rho_T \eta_T e^{-\sigma 2R}}{\pi R^2} \quad \frac{\text{watts}}{\text{cm}^2} \quad (2.1)$$

where P_L = laser power = 40 watts

ρ_T = target reflectivity = 0.1

η_T = fraction of energy on target = 0.75

σ = atmospheric extinction coefficient (m^{-1})

R = range (meters)

Calculations of received power density, at 300, 400, and 500 meters are presented in Table 2.1 for two values of atmospheric visibility corresponding to good and poor seeing conditions.

UNCLASSIFIED

TABLE 2.1

Received Power Density (watts/cm²)

<u>Range (M)</u>	<u>$\sigma = 8 \times 10^{-5} \text{ m}^{-1}$</u>	<u>$\sigma = 8 \times 10^{-4} \text{ m}^{-1}$</u>
300	1.01×10^{-9}	0.66×10^{-9}
400	0.56×10^{-9}	3.14×10^{-10}
500	3.52×10^{-10}	1.72×10^{-10}

2.2 Receiver Considerations

2.2.1 Signal

The optical power reflected back from the target is converted into an electrical signal by way of the receiving optics and the detector. The magnitude of this signal is proportional to the effective area A_o of the receiving optics, the optical power density, and the sensitivity of the detector. Thus, the signal current from the detector may be expressed by

$$I_s = S P_D A_o \tau_o \text{ amps} \quad (2.2)$$

where

- S = detector sensitivity - amp/watt
- P_D = received power density - watt/cm²
- A_o = effective area of receiving optics - cm²
- τ_o = transmission of optical system

UNCLASSIFIED

2.2.2 Noise

There are two principal sources of noise to contend with in this system; noise due to background induced current in the photodetector, and noise sources within the preamplifier following the detector. Practical preamplifiers produce noise equivalent to an input noise current of 1.5×10^{-12} amps/ $\sqrt{\text{Hz}}$.

The optical background power at the detector is given by

$$P_B = A_O \tau_O \Omega \int_{\lambda_1}^{\lambda_2} N_{B\lambda} d\lambda \quad (2.3)$$
$$\approx A_O \tau_O \Omega N_B \int_{\lambda_1}^{\lambda_2} d\lambda = A_O \tau_O \Omega N_B \Delta\lambda \text{ watts}$$

where $N_{B\lambda} = \frac{H_{B\lambda} \gamma_B}{\pi} = \text{Background Radiance watts/cm}^2 \text{ ster}$

$A_O = \text{effective receiver optics area, cm}^2$

$\tau_O = .72 = \text{optics and filter transmission}$

$\Omega = \text{receiver solid angle field of view steradians}$

$H_{B\lambda} = 6 \times 10^{-6} \text{ watts/cm}^2/\text{\AA} = \text{solar irradiance}$

$\gamma_B = 0.7 = \text{assumed background reflectance}$

$\Delta\lambda = 500 \text{\AA} = \text{spectral filter bandwidth}$

UNCLASSIFIED

The minimum spectral bandwidth, $\Delta\lambda$, which can be used will depend to a large extent on receiver F/number and laser frequency drift due to temperature changes. For the purpose of calculations, a value of 500 \AA will be used. However, it is noteworthy that the ranging capability of the device is not particularly sensitive to the quantity, as will become apparent.

Using the values above in Equation (2.3) yields

$$P_B = 4.80 \times 10^{-4} A_O \Omega \text{ watts} \quad (2.4)$$

In theory the receiver FOV need not exceed the transmitter beam divergence. In practice, however, it will be desirable, in order to minimize alignment problems to double this value. Thus assuming a beam divergence of .01 radians yields

$$\Omega = \frac{\pi}{4} (2 \times .01)^2 = 3.14 \times 10^{-4} \text{ steradians} \quad (2.5)$$

so that

$$P_B = 1.51 \times 10^{-7} A_O \text{ watts} \quad (2.6)$$

The detector current due to this optical power is

$$I_B = S P_B \text{ amps} \quad (2.7)$$

where $S = 0.65 \text{ amp/watt}$

Therefore

$$I_B = 9.8 \times 10^{-8} A_O \text{ amps.} \quad (2.8)$$

UNCLASSIFIED

This current of itself does not interfere with signal detection. Statistical fluctuations in this current due to its quantized nature does, however. The rms noise current i_b due to this fluctuation is given by

$$i_b = \sqrt{2e I_B B_n} \text{ amps} \quad (2.9)$$

where e = the charge on an electron
 B_n = the noise bandwidth of the receiver

The required range resolution of ± 10 meters is equivalent to about 140 nanoseconds timing resolution in the optical radar. Since the range determination in the system will be made by setting a range gate in coincidence with the received signal, the optical pulse length and range gate will be set at one-half this value or 70 nanoseconds so that in the convolution of the range gate with the received pulse, the required range accuracy may be maintained.

Good signal-to-noise performance as well as minimum pulse stretching will be obtained if

$$B\tau = 1/2 \quad (2.10)$$

where B = 3 db bandwidth of receiver (single pole)
 τ = transmitter pulse length = 70 ns

UNCLASSIFIED

Then

$$B = \frac{1}{2 \times 70 \times 10^{-9}} = 7.15 \times 10^6 \text{ Hz} \quad (2.11)$$

The equivalent noise bandwidth is

$$B_n = \frac{\pi}{2} B = 11.2 \text{ MHz} \quad (2.12)$$

so that

$$i_b = (5.92 \times 10^{-10}) A_o^{1/2} \text{ amps} \quad (2.13)$$

The equivalent noise current due to the preamplifier is

$$\begin{aligned} i_p &= 1.5 \times 10^{-12} \times B_n^{1/2} \\ &= 5.02 \times 10^{-9} \text{ amps} \end{aligned} \quad (2.14)$$

The total noise current due to both background and preamplifier noise is

$$\begin{aligned} i_n &= \sqrt{i_b^2 + i_p^2} \\ &= \sqrt{(5.92)^2 + (50.2)^2} \times 10^{-10} \text{ amps} \end{aligned} \quad (2.15)$$

We notice that for effective apertures less than about 72 cm^2 the system will be preamplifier noise limited.

2.2.3 Signal-to-Noise Ratio

The signal-to-noise ratio for the system may now be obtained from Equations (2.2) and (2.15):

UNCLASSIFIED

$$\left(\frac{S}{N}\right) = \frac{I_s}{i_n} = \frac{S P_D A_o \tau_o}{\sqrt{(5.92)^2 A_o + (50.2)^2} \times 10^{-10}} \quad (2.16)$$

Using the values of P_D derived in Table 2.1, calculations for signal-to-noise at 300, 400, and 500 meters, as a function of receiver aperture, for good and poor seeing conditions are presented in Table 2.2.

TABLE 2.2

Signal-to-Noise Ratio at Ranges of 300, 400, and 500 Meters as a Function of Receiving Aperture for Good ($\sigma = 8 \times 10^{-5} \text{ m}^{-1}$) and Poor ($8 \times 10^{-4} \text{ m}^{-1}$) Seeing Conditions

Receiving Aperture A_o , cm^2	Signal-to-Noise Ratio					
Range	300 M		400 M		500 M	
Seeing Condition	Poor	Good	Poor	Good	Poor	Good
10	0.58	0.88	0.27	0.49	0.15	0.31
15	0.84	1.28	0.40	0.71	0.22	0.45
20	1.09	1.66	0.52	0.92	0.28	0.58
25	1.32	2.02	0.63	1.12	0.34	0.71
30	1.55	2.37	0.74	1.32	0.40	0.83
35	1.77	2.70	0.84	1.50	0.46	0.94
40	1.97	3.02	0.94	1.67	0.51	1.05

UNCLASSIFIED

2.3 Signal Integration and Detection

Examination of Table 2.2 shows that even for large receiver apertures the signal-to-noise ratio is less than adequate for reasonable detection probability. (It will be shown that a signal-to-noise greater than about 4 is required). Improvement in the system signal-to-noise ratio and thus detection capability can be obtained by integrating a number of received pulses from the target. In fact, it will be shown that this improvement is directly proportional to the square root of the number of pulses integrated.

The number of pulses that may be integrated will depend on the pulse repetition rate and the length of time the target can be held in the range gate. This time will depend on operational considerations. The maximum pulse repetition rate PRF_{max} will depend on the average power capabilities of the diode laser. The ratio of average power to peak power, the so-called duty factor D_f , determines the PRF_{max} by

$$PRF_{max} = \frac{D_f}{\tau} \quad (2.17)$$

where $\tau =$ laser pulse width $= 7 \times 10^{-8}$ seconds

For the GaAs diode $D_f = .0004$

$$\text{Thus } PRF_{max} = \frac{4 \times 10^{-4}}{7 \times 10^{-8}} = 5.7 \text{ KHz}$$

UNCLASSIFIED

The length of time the target can be held within a range gate will depend on the length of time allowed for searching the range gates through 0 to 500 meters. Since the range gate is set at 70 ns, the equivalent range cell is 10 meters. The number of such range cells in 500 meters is 50 so that if the allowed search time is t_s , the length of time allowed in each cell is $t_s/50$. The maximum number of pulses that may be integrated is then

$$N_{\max} = \frac{t_s \text{ PRF}_{\max}}{50} \quad (2.18)$$

If we, for example, allow a search time t_s of 2 seconds, then for this case

$$N_{\max} = \frac{2 \times 5.7 \times 10^3}{50} = 228$$

The noise output from an ideal integrator will be the sum of N input samples of noise in the range gate thus

$$Y = \sum_{i=1}^N y_i$$

where Y = integrator output
 y = integrator input

The probability density of y is gaussian and may be expressed by

$$P(y) = \frac{1}{\sigma\sqrt{2\pi}} e^{-y^2/2\sigma^2} \quad (2-19)$$

UNCLASSIFIED

The output probability density is the n-fold convolution of P(y). This result may be most conveniently computed by taking n-fold product of the characteristic function of P(y). The characteristic function of P(y) is

$$C_Y(\xi) = \int_{-\infty}^{\infty} P(y) e^{j2\pi\xi y} dy \quad (2.20)$$

or

$$C_Y(\xi) = \frac{1}{\sigma\sqrt{2\pi}} \int_{-\infty}^{\infty} e^{-y^2/2\sigma^2 + j2\pi\xi y} dy \quad (2.21)$$

This integral is easily evaluated by completing the square in the exponent to yield

$$C_Y(\xi) = e^{-2(\pi\sigma\xi)^2} \quad (2.22)$$

from which

$$C_Y(\xi) = [C_Y(\xi)]^N = e^{-2N(\pi\sigma\xi)^2} \quad (2.23)$$

We now obtain the desired probability density by taking the Fourier transform of (2.23) thus

$$P(Y) = \frac{1}{\sqrt{N} \sigma \sqrt{2\pi}} e^{-Y^2/2N\sigma^2} \quad (2.24)$$

UNCLASSIFIED

Comparing (2.24) with (2.19) we see that the rms noise amplitude σ has been increased by a factor \sqrt{N} that is

$$\sigma_o = \sigma \sqrt{N} \quad (2.25)$$

Since at optical wavelengths the scintillation effects on reflection from the target are negligible (due primarily to the short wavelength and the relative incoherence of the diode laser) we may assume that the target return signal is of constant amplitude S . The action of the integrator is then to take the n -fold sum of the constant signal or

$$S_o = NS \quad (2.26)$$

The signal-to-noise ratio at the output of the integrator is then

$$\frac{S_o}{\sigma_o} = \frac{NS}{\sigma \sqrt{N}} = \frac{S}{\sigma} \sqrt{N} \quad (2.27)$$

Hence, as previously stated, the output signal-to-noise ratio is equal to the input signal-to-noise ratio times the square root of number of pulses integrated.

An ideal integrator is somewhat difficult to implement in practice. It can be shown that identical results may be obtained using a low pass filter in place of the integrator. If a single stage RC low pass filter is used, we may replace N in Equations (2.24), (2.25), (2.26) and (2.27) by $1/\alpha T$ where $\alpha = 1/RC$ and $T =$ interpulse time period, i.e. $T = 1/PRF$.

UNCLASSIFIED

In determining the probability of detection we must set some threshold at the output of the integrator such that when the signal plus noise is above this threshold, we assume signal detection has taken place. To do this we must set the threshold so that in the absence of a signal, the false alarm rate, FAR, is below some acceptable level. The FAR is expressed by

$$\text{FAR} = P_{\text{FA}} \frac{\text{PRF}}{N} \quad (2.28)$$

or in terms of the RC network

$$\text{FAR} = P_{\text{FA}} \text{PRF}(\alpha T) = P_{\text{FA}} \alpha$$

where P_{FA} = probability of false alarm.

The required threshold T_n may be expressed in terms of P_{FA} by

$$\frac{T_n}{\sigma_o} = \text{erfc}^{-1*}(P_{\text{FA}}) \quad (2.29)$$

where $\text{erfc}^{-1*}(\)$ is the inverse complementary error function. The complementary error function is defined by

$$\text{erfc}^*(z) = \frac{1}{\sqrt{2\pi}} \int_z^{\infty} e^{-y^2/2} dy \quad (2.30)$$

the probability of detection then is expressed by

$$P_D = \text{erfc}^* \left(\frac{T_n}{\sigma_o} - \frac{S_o}{\sigma_o} \right) \quad (2.31)$$

UNCLASSIFIED

If we assume an acceptable FAR of one every 10 seconds and a value of $N = 225$, then

$$\frac{T_n}{\sigma_o} = \text{erfc}^{-1}(P_{FA}) = \text{erfc}^{-1}\left(\frac{N(\text{FAR})}{\text{PRF}}\right) = 2.65 \quad (2.32)$$

and

$$P_D = \text{erfc}^{-1}\left(2.65 - \frac{S_o}{\sigma_o}\right) \quad (2.33)$$

The mean time to detection is related to the probability of detection by

$$T_D = \frac{N}{P_D \times \text{PRF}} = \frac{.0395}{P_D} \quad (2.34)$$

In Table 2.3 we present calculations of the probability of detection and mean time to detection as a function of both input and output signal-to-noise of the integrator.

Examination of Table 2.3 shows that even with an input signal-to-noise ratio of as low as .067, there is about a 5% probability of detection and on the average a detection event will occur every 0.8 seconds or about 10 times more often than if there were no target present in the range gate. While this might be adequate, a more certain indication should be required. In addition the scan rate of 2 sec/500 meters dictates that the target can remain in the range gate for only $2/50 = .04$ seconds. The mean time to detection should be of this order or less if detection is to take place reliably. With an output signal-to-noise ratio greater than 4 (input greater than 0.267) this condition will be met.

UNCLASSIFIED

TABLE 2.3

Input $\left(\frac{S}{N}\right)$	Output $\left(\frac{S}{N}\right)$	Probability of Detection	Mean Time To Detection
$\frac{S}{\sigma}$	$\frac{S}{\sigma_o} = 15 \frac{S}{\sigma}$	P_D	T_D (Sec.)
0.067	1.0	.0495	0.8
0.133	2.0	.2578	0.153
0.200	3.0	.6368	0.062
0.267	4.0	.9115	0.0434
0.333	5.0	.9906	0.0399
0.400	6.0	.9996	0.0396
0.466	7.0	.9999	0.0395

From Table 2.2 we notice that if the receiving aperture is made to be 25 CM² or greater, reliable operation will be assured at 500 M range even under poor seeing conditions.

It should be noted that if more time is taken in range scanning, operation at longer ranges and/or poorer seeing condition and/or smaller receiving optics etc. is possible. It is clear that a number of technical as well as operational and cost tradeoffs are possible with this system. The next section will detail some of these operational tradeoffs in terms of the demonstration range finder.

UNCLASSIFIED

3. Demonstration Rangefinder

This section is concerned with the implementation of a specific set of the range finder parameters as discussed in Section 2. The result of this implementation is a demonstration device which serves as the baseline for the discussion of a low cost rangefinder which is presented in Section 4.

Figure 3.1 is a photograph of the initially fabricated demonstration range finder. This prototype model is a simple optical monopulse transceiver system utilizing pulse transit time range measurement averaged over 100 samples in a manually set range gate. Signal-to-noise ratio enhancement is achieved by pulse integration. Desensitization to transmitted pulse feedthrough and other close range effects is achieved by variation of the detection comparator threshold with time. A block diagram of the system is given in Figure 3.2.

Manual adjustments of the range gate delay are made with a 10 turn potentiometer until an indicator LED in the viewfinder lights up, signalling that the target is in the range gate. Range is then read from the adjustment pot dial directly. For implementation on the LAW weapon, a thumb-wheel and screw would be coupled to the potentiometer (the pistol grip shown in Figure 3.1 would be eliminated) and would change the angle between the rangefinder line-of-sight and weapon in accordance with the range-elevation function rather than give a range reading, as discussed in Section 4. In essence, it would be an optically sensed superelevation control system with a simple-aim, target sense, fire-sequence. Thus eliminated are complex dials, read-outs and fire control charts, while providing accuracy of ± 10 M

UNCLASSIFIED

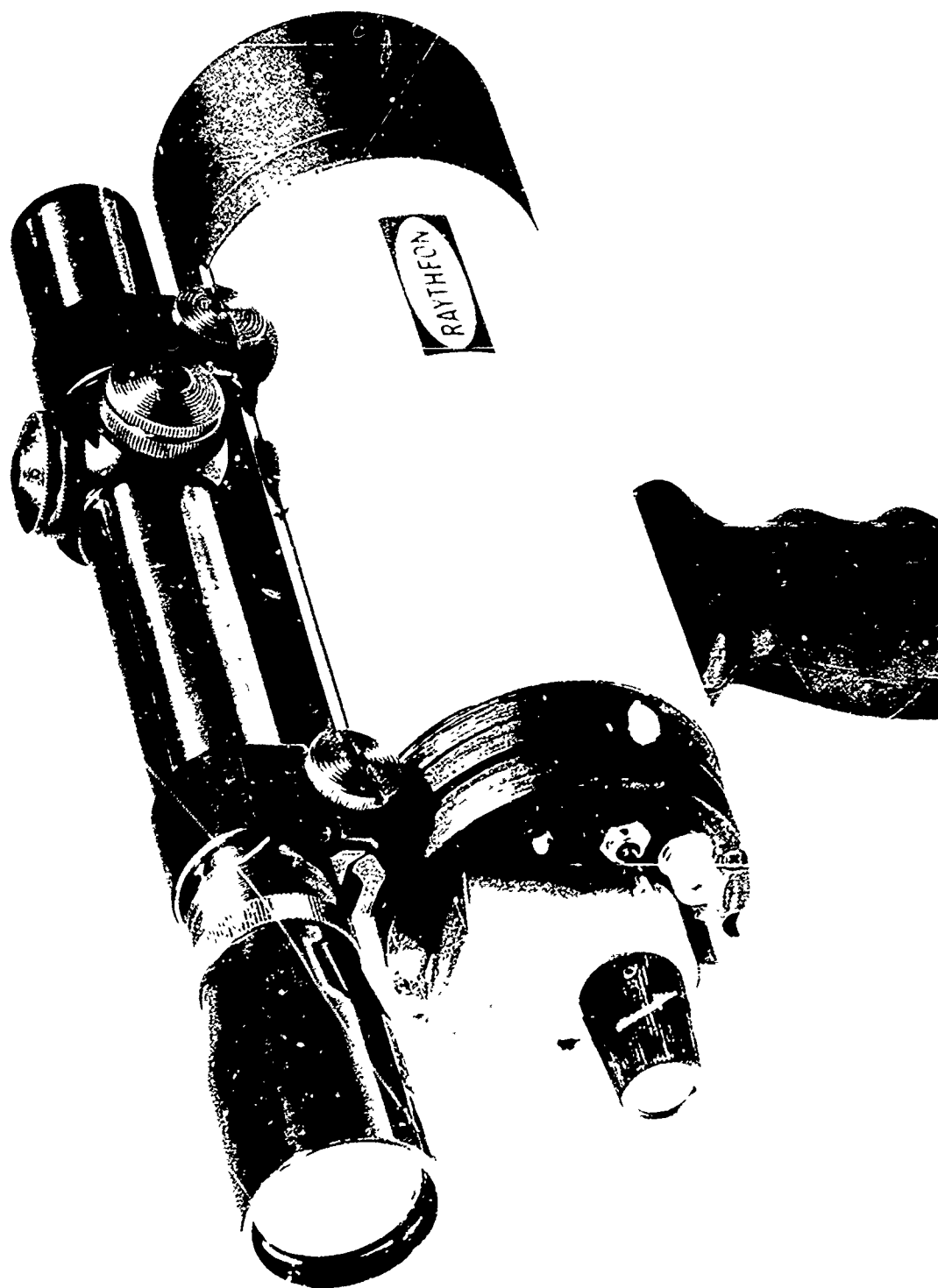


Figure 3-1 Demonstration Rangefinder Model

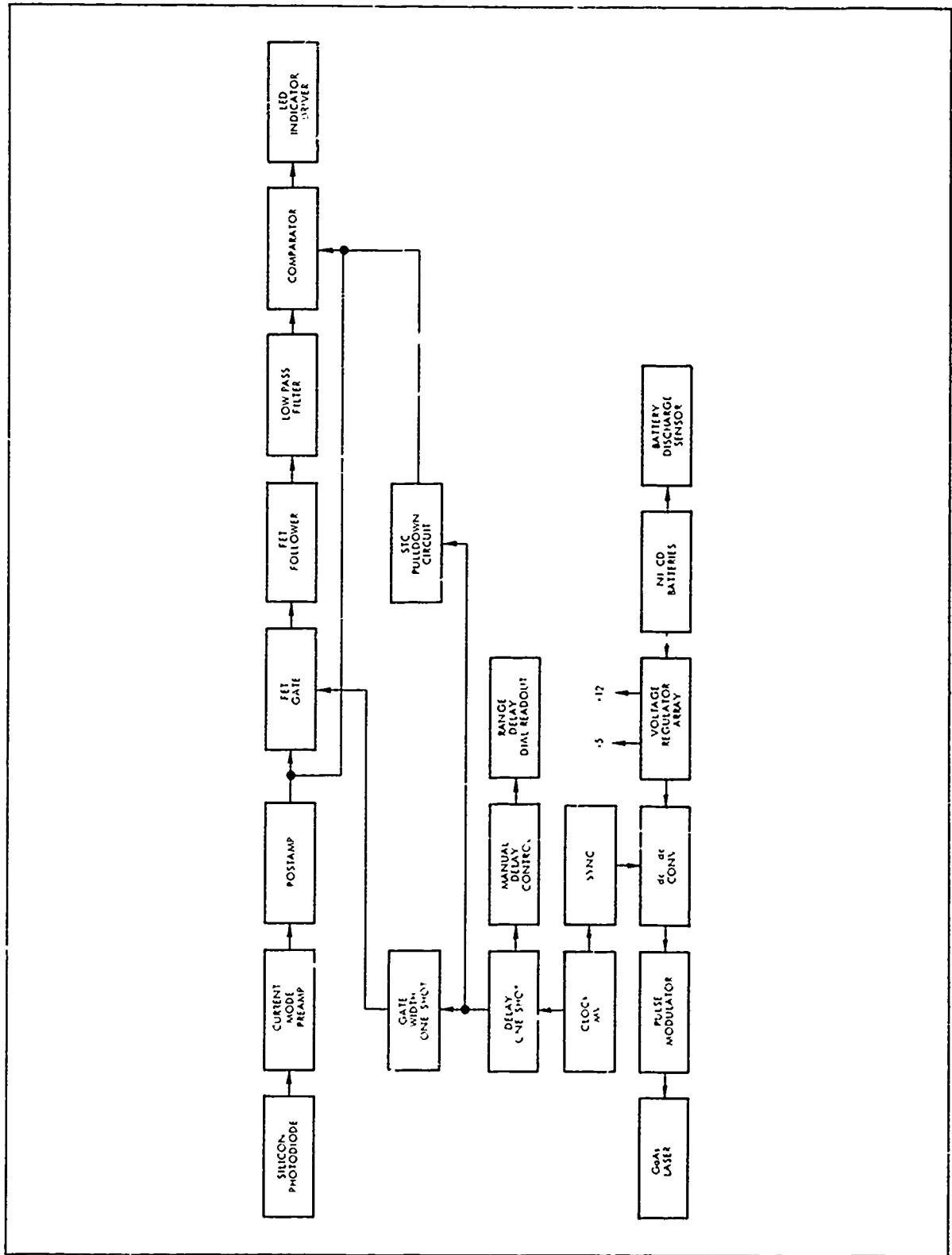


Figure 3.2 LAW Rangefinder Prototype

UNCLASSIFIED

or better with operation simplicity. The complete system is contained within a cylindrical package of 2.75 inches diameter and approximately eight inches in length.

3.1 Receiver

The basic functions of the receiver are to collect reflected light pulses, generate the resulting electrical signals, and provide the necessary signal processing in order to make a decision as to the presence or absence of a target within a range gate. The various electronic subsystems involved in this sequence are discussed below.

3.1.1 Preamplifier and Postamplifier

The video signal processing section consists of a low noise current-mode (transresistance) preamplifier, two cascaded IC postamplifiers and interstage bandpass shaping. The schematic is shown in Figure 3.3.

The input stage, 2N4416 FET, Q1 is in the common source configuration. The drain load for Q1 is formed by a common base constant current source, another 2N4416 FET, Q2. Since DC coupling is used and bootstrapped DC feedback used, the drops across Q1 and Q2 must be matched. This is done initially by obtaining FET pairs with I_{DSS} values nearly equal. The final matching is achieved by adjusting the I_{D2} (drain current) of constant current load Q2 by means of its gate-source bias resistor, R_{S2} until it matches the I_{DSS} of Q1. The value of R_{S2} is given by

UNCLASSIFIED

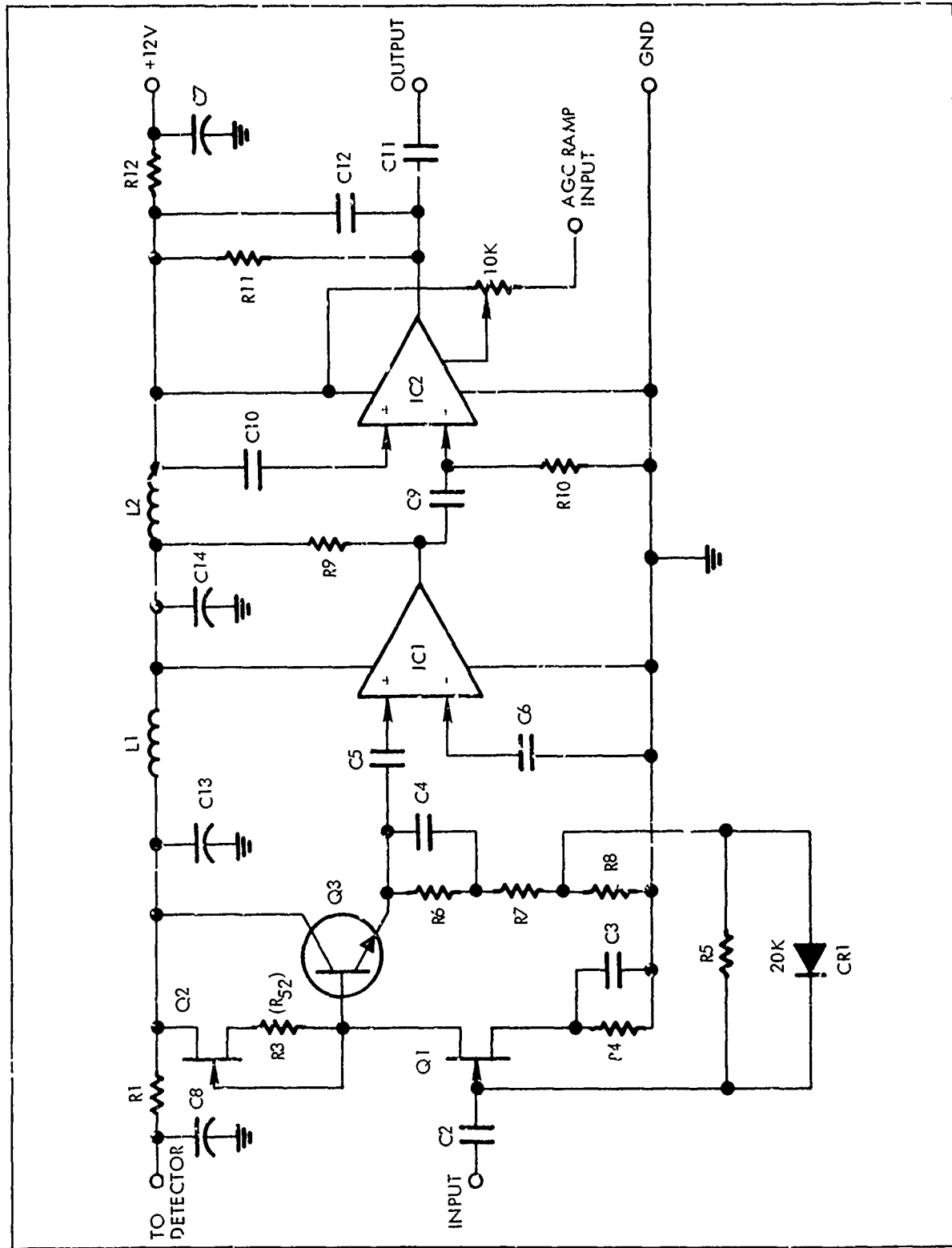


Figure 3.3 Preamplifier - Postamplifier (Receiver)

UNCLASSIFIED

$$R_{S_2} = \left(\frac{V_{P_2}}{I_{D_1}} \right) \left[1 - \left(\frac{I_{D_1}}{I_{DSS_2}} \right)^{1/2} \right]$$

where

V_{P_2} is the Q2 pinch-off

I_{D_1} is the Q1 drain current

I_{DSS_2} is the $V_{gs(o)}$ drain current, Q2

and

$$I_{D_1} = I_{DSS_1} \left[1 - \left(\frac{I_{DSS_1} R_{S_1}}{V_{P_1}} \right) \right]^2$$

where

I_{DSS_1} is the $V_{gs(o)}$ drain current, Q1

V_{P_1} is the Q1 pinch-off

R_{S_2} is typically between 0 and 50 ohms.

The output of the Q1-Q2 pair at the drain of Q1 is applied to output emitter follower Q3. Part of the emitter-follower output is tapped off across R8 and fed back to the Q1 input through feedback resistor R5. Diode C1 limits the pre-amplifier overload effects.

UNCLASSIFIED

Open loop gain of the preamplifier is 40. In the current mode or transresistance amplifier, the input terminal is at virtual ground and the output voltage is the input current flowing through the feedback resistor R_5 or

$$e_{out} = i_{in} R_5$$

Using a value of 20K for transresistance R_5 , the output scale factor, S_o , for a detector sensitivity of 0.65 A/W is

$$S_o = 1.3 \times 10^4 \text{ volts/watt}$$

The input resistance looking into the gate of Q1 is related to R_5 and open loop gain, A_o by

$$r_{in} = \frac{R_5}{A_o} = \frac{2 \times 10^4}{4 \times 10^1} = 500 \text{ ohms}$$

The response time of the preamplifier is determined by source capacitance, C_s , Q1 input capacitance, C_{SS} , and stray capacitance, C_{Sr} and input resistance, r_{in} by

$$t_{pr} = 2.2 r_{in} (C_s + C_{SS} + C_{Sr})$$

Assuming $C_s = 20 \text{ pf}$, $C_{SS} = 0.5 \text{ pf}$ and $C_{Sr} = 2 \text{ pf}$

$$t_{pr} = 2.2 (5 \times 10^2) (22.5 \times 10^{-12}) = 24.8 \text{ nsc}$$

UNCLASSIFIED

In practice this is not limited by the closed loop bandwidth of approximately 25 MHz for $C_S = 0$. Further roll-off to 2.5 MHz bandwidth is added in the postamplifier. Further reduction in input response time is achieved by only reducing R_5 or detector capacitance C_S .

The output of the preamplifier is AC coupled by C_5 to IC1, an MC1590 wideband amplifier with a gain of 200. This amplifier is cascaded with a second MC1590, IC2, with a gain of up to 200 bringing the preamp output noise level up to 1 V. High frequency cut is achieved by R11-C12. The values shown give a 2.5 MHz cut.

The 3 db bandwidth of the entire analog processor is from 80 KHz to 2.5 MHz.

The IC amplifiers chosen have AGC capability if needed to suppress transmitted pulse feedthrough, noise, etc. Up to 20 db of AGC per stage is possible.

To minimize interstage coupling problems, all of the circuitry associated with Q1 and Q2 is shielded and decoupled by R1-C8. The IC amplifiers were decoupled by L1, L2, C13, and C14 and the receiver board further decoupled from the +12V regulated line by R12-C7. High frequency layout techniques were used with extensive ground plane maintained.

UNCLASSIFIED

3.1.2 Pulse Integrator

The pulse integrator consists of the input buffer, sample-hold and integrator. The pulse integrator circuitry is shown in Figure 3.4. Its operation is described in the following section.

Negative going video is applied to the PNP emitter follower Q1 causing the emitter to swing negative from a 7.2 V reference level set by

$$V_{\text{ref}} = V_{\text{CC}} \left(\frac{R_2}{R_1 + R_2} \right)$$

in proportion to the signal. This is the input buffer stage.

The sample-hold circuit consists of the analog gate, Q2, gate driver, Q3, and FET voltage follower IC1. The zero signal reference level is the 7.2 V at the emitter of Q1. When the base of driver transistor Q3 is high, Q3 conducts and the 7.2 V at point A divides across R_4 , CR1 and Q3, keeping the gate of the N-channel JFET, Q2 about 6 V below the source terminal of Q2, thus keeping Q2 off. When the base of Q3 goes to ground and Q3 goes into cutoff, C2 charges positive during the switching transition and supplies a small amount of charge to replace the depleted charge in diode CR1 to ensure a clean turn-on of the JFET gate. With Q3 off, the gate of Q2 goes to the source voltage through referencing resistor R4 and turns on, passing data from Q1 to the holding capacitor C4.

The data acquisition time constant is determined by the "ON" resistance, $r_{\text{ds(on)}}$, of Q2 and the value of C4. With

UNCLASSIFIED

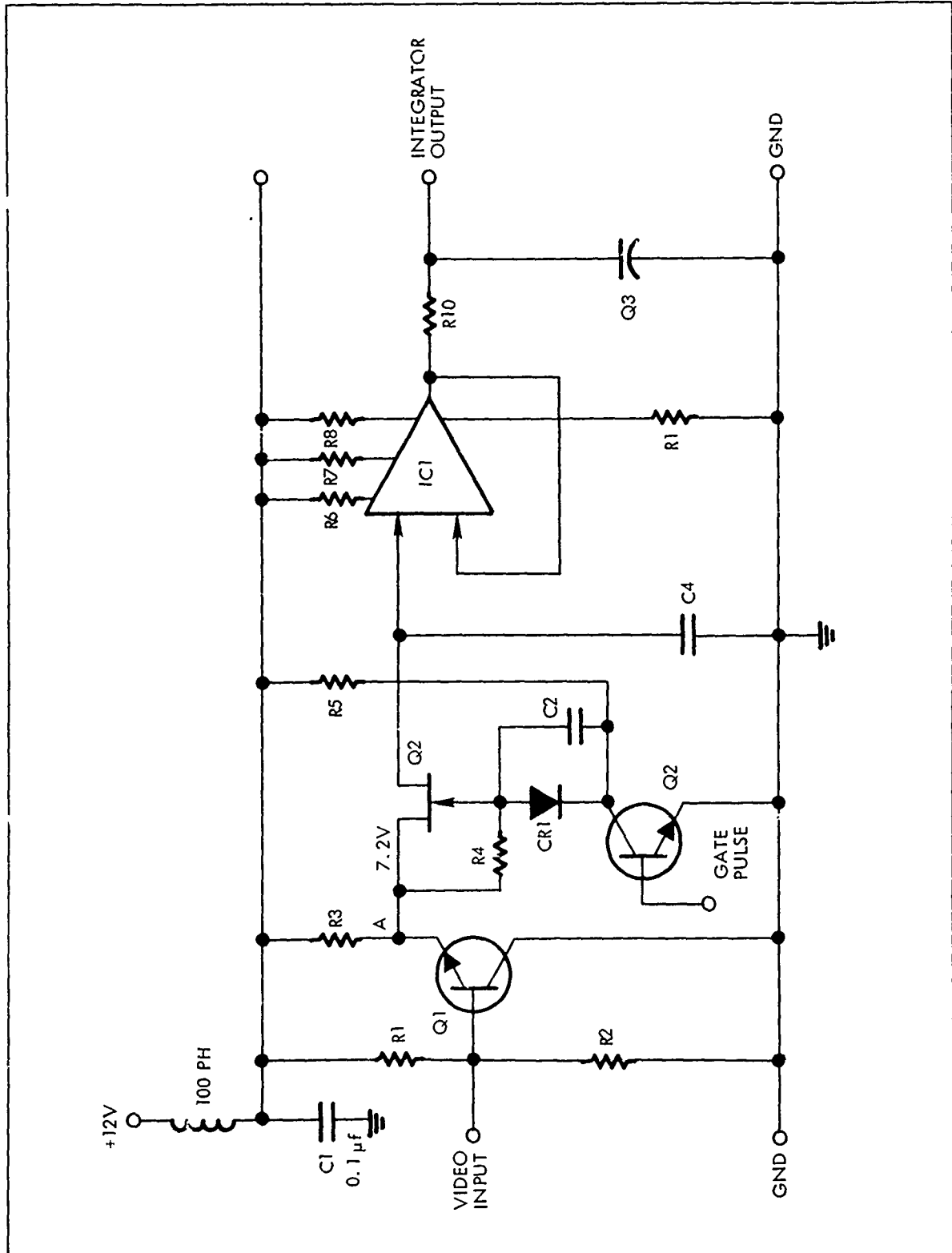


Figure 3.4 Pulse Integrator Schematic

UNCLASSIFIED

$r_{ds(on)}$ of typically 70Ω and $C4 = 560 \text{ pf}$, the acquisition time is about 40 nsc. It should be noted that while decreasing this time constant increases the time resolution, it also decreases immunity to noise spikes such as gate switching spikes, laser noise, ringing, etc. Increasing the time constant above 50 nsc (the gate interval) reduces the amplitude response. The 40 nsc value is a good compromise that provides good performance and minimizes design problems and costs.

When the range gate pulse (0 level) is at the base of Q3, C4 tracks the video at the source of Q2. When the range gate turns off, C4 holds the last analog level present at the Q2 input. It holds this value for one clock period when the next range gate appears and the sample-and-hold updates. Since the charge on C4 can decay with time due to the "OFF" leakage of Q2, leakage in C4 itself and leakage due to the input bias current of IC1, these terms must all be minimized. Using a high quality capacitor for C4, we can reduce this to a negligible value leaving only the error (drift) due to $i_{dss(o)}$ and i_p . This turns out to be about 0.1 V/sec or 10^{-4} V drift between samples. Use of a high quality JFET minimizes the $i_{dss(o)}$ loss. While MOSFETS are superior, they have inherent driver problems and insufficient switching speed. The JFET selected is a high reliability, low cost MIL-SPEC N-channel unit, the 2N4416, recommended for high speed video applications. It has a typical $i_{dss(o)}$ of 10 pa .

UNCLASSIFIED

The voltage follower bias current effect is minimized by using a FET input voltage follower. This can be any of a number of devices such as the $\mu\text{A 2050}$, LM 740, NH 0022, $\mu\text{A 740}$, AD 503, AD 506, or AD 540. While input bias current is one criteria for selecting this component, the offset drift with temperature must also be considered since it determines the minimum threshold level for the post integrator comparator. With our detection threshold set at about 10 mV, then over a 100°C temperature range, a $100 \mu\text{V}/^\circ\text{C}$ drift rate would cause the comparator to fire. It thus should be less than $50 \mu\text{V}/^\circ\text{C}$ and unity gain operation is mandatory since this offset is multiplied by the follower gain. Achieving low drift is possible by merely externally trimming and matching drain currents of the input FETS. Drifts of less than $1 \mu\text{V}/^\circ\text{C}$ are possible using complex drift sense amplifiers, active compensation in the feedback loop and thermistors. It was found, however, that $30 \mu\text{V}/^\circ\text{C}$ to $50 \mu\text{V}/^\circ\text{C}$ is possible without such remedies.

The FET input voltage follower used, $\mu\text{A 740}$, has an input bias current of 100 pa and drift of $50 \mu\text{V}/^\circ\text{C}$.

Using the values of $i_{\text{dss}(o)} = 10 \text{ pa}$ and $i_{\text{b}} = 100 \text{ pa}$ we find

$$\frac{\Delta e_o}{\Delta t} \text{ is } 0.2\text{V/sec}$$

For an interpulse period (between gates) of 1 msec the sample-hold drift towards the 7.2 V reference would be about $100 \mu\text{V}$ or 5×10^{-3} percent for a 2 V signal. This turns out to be negligible in regard to degrading the pulse integrator output signal-noise ratio and also in regard to amplitude data accuracy.

UNCLASSIFIED

The voltage follower transfers the data on C4 to the simple RC low pass filter "integrator", R10-C3. The time constant, T_i of the integrator is equal to 100 pulse intervals or 10^{-1} sec. The output represents the RMS noise during the sampling interval (gate) averaged over 100 interpulse periods plus the integral of the signals detected during 100 consecutive gate periods. This noise sampling is shown in Figure 3.5. The noise is reduced by a factor of 10 for 100 pulse integration, giving a signal-to-noise enhancement of 10 x. Input and output signal-to-noise ratio enhancement is shown in Figure 3.6 for the design breadboard.

3.1.3 Detection Comparator and Sensitivity Time Control

The pulse integrator output is thresholds detected to determine target presence or absence. To minimize receiver overload and "main bang" noise, the comparator threshold sensitivity is varied with time by the sensitivity time control (STC) circuits. These circuits are shown in Figure 3.7.

The comparator used is a National LM 311 which is a high accuracy, medium speed, low power unit readily suited to single ended operation with high common mode voltages and input voltages.

The integrator output is applied to one input of IC2. The reference level is applied to the other input. The initial reference level is set by the variable voltage divider R3, R4, and R5. The threshold potentiometer R5 is set for the desired false alarm rate. The comparator output stage uses

UNCLASSIFIED

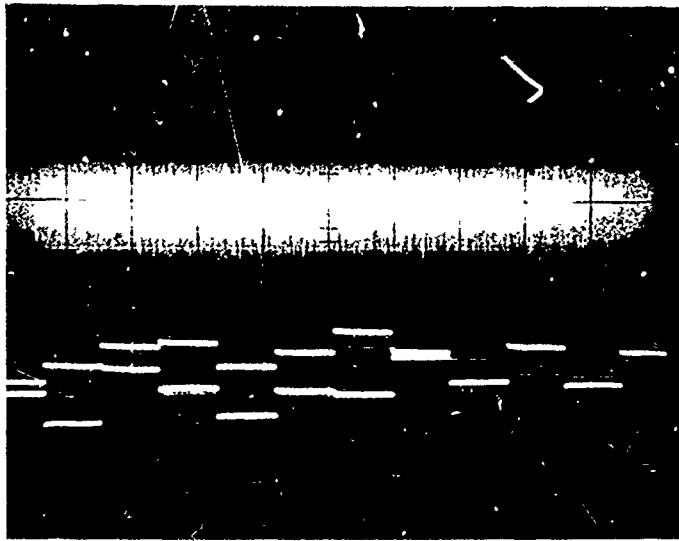


Figure 3.5 RMS Noise Sample

UNCLASSIFIED

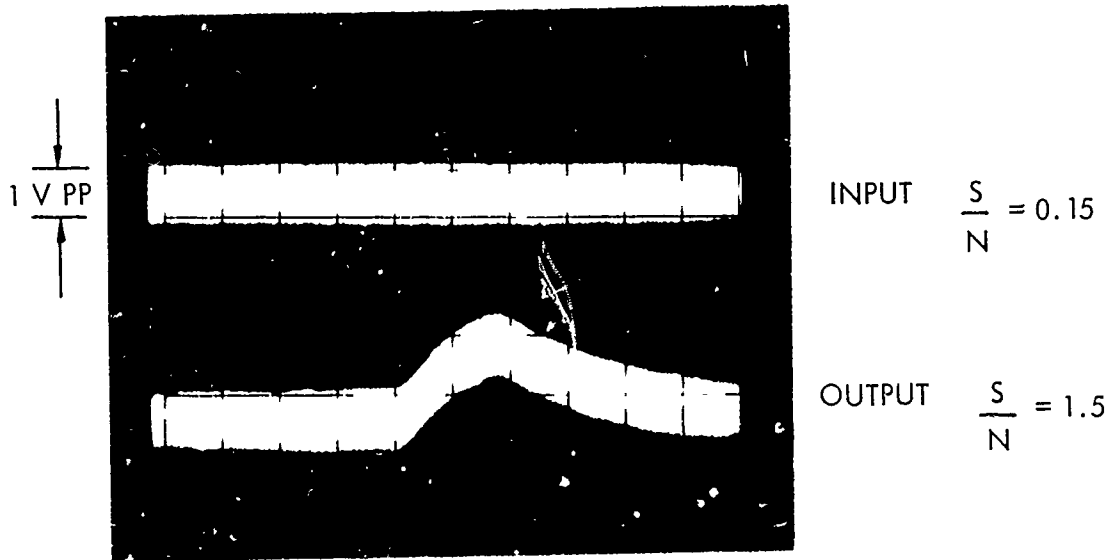


Figure 3.6 Signal-Noise Enhancement
Input/Output Waveforms

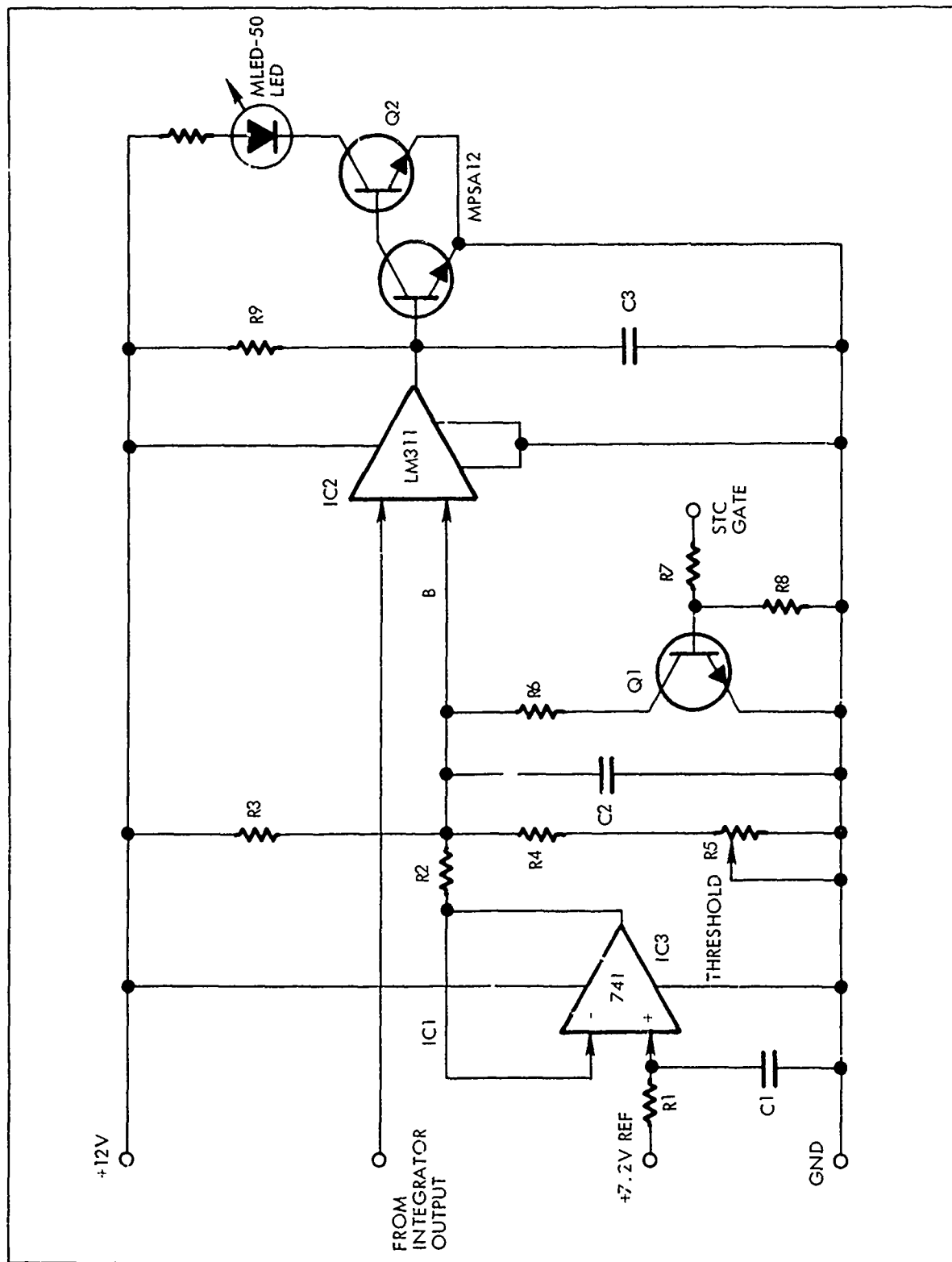


Figure 3.7 Comparator and Sensitivity Time Control

UNCLASSIFIED

an external collector resistor, R9. The comparator output then drives an LED indicator by means of an external stage, Q2.

The comparator reference level is varied with time by the STC circuits. The STC reference level is 7.2 V derived from the sample and hold emitter follower output. To remove video from the STC, a series low pass filter with 10^{-4} sec time constant was used (R1-C1), fed to a 741 unity gain voltage follower, IC3. The 7.2 V output of IC3 is applied to STC pull-down transistor, Q1, through resistor R2. This transistor serves to switch in a resistor, R6, to shunt potentiometer, R5 and decrease sensitivity. With a 1 level at the base of Q1 prior to the transmit clock pulse, Q1 is conducting pulling point B down to a voltage level of e_{BL} where

$$e_{BL} = e_{ref} \left[\frac{\left(\frac{R4R6}{R4 + R6} \right)}{R2 + \left(\frac{R4R6}{R4 + R6} \right)} \right]$$

The switching of the input level at the Q1 base to a 0 causes Q1 to go into cutoff allowing capacitor C2 to charge to a voltage e_{BH} where

$$e_{BH} = e_{ref} \left[\left(\frac{R4}{R4 + R2} \right) \right]$$

UNCLASSIFIED

The STC time constant (10% of $e_{BH} - e_{BL}$ to 90% of $e_{BH} - e_{BL}$) is set by resistor R6 and C2 and is nominally about 500 ns. The STC waveforms are shown in Figure 3.8. The STC amplitude is controlled by R2 and R6.

3.1.4 Indicator and Driver

The LM 311 comparator output, (Figure 3.7) is applied directly to an external NPN transistor, Q2, a Motorola MPSA12. With no target the comparator output is normally low and the MPSA12 is in cut-off. When the comparator switches, it charges C3 through resistor R9, thus stretching the output transition of the comparator. This stretched pulse turns on the Q2 and drives a Motorola MLED-50 red light emitting diode located in the viewfinder to indicate the presence of a target. The time constant, R9 C3, was chosen to minimize transient LED firings that would be of low visibility due to short duration. This could occur if the gate is scanned too fast.

3.1.5 Clock Generator

The basic system clock generator is a unijunction transistor oscillator. The frequency of oscillation is determined by

$$f_r \approx \frac{1}{2.2 \left[\frac{(R5+R6)(1.7)}{(R5+R6+R7)} \right] C1}$$

The limits of adjustment are about 250 Hz to 1250 Hz for the circuit shown in Figure 3.9. Generation of a pulse rather than

UNCLASSIFIED

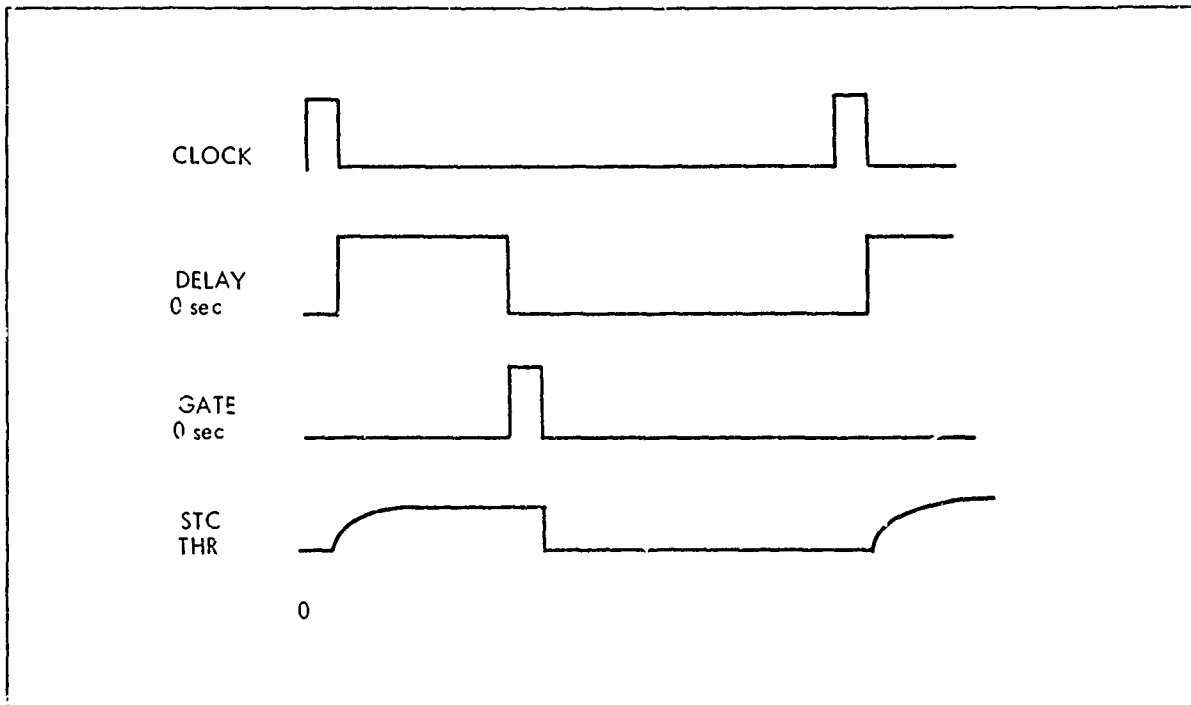


Figure 3.8 Sensitivity Time Control (STC) Timing Synchrogram

UNCLASSIFIED

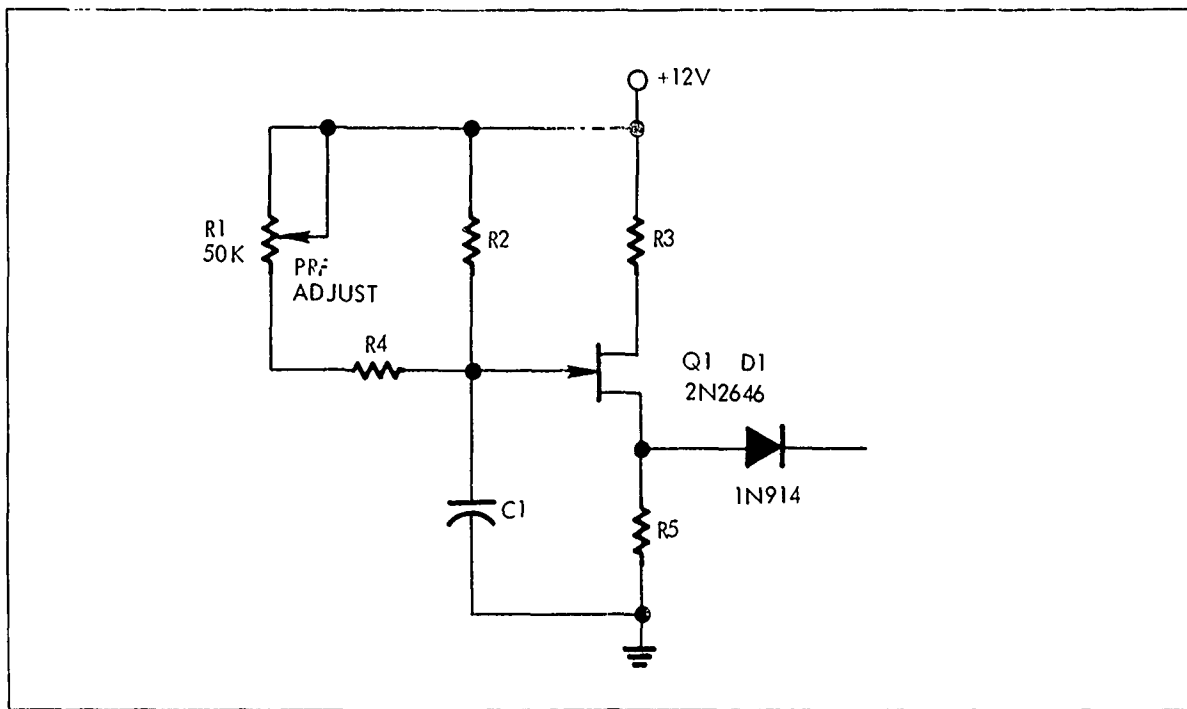


Figure 3.9 Clock PRF Generator

UNCLASSIFIED

a sinusoid is achieved by keeping the UJT in cut-off until the last portion of the C1 charging cycle.

The triggering of the laser modulator is initiated by the UJT oscillator output. Timing pulses for gating, etc. are then derived by means of the SCR discharge current flowing through the SCR gate circuit. This generates a fast pulse coincident with actual modulator firing. The circuitry is shown in Figure 3.9.

3.1.6 Gating Pulse Generator

The range gate is generated in two steps: generation of the range delay and shaping of the gate pulse.

When the clock goes high, the leading edge triggers the first half of a dual monostable which has an external RC timing network selected to give the required range delay. This timing can be varied by means of a potentiometer for manual "range search" or scanned electronically. In this case, manual adjustment was used. At the termination of the delay interval, a second half of the dual monostable is triggered. This monostable section has its timing interval set to the desired gate width, in this case 70 nsc. Rise and fall times of the gate are under 10 nsc. We now have a range gate that can be delayed with reference to time zero by an easily varied amount to permit range search. In this case the delay is variable from 330 nsc to 6600 nsc, which corresponds to detection ranges of 50M to 1000 M.

The gating generator is shown in Figure 3.10.

UNCLASSIFIED

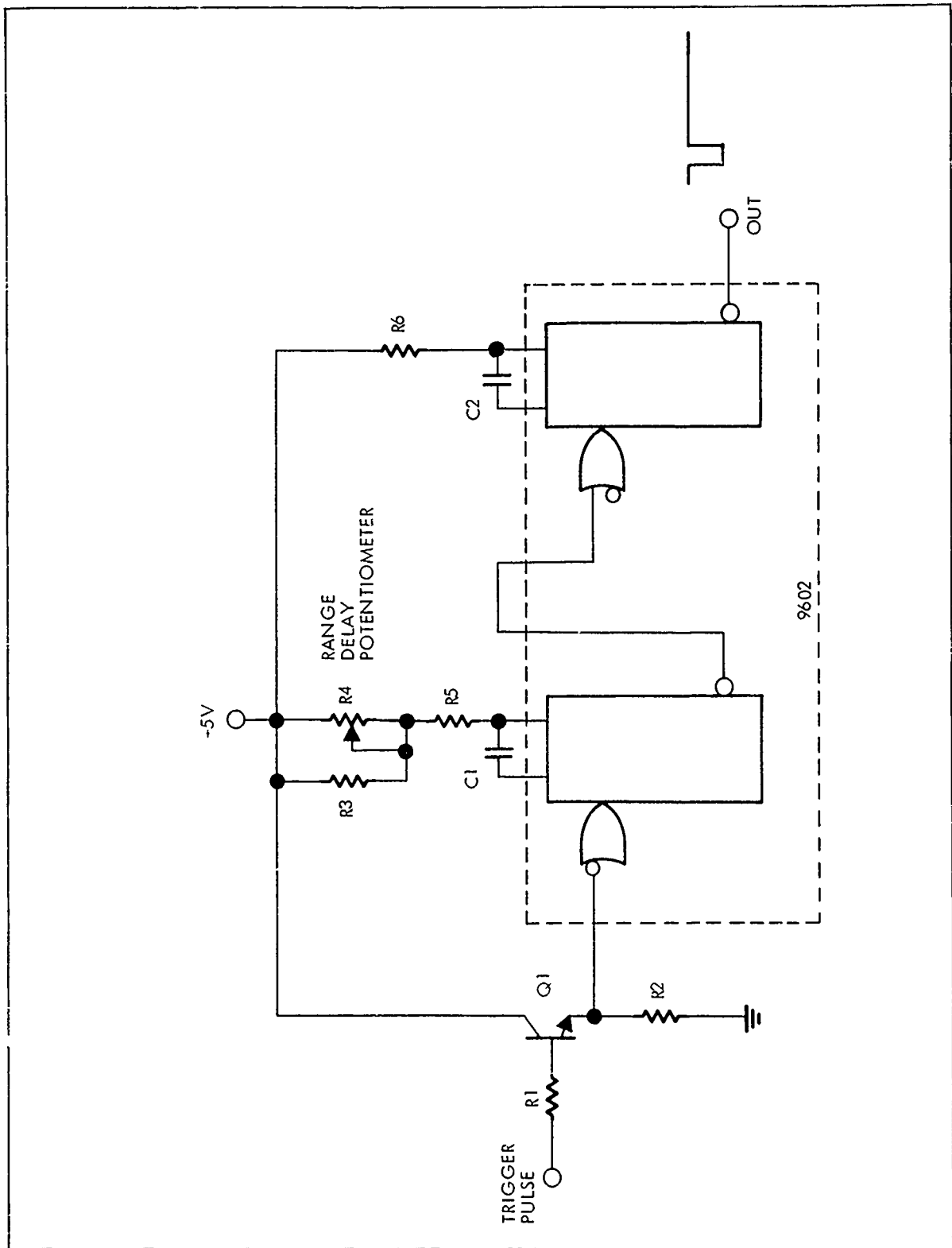


Figure 3.10 Gating Generator

UNCLASSIFIED

3.2 Transmitter

Included within the transmitter, in addition to the laser, are the pulse modulator circuitry and DC-DC converter. Each of these components is discussed below.

3.2.1 Laser Pulse Modulator

The laser pulse modulator is of the capacitive discharge type using a simple LC pulse shaping network and an SCR switch to discharge the pulse forming network through the laser. The schematic is shown in Figure 3.11.

The pulse forming network is essentially a lumped constant delay line with propagation delay, t_D , risetime, t_r , falltime, t_f and n sections. The design is straightforward. The delay line impedance, Z_D , should match the load impedance, Z_L , which is composed of the "ON" impedance of the SCR switch, Z_S , and laser diode "ON" impedance Z_Z as well as the interconnecting circuit characteristic impedance resulting from lead inductances and stray or distributed capacitance. With Z_L equal to about 1.0 ohm typically, we can determine the values of L and C for given rise and fall times for n sections. The pulse forming network (PFN) schematic is shown in Figure 3.12.

To determine the energy required from the PFN we must know the peak pulse current, i_2 , pulse width, t_w , and circuit load impedance, Z_L . The energy per pulse, E_E is

$$E_E = t_w i_2^2 Z_L$$

$$E_E = (10^{-7}) (75)^2 (1) = 0.56 \text{ millijoule/pulse}$$

UNCLASSIFIED

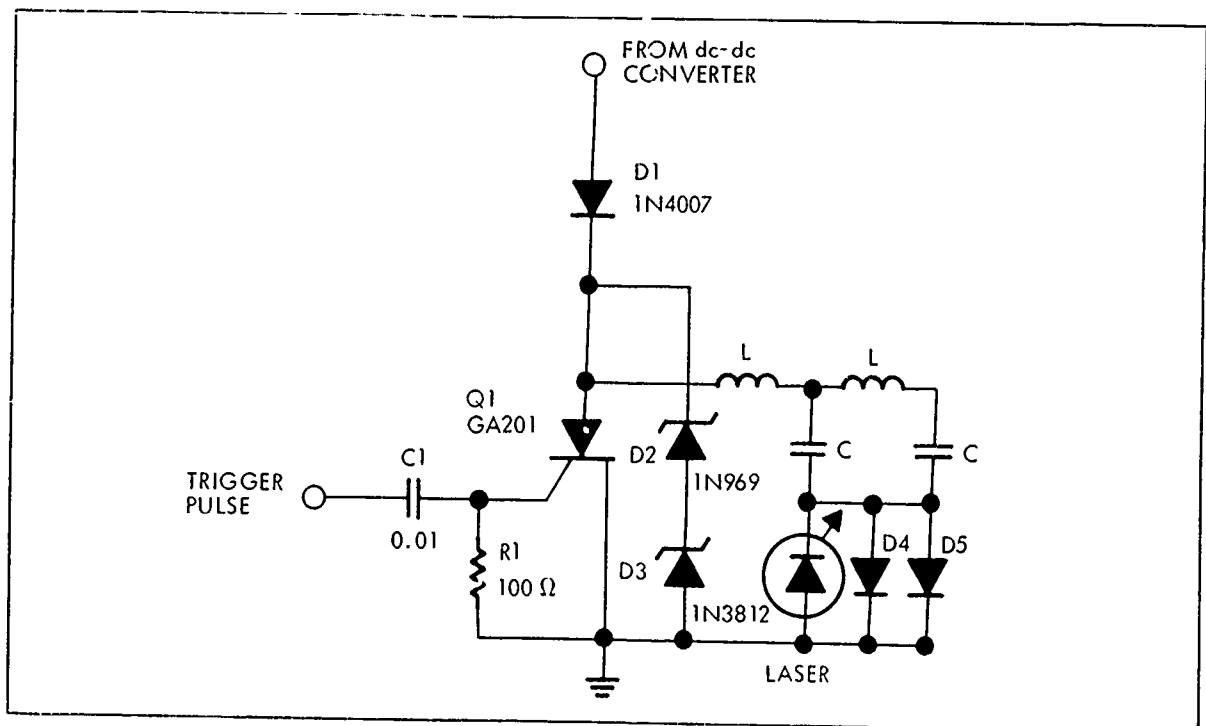


Figure 3.11 Pulse Modulator

UNCLASSIFIED

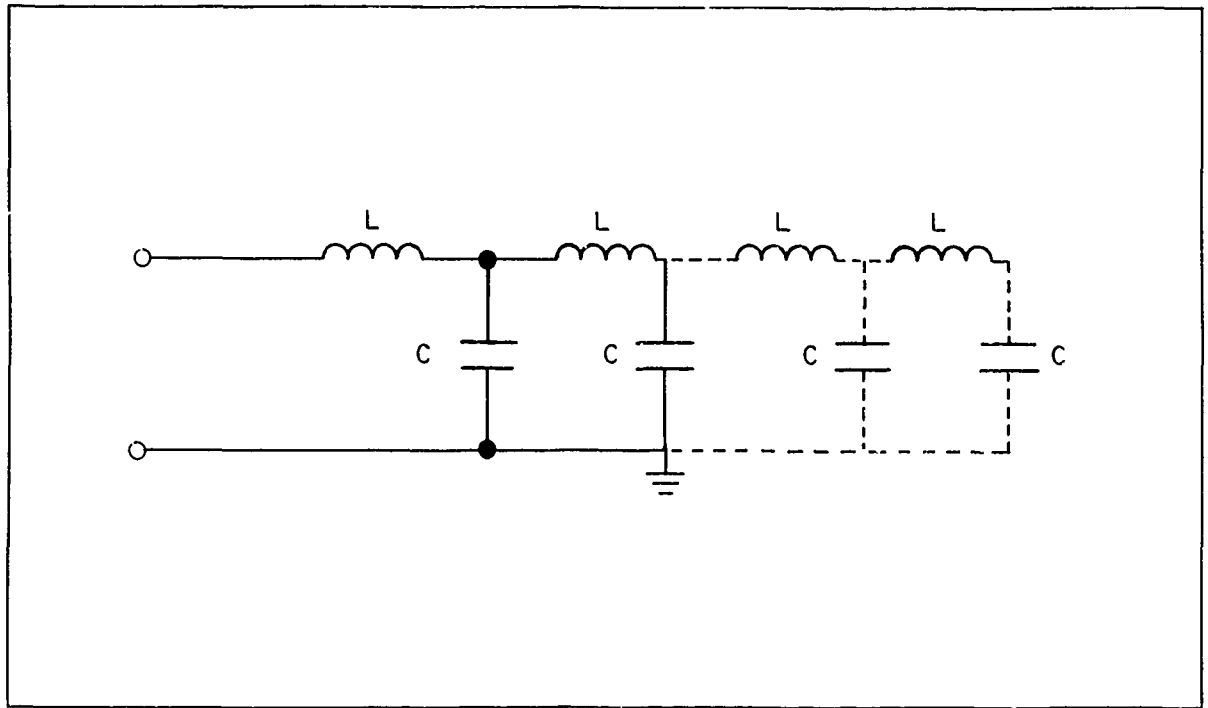


Figure 3. 12 LC Pulse Forming Network

UNCLASSIFIED

Since the energy stored in the PFN total capacitance, C_T , is determined by C_T and the charging voltage V_C , if $V_C = 100$ V we we find

$$E_E = \frac{1}{2} C_T V_C^2$$

Since we determined E_E to be 0.56 mj and $V_C = 100$ V then

$$C_T = \frac{2 E_E}{V_C^2}$$

$$C_T = \frac{2 (0.56) \times 10^{-3}}{(10^2)^2} = 0.11 \text{ } \mu\text{fd}$$

Now if we let the PFN characteristic impedance, R_O be equal to the circuit load impedance, Z_L , or

$$R_O = \left(\frac{L_T}{C_T} \right)^{1/2}$$

then the values of L and C can be calculated for n sections with delay time t_D by

$$L = \frac{t_d R_O}{1.07 n}$$

$$C = \frac{t_d}{1.07 n R_O}$$

Assuming $n = 2$, $R_O = 1$ ohm, $t_d = 1 \times 10^{-7}$

UNCLASSIFIED

$$C = \frac{(10^{-7})}{(1.07)(2)(1)} = .046 \mu\text{fd}$$

$$L = \frac{(10^{-7})(1)}{(1.07)(2)} = 46 \text{ nanohenries}$$

the nearest standard value of 0.05 μfd is used for C.

The SCR selected to discharge the PFN must have a fast turn-on (<10 nsc) or excessive voltage will be dropped across the SCR as the PFN discharges and higher supply voltages will be needed.

The SCR chosen is the Unitrode GA201 Nanosecond Thyristor. This high reliability device, packaged in a TO-18 package will handle peak currents to 100A @ 100 V with 1% duty cycle or less, has a turn-on time of 10-20 nsc and turn-off time of under 500 nsc. The holding current is typically 5 ma for this device. The PFN charging resistor is made large enough to limit the "ON" current (average) to less than the holding current ensuring that the SCR does not latch up and turns off after the PFN has discharged.

Pulser operation is as follows. When positive pulse of at least 20 nsc duration is applied to the gate causing a current of at least 100 μa to flow through the gate-cathode junction then the SCR turns-on and the PFN, which has charged to V_{CC} through R3, discharges through the SCR and laser diode. As soon as the current drops below the holding current value, the SCR switches off and the PFN begins recharging through R3.

UNCLASSIFIED

3.2.2 DC-DC Converter

The laser pulse modulator used in the LAW laser rangefinder requires 100V to charge the PFN. Since the regulated primary supply voltage is +12V, a DC step-up ratio of $\left(\frac{100}{12}\right)$ or 8.4 x is required. This can be obtained either by means of switching mode, driven oscillator or free-running blocking oscillator DC-DC converters. In this case, the simplest approach is the blocking oscillator design shown in the schematic of Figure 3.13. Operation is inherently simple, requiring only one transistor and a transformer. The oscillation frequency is set at a minimum of 10 x the laser PRF to ensure efficient PFN charging between laser trigger pulses.

3.3 Battery and Power Regulators

The primary supply for the laser rangefinder is a nickel-cadmium battery pack consisting of 3 Burgess CD-22 , batteries. The output is 18V with a discharge profile as shown in Figure 3.14 for a 90 Ω load. Operating voltages for the laser power converter (DC-DC converter), receiver, pulse integrator and other circuits are derived from 3 terminal voltage regulators of the MC7805 and MC7812 types. The supply circuitry is shown in Figure 3.15

UNCLASSIFIED

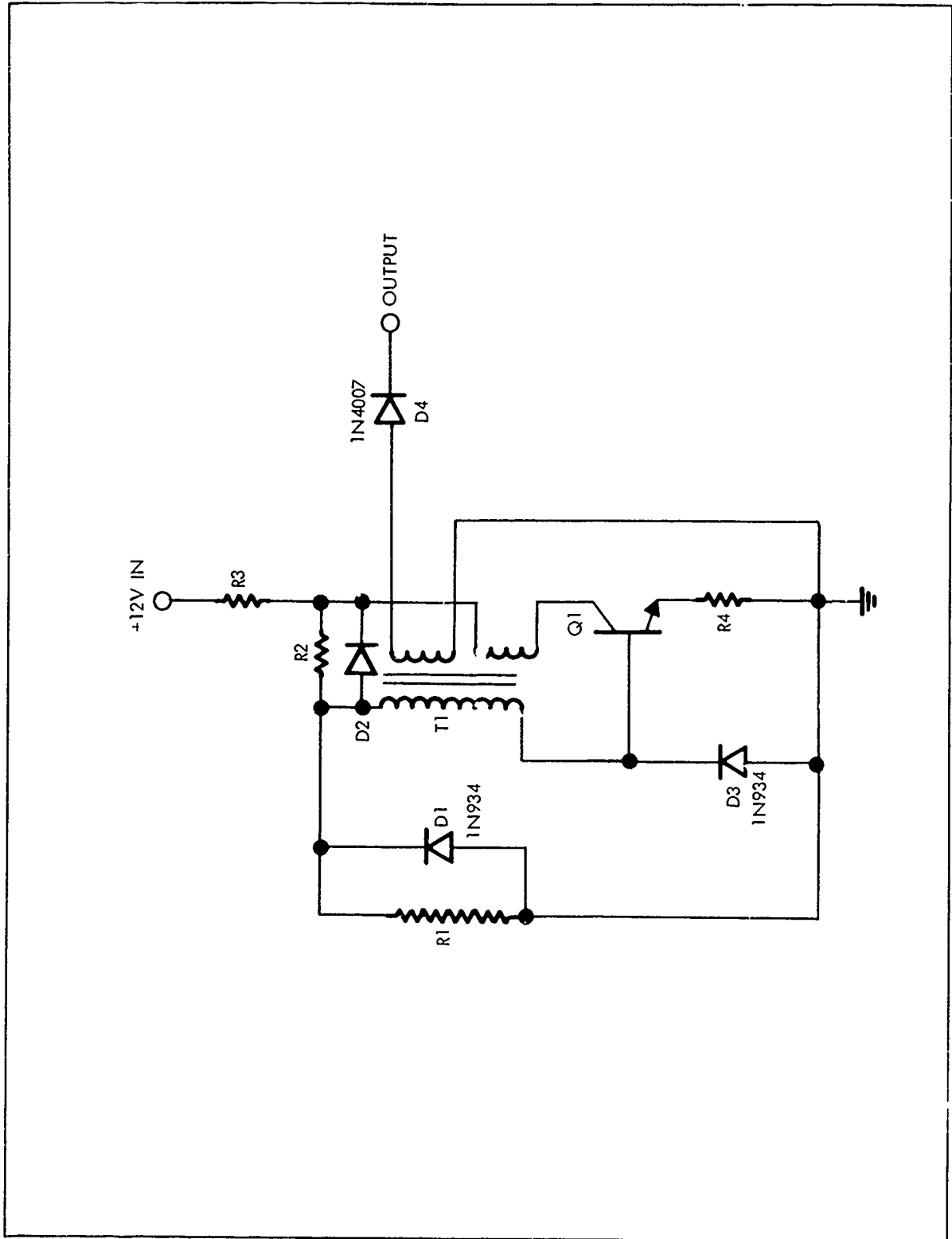


Figure 3.13 DC-DC Converter

UNCLASSIFIED

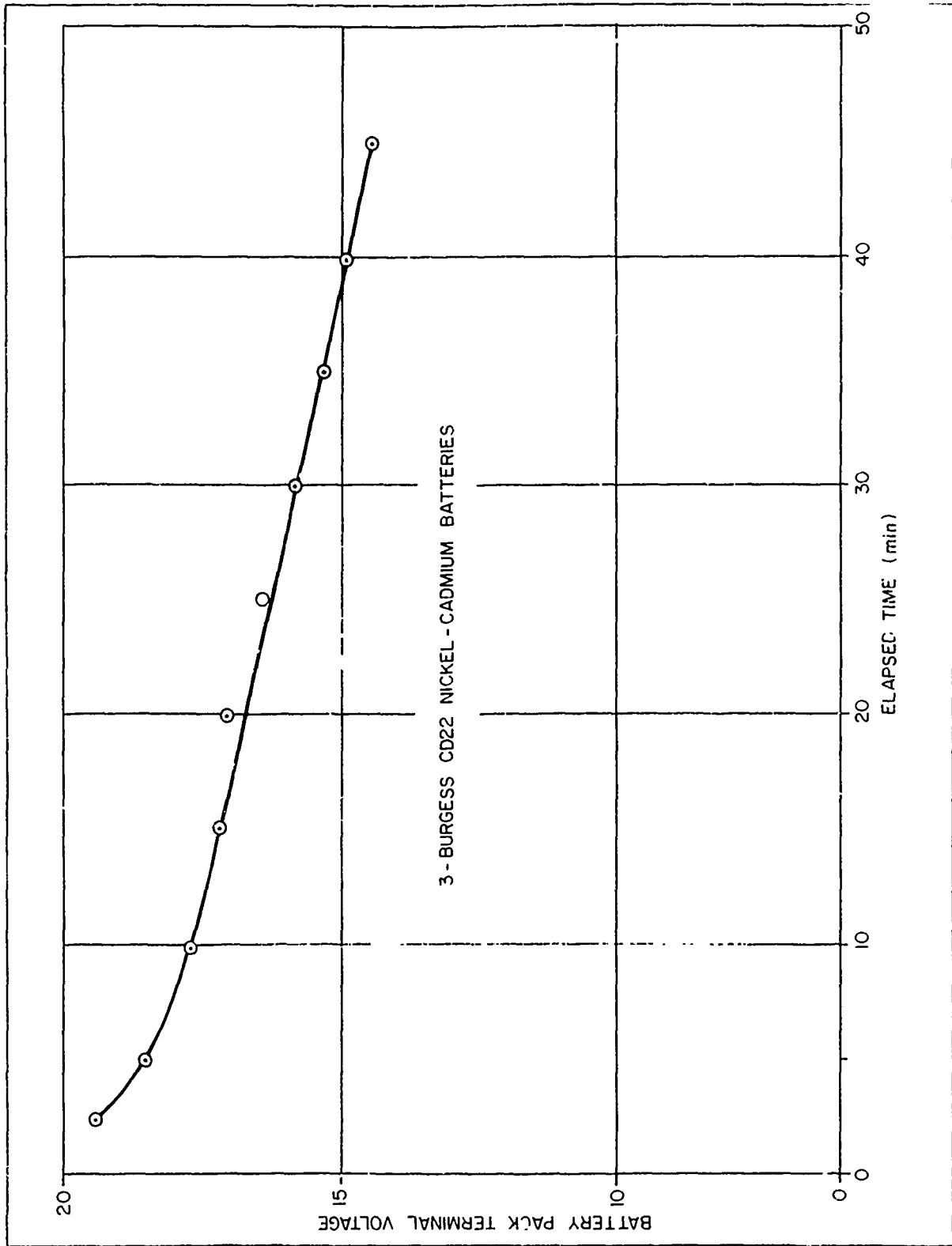


Figure 3.14 Battery Pack Discharge Profile

UNCLASSIFIED

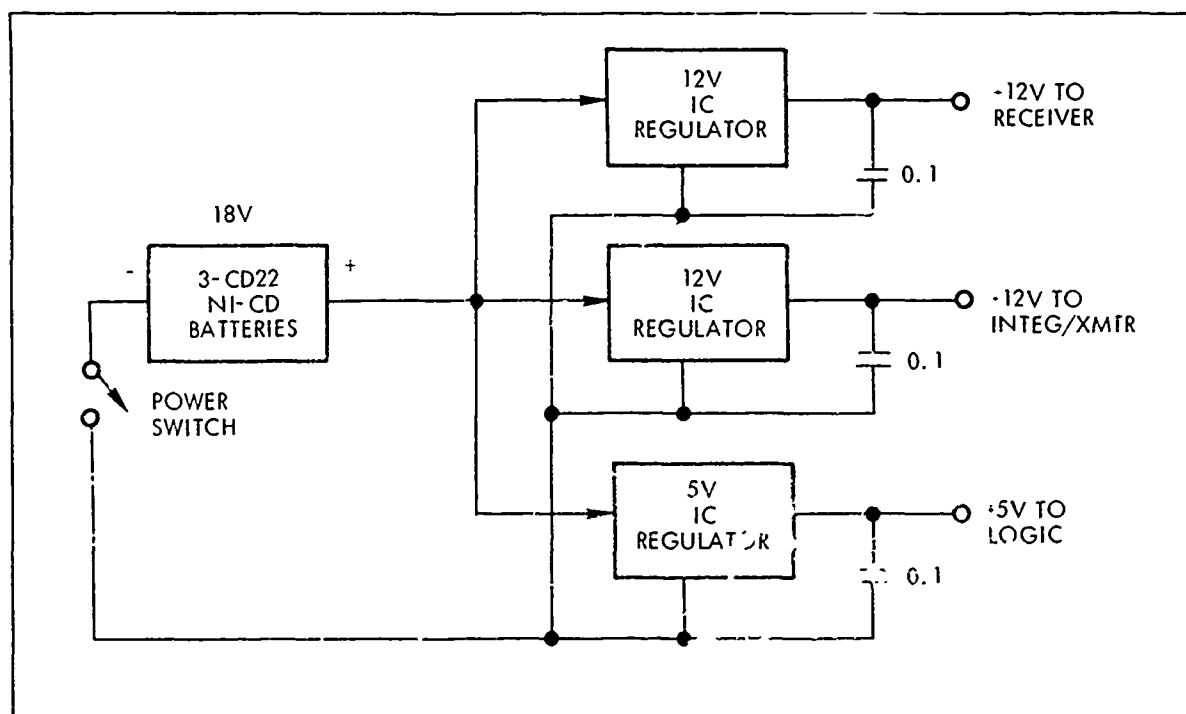


Figure 3.15 Power Supply Schematic

UNCLASSIFIED

3.4 System Calibration, Demonstration Model

The range readout was calibrated by means of trim resistors in the gate timing circuit so that the dial reading of the 10 turn potentiometer corresponds to the range delay. The reading is in meters, from 50 M to 999 M and corresponds to time delays of 660 nsc/turn or 300 ft/turn of the dial. Calibration of the delay was measured with a precision time interval meter.

The inherent range errors are due to 2 sources: readout indexing errors and ambiguity of the gate coincidence. The overall error function is shown in Figure 3-16 and shows a periodicity characteristic of the dial-pot gearing. The system calibration curve is shown in Figure 3.17

3.5 Optical System, Demonstration Model

The optical system consists of two coaxially-mounted lens as shown in Figure 3.18, which serve as transmitter (collimating) optics and receiver optics, and an optical filter. Both lens are made of SF1 which has a relatively high refractive index (approximately 1.7) resulting in less spherical aberration than lower index glasses. It is relatively inexpensive, rugged, and resistant to climatic attack. The high chromatic dispersion of SF1 is not a problem in this system due to the essentially monochromatic radiation (0.9 μ). The radiation source is a GaAs diode with a maximum dimension of 0.016 inch (line pair) and the detector is a 2.5 mm diameter silicon detector. The transmitter and receiver characteristics are discussed below.

UNCLASSIFIED

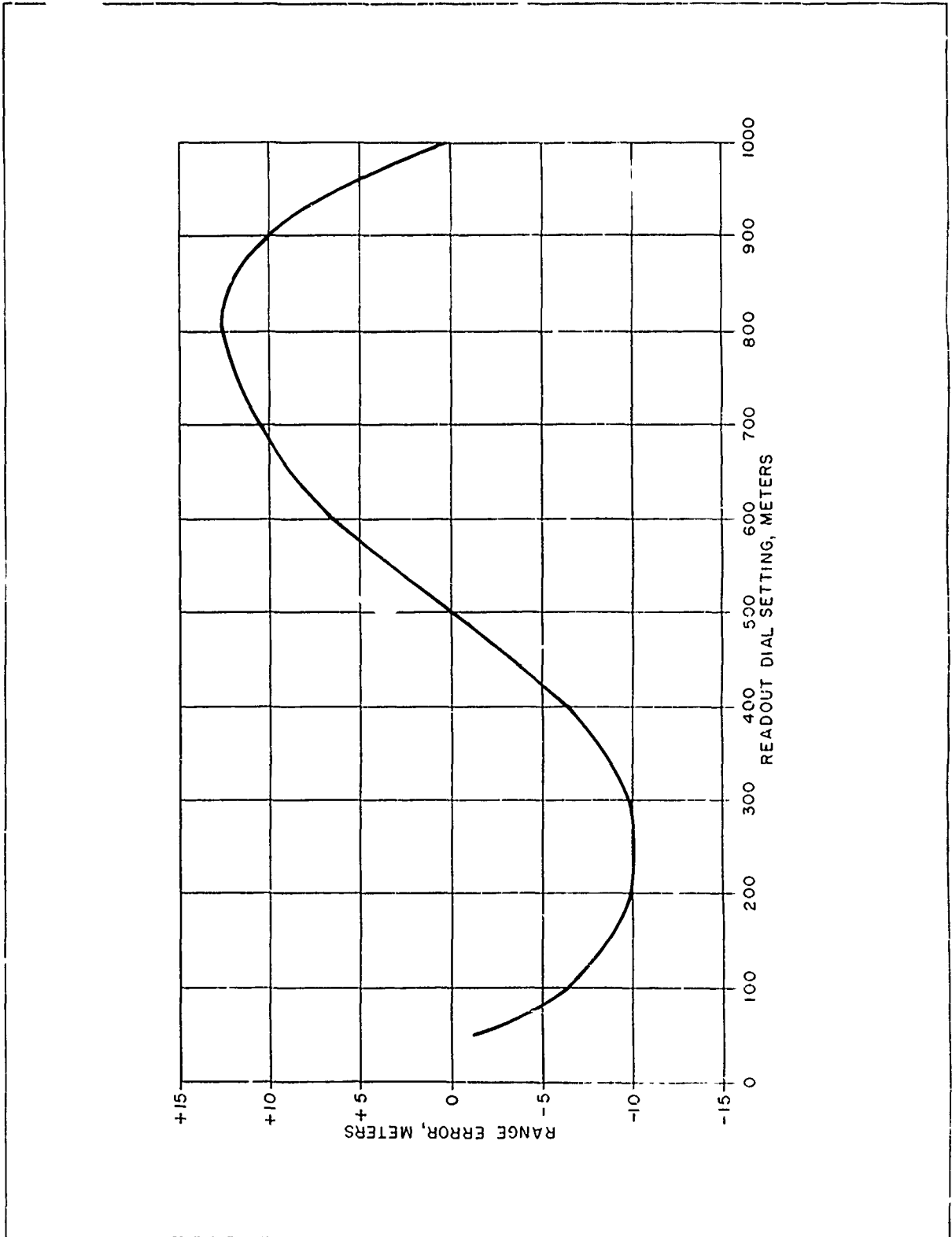


Figure 3.16 LAW Rangefinder, Range Error Function

UNCLASSIFIED

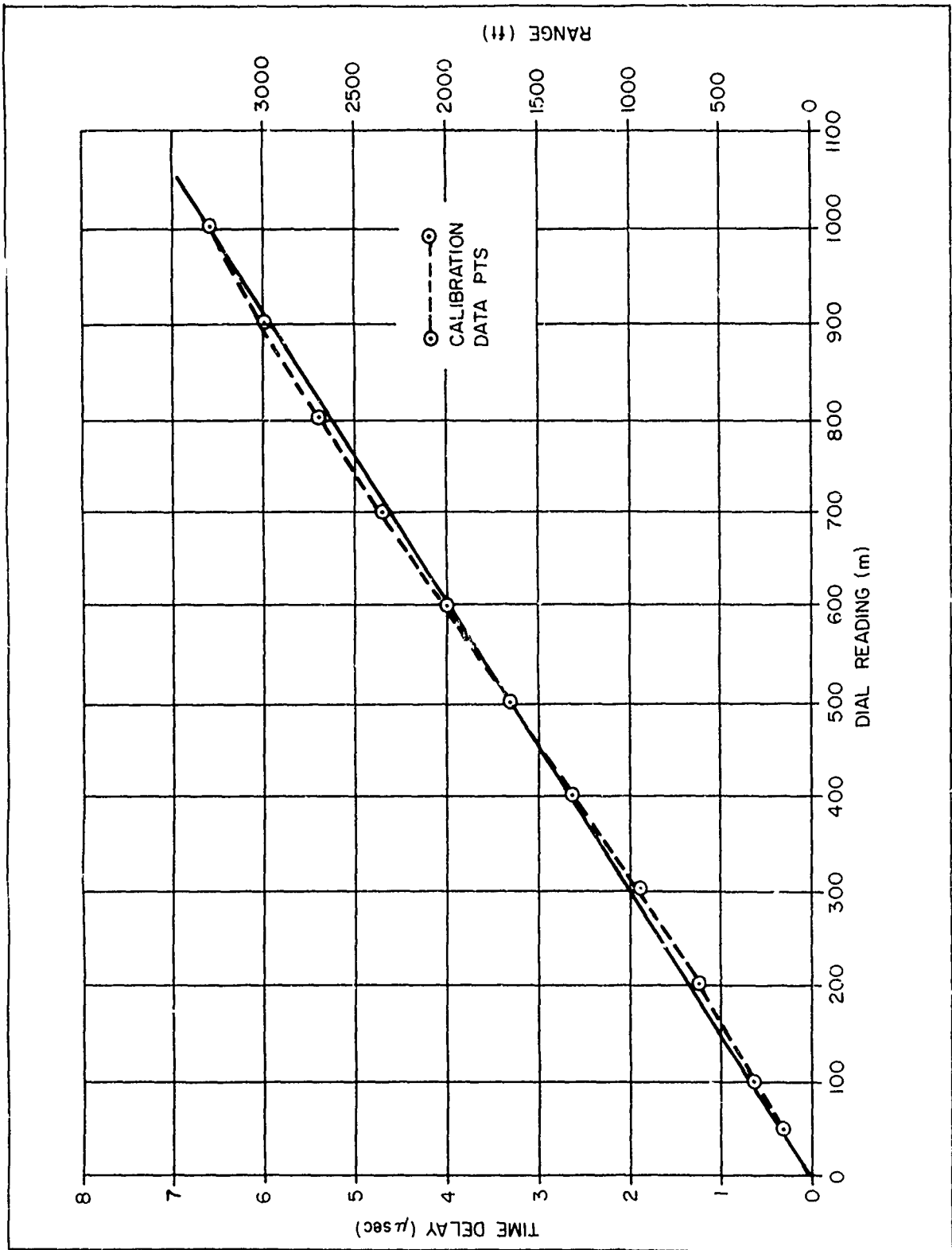


Figure 3.17 LAW Rangefinder Range Readout Calibration

UNCLASSIFIED

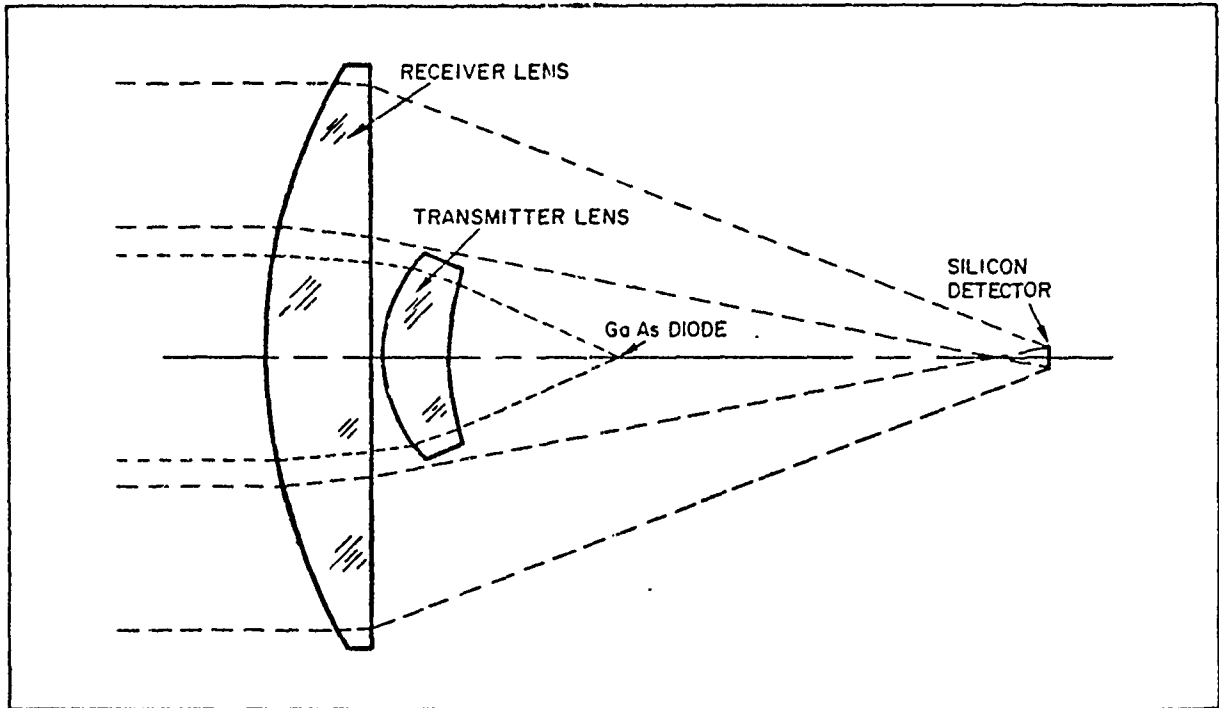


Figure 3-18 -- Receiver and Transmitter Lens Coaxial Configuration

The receiver lens is a plano-convex lens as shown in Figure 3.18 with the prescription given in Table 3.1. The lens has a focal length of 3.701 inches (94 mm) with a speed of F/1.47, and with the central blockage required for the transmitter the collecting area is 25 CM². The blur spot for the field-of-view subtended by the above detector (>50 percent collection) is 1.52 degrees.

UNCLASSIFIED

TABLE 3.1
RECEIVER OPTICS PRESCRIPTION

Lens Type - Convex-Plano Singlet Focal Length = 3.701 inches (94 mm) F/number = 1.47 Pupil Outer Diameter = 2.525 inches Pupil Blockage Diameter = 1.2 inch (approximately) Collecting Area (without spider) = 25.0 cm ² Approximate Blur Spot Diameter = 0.075 inch (1.9 mm) Detector Diameter = 2.5 mm Approximate Field-of-View (80 percent collection) = 1.14 deg							
Element	Material	Thickness (inches)	Surface	Radius (inches)	Position* (inches)	Outer Diameter (inches)	Inner Diameter (inches)
Receiver Lens	SF1	0.5000	1	2.5761	0.0000	2.525	1.200
			2		0.5000	2.500	1.100
Detector	Air	3.1930	3	---	3.6930	---	---
* Position to right of first surface vertex.							

The transmitter lens consists of a positive meniscus singlet lens located behind the receiver lens as shown in Figure 3.18 with the prescription given in Table 3.2. The focal length of the combination is 1.23 inches with a speed of F/1.3. The total beam divergence including aberrations and the finite source size is 1.09 deg. Based on RCA data (GaAs diode manufacturer) a faster lens would collect somewhat more radiation; however, this

UNCLASSIFIED

was avoided because another lens element would be required to correct the aberrations, and the transmitter size would increase and probably introduce as much or more loss into the receiver path as would be gained in the transmitter.

TABLE 3.2
TRANSMITTER OPTICS PRESCRIPTION

Element	Material	Thickness (inches)	Surface	Radius (inches)	Position * (inches)	Outer Diameter (inches)	Inner Diameter (inches)
Lens Type - Positive Meniscus Focal Length - 1.23 inch F/number - 1.3 Diode Size - 0.016 inch (maximum dimension) Total Divergence - 1.09 deg							
Receiver	SF1	0.5000	1	2.5761	0.00	0.945	0.0
	Air	0.0500	2		0.5000	0.872	0.0
Lens	SF1	0.314	3	0.674	0.5500	0.824	0.0
	Air	0.811	4	1.226	0.864	0.663	0.0
Diode			5	---	1.675	---	---
* Position to right of first surface vertex.							

UNCLASSIFIED

3.6 Test Results

The prototype model was tested at Aberdeen Proving Grounds, Frankford Arsenal, and Picatinny Arsenal and at Raytheon MSD against various targets of opportunity. Extended area targets such as buildings, trees, trucks, and tank mockups were detected consistently at ranges out to 500 M. Some foliage and buildings were detected at ranges as great as 930 M.

Due to the scope of the program, only qualitative tests rather than exacting quantitative data were possible. The test results showed close agreement with the predicted performance values and served as a baseline for future advanced model designs such as given in Section 3.7 below and in Section 4.

3.7 Advanced Model Design Description

A change in scope regarding the features to be incorporated within the range finder to be delivered was requested by the Frankford Arsenal Program Office. This section describes those features incorporated which are unique to this device. Figure 3.19 and Figure 3.20 contain photographs of the deliverable range finder.

3.7.1 Dual Gate Signal Processor

Since the laser pulse rise time is on the order of 30-40 nsc with a 100 nsc pulse width, one of two techniques must be used if the range accuracy of ± 5 M or less is to be achieved with minimum complexity. The first is measurement of amplitude of each pulse and subsequent determination of the half-amplitude threshold crossing. This is not readily implemented or compatible with pulse integration processing such as

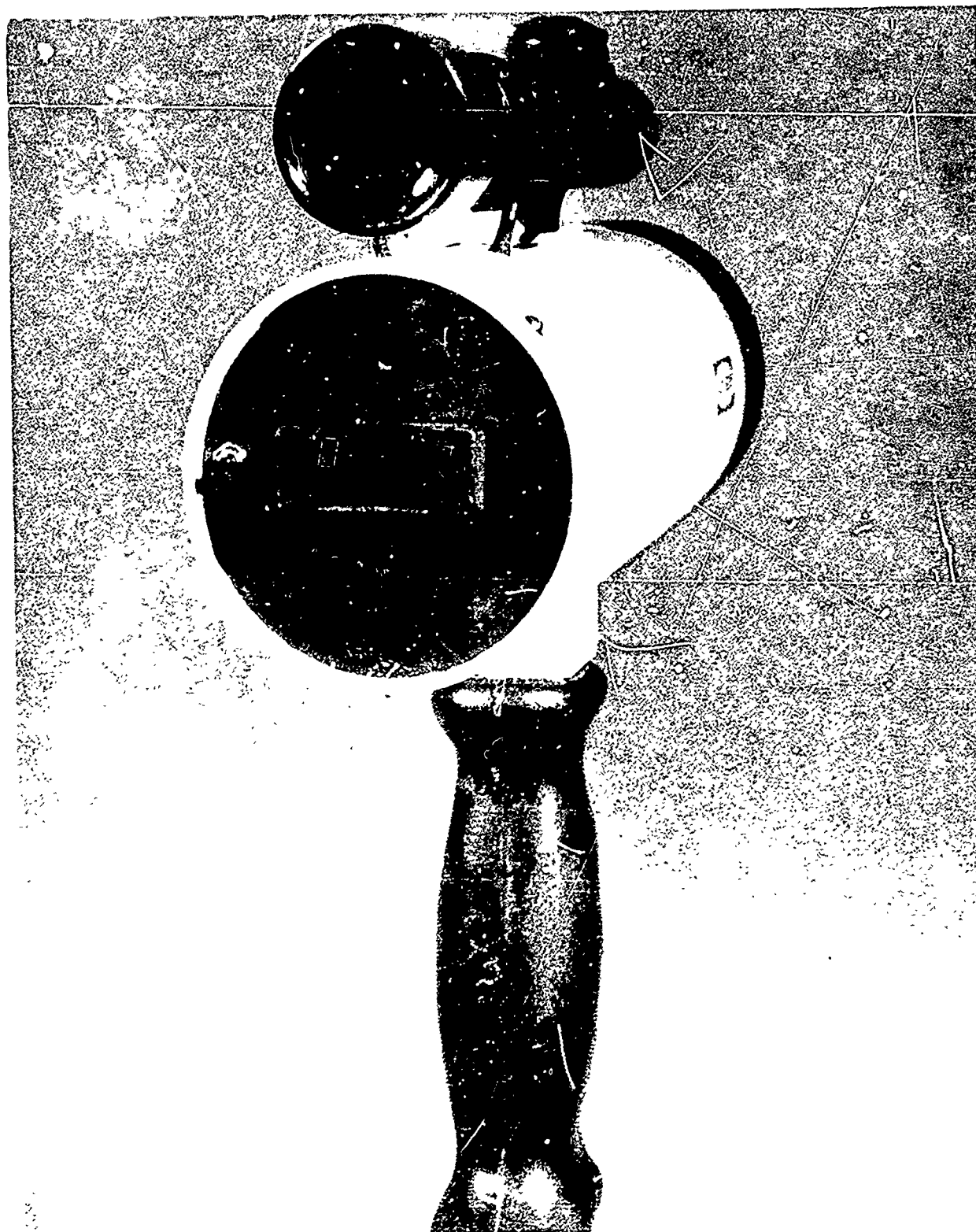
UNCLASSIFIED



Figure 3.19 Demonstration Model, Front View

CN-22-199

UNCLASSIFIED



CN-27-201

Figure 3.20 Demonstration Model Showing Range Readout Display

UNCLASSIFIED

needed for signal-to-noise ratio enhancement. The other technique evolves from optimum filter theory. If the pulse in Figure 3.21(a) is differentiated as shown in 3.21(b), the rectangular approximation matched filter takes the form shown in 3.21(c). In practice, this filter can be implemented without differentiation and bipolar processing by means of parallel processing using two rectangular matched filters (sampling gates) as shown in Figure 3.22. The implementation of this technique is shown in block diagram form in Figure 3-23.

This particular implementation of the dual-gate signal processor serves two basic functions: optimum range detection filter and capability of implementing a range tracking function. The pseudo-matched filter approach permits range measurement by interpolation between the leading and trailing edges of the signal pulse. This effectively eliminates the gross ambiguity inherent with threshold detection within a single sampling gate.

Referring to the block diagram of Figure 3-23 we see that the dual-gate signal processor consists of "near gate" and "far gate" sample-holds and integrators, "sum" and "difference" level detectors and tracking logic. A schematic is given in Figure 3.24.

Negative going video pulses from the postamplifier are applied to the input stage of the dual gate processor, a PNP emitter follower, Q1 which is biased at above 7.2V. The emitter of Q1 drives both the "near" and "far" gate sample-holds.

UNCLASSIFIED

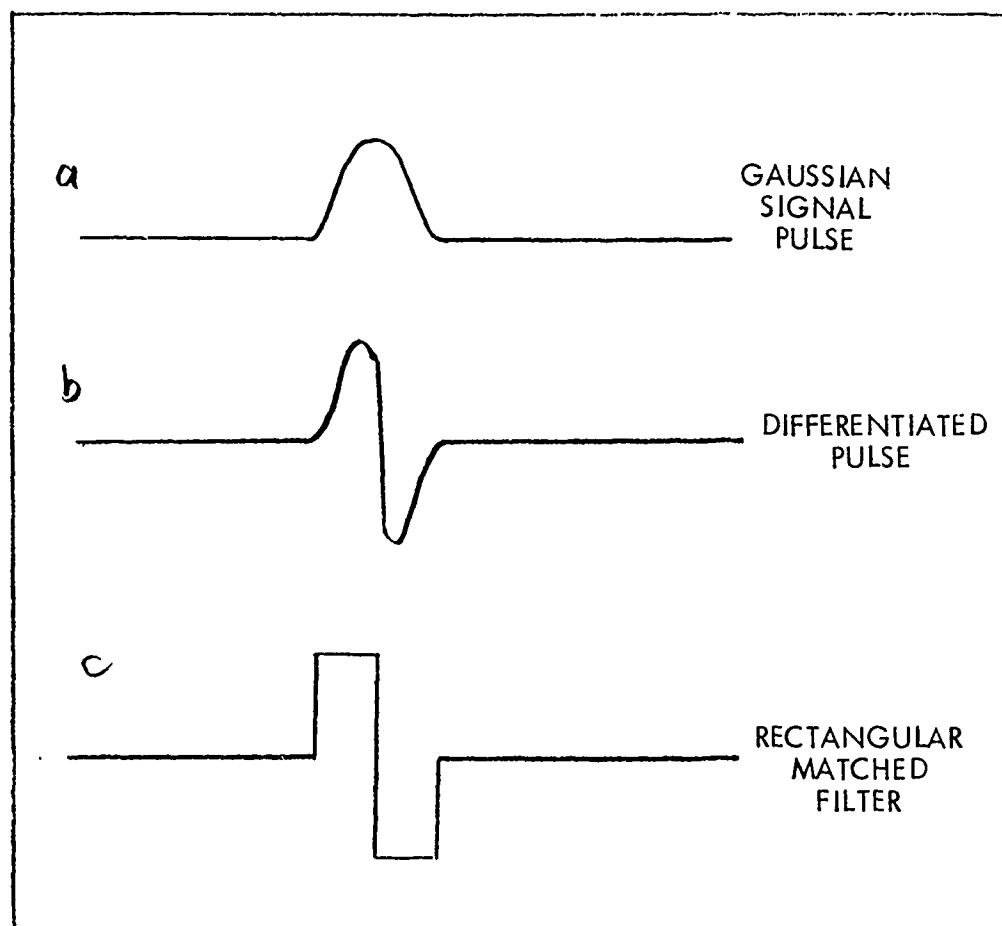


Figure 3.21 Pseudo-Optimum Filter Derivation

UNCLASSIFIED

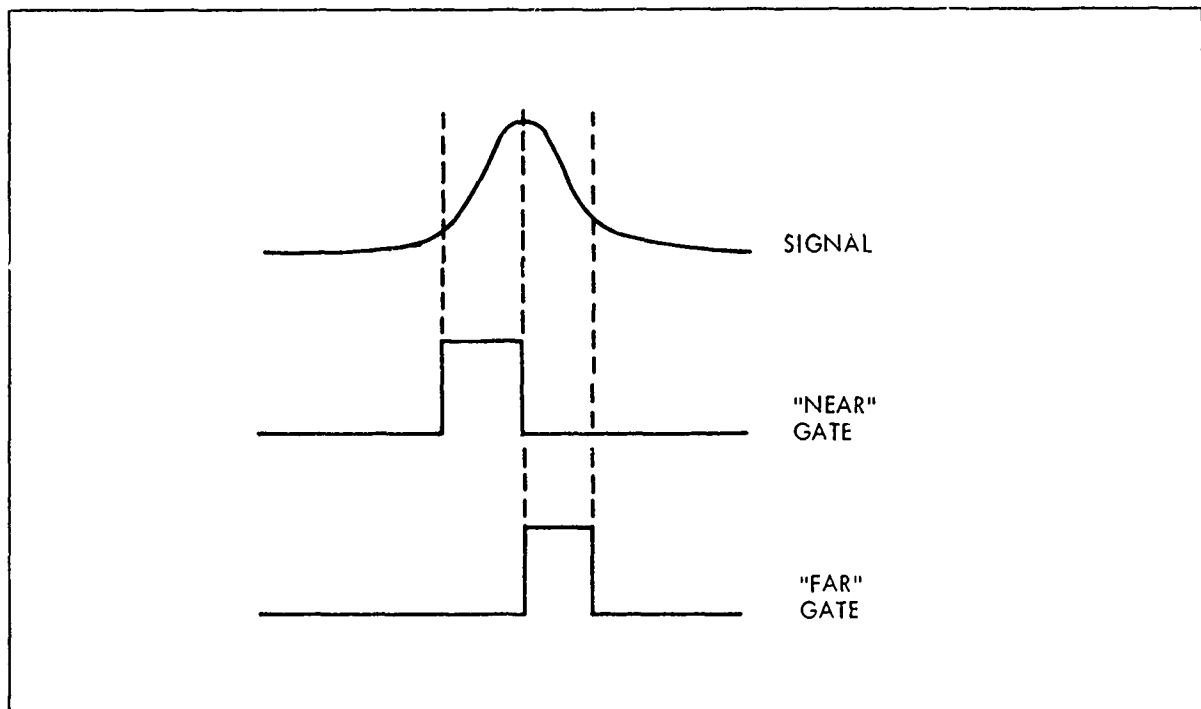


Figure 3.22 Dual Sampling Gates

UNCLASSIFIED

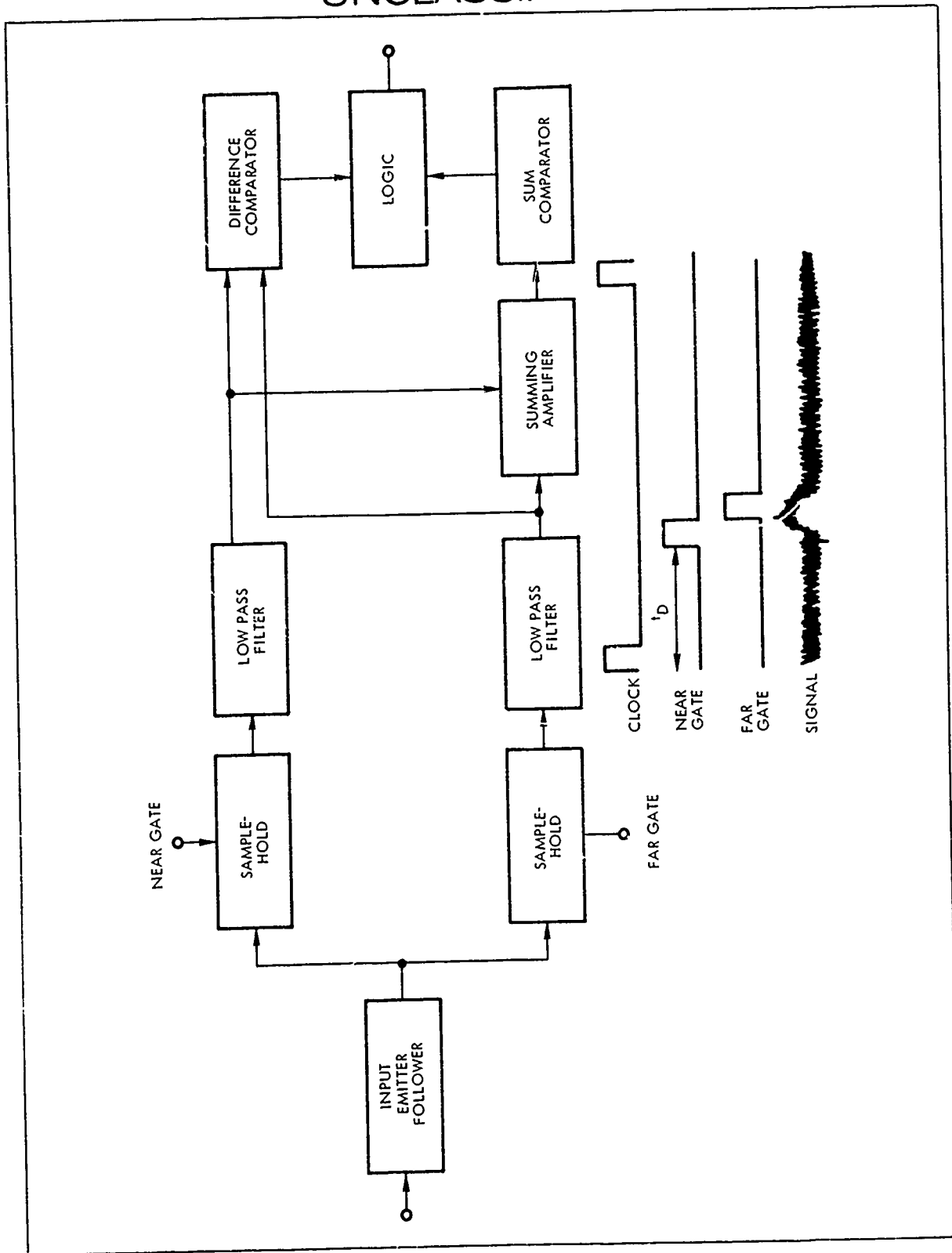


Figure 3.23 Dual-Gate Signal Processor

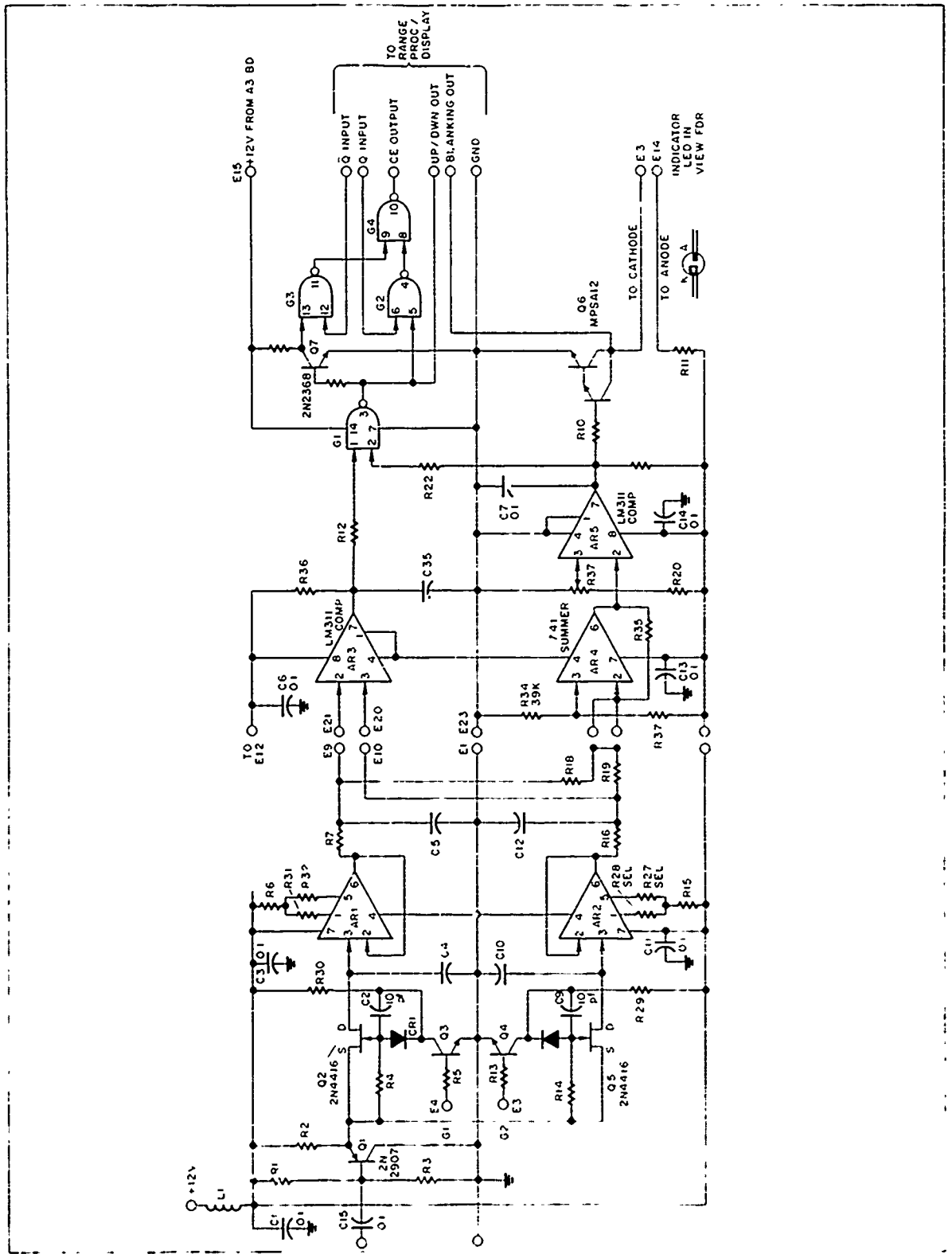


Figure 3.24 Logic Schematic (Dual-Gate Processor)

UNCLASSIFIED

The integrator is simply a single section RC low pass filter with a time constant, T_2 , of 0.1 sec

The outputs of the "near" and "far" gate integrators are applied to the "difference" channel comparator, AR3. Offsets are set for the two integrator channels so that the "difference" comparator is normally at a Logic "1", switching randomly with noise.

The "near" and "far" gate integrators are also applied to a summing amplifier, in Figure 3-24 AR4 which has a gain determined by

$$G = \left[\left(\frac{R3}{R1} \right) + \left(\frac{R3}{R2} \right) \right]$$

and output. $e_o = -R3 \left[\left(\frac{e1}{R1} \right) + \left(\frac{e2}{R2} \right) \right] + V_{OS}$

This is detailed in Figure 3.25

The output of the 741 summing amplifier, AR4, is applied to one input of the "sum" comparator, AR5 (Figure 3.24). A variable reference voltage determined by the voltage dividers R37 and R20 is applied to the other input of AR5 and is set to give a normal logic 0 level out. The difference and sum comparator outputs are combined in a CMOS NAND gate to determine which gates the target is in and generate the UP/DOWN commands to the range display/D/A counters to achieve range lock and range track.

UNCLASSIFIED

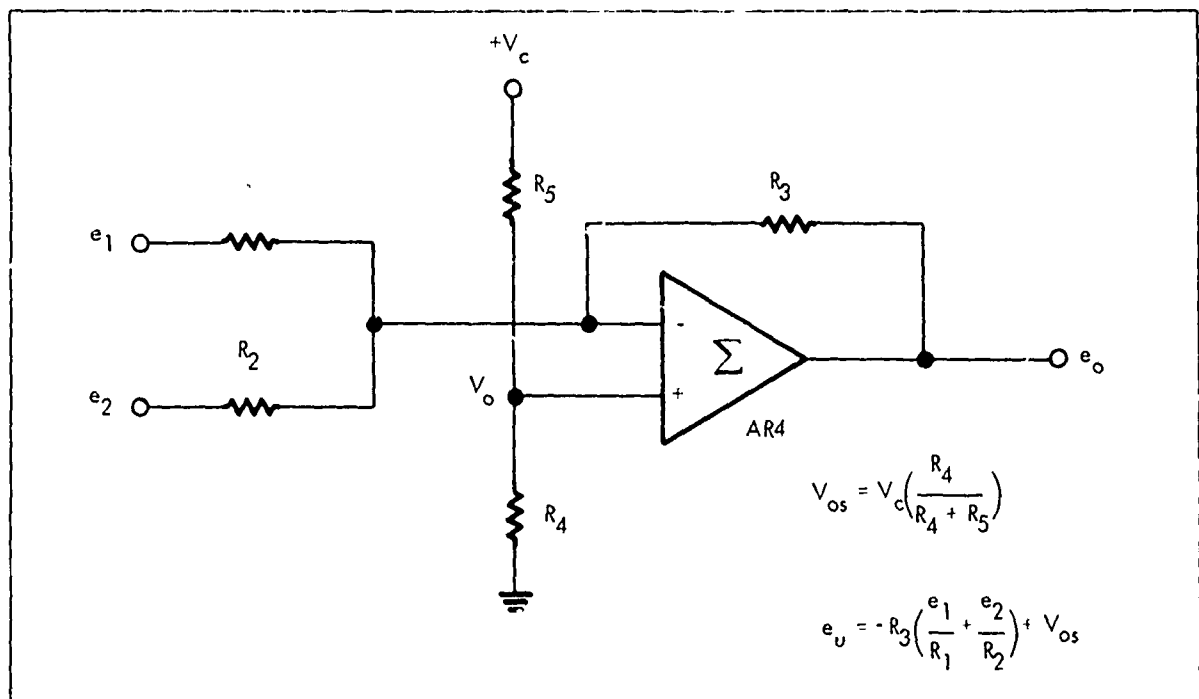


Figure 3.25 Summing Amplifier, Inverting

UNCLASSIFIED

The detection/tracking logic truth table is given in Table 3.3

TABLE 3.3

	<u>TARGET LOCATION</u>			
	<u>Neither Gate</u>	<u>Near Gate</u>	<u>Far Gate</u>	<u>Both Gates</u>
Sum Comparator	0	1	1	1
Difference Comparator	1/0	1	0	0
UP/DOWN NAND GATE	1	0	1	1

With no target in the gates, the gates sweep out in range. When a target appears in the "far" gate or both gates, the "sum" and "difference" comparators both switch and the gates continue sweeping out in range. When the target appears in only the "near" gate, both comparators switch to the "1" level and the NAND gate goes to "0" causing the gates to backup or sweep in. When the near gate backs up until the target is in both gates, the sweep reverses again and begins to bat back and forth between the target leading and trailing edges. This is the "range lock" condition and once achieved, the target can be tracked in range at velocities of up to about 180 MPH.

UNCLASSIFIED

Stability of the loop is enhanced by slowing down the gate sweep when backing up or sweeping inward in range. This is done by controlling the count rate in the range count/D/A module. The "sum" comparator output also generates two other commands. One is the drive for the range presence LED in the viewfinder to tell the operator the target was acquired and the other is to strobe the 3 digit display on.

The LED in the viewfinder is driven with an MPSA12 Darlington transistor.

3.7.2 Sweep, Timing, and Display

The sweep, timing and display unit generates all timing pulses, range gate sweep and range count conversion and display. The functional block diagram is shown in Figure 3.26.

The basic 1 KHz clock frequency from the transmitter unit is divided down by 25 in the normal UP count mode. A precision IC dual monostable operated in the closed loop frequency division mode is used for this function. The division ratio is changed upon application of the COUNT DOWN command to divide by 50. This is done by switching in a shunt timing element. The divide by 25/50 output is fed into a CMOS flip-flop. The flip-flop Q and \bar{Q} outputs are applied to CMOS gates wired to perform the EXCLUSIVE OR function and control synchronous data carry from the 0/5 M range flip-flop. The Q or \bar{Q} rail data selected by the OR gate is transferred to the first counter for the 10's column. The flip-flop output also drives a MAN-4 display hardwired to read 0 or 5 meters. The count is transferred

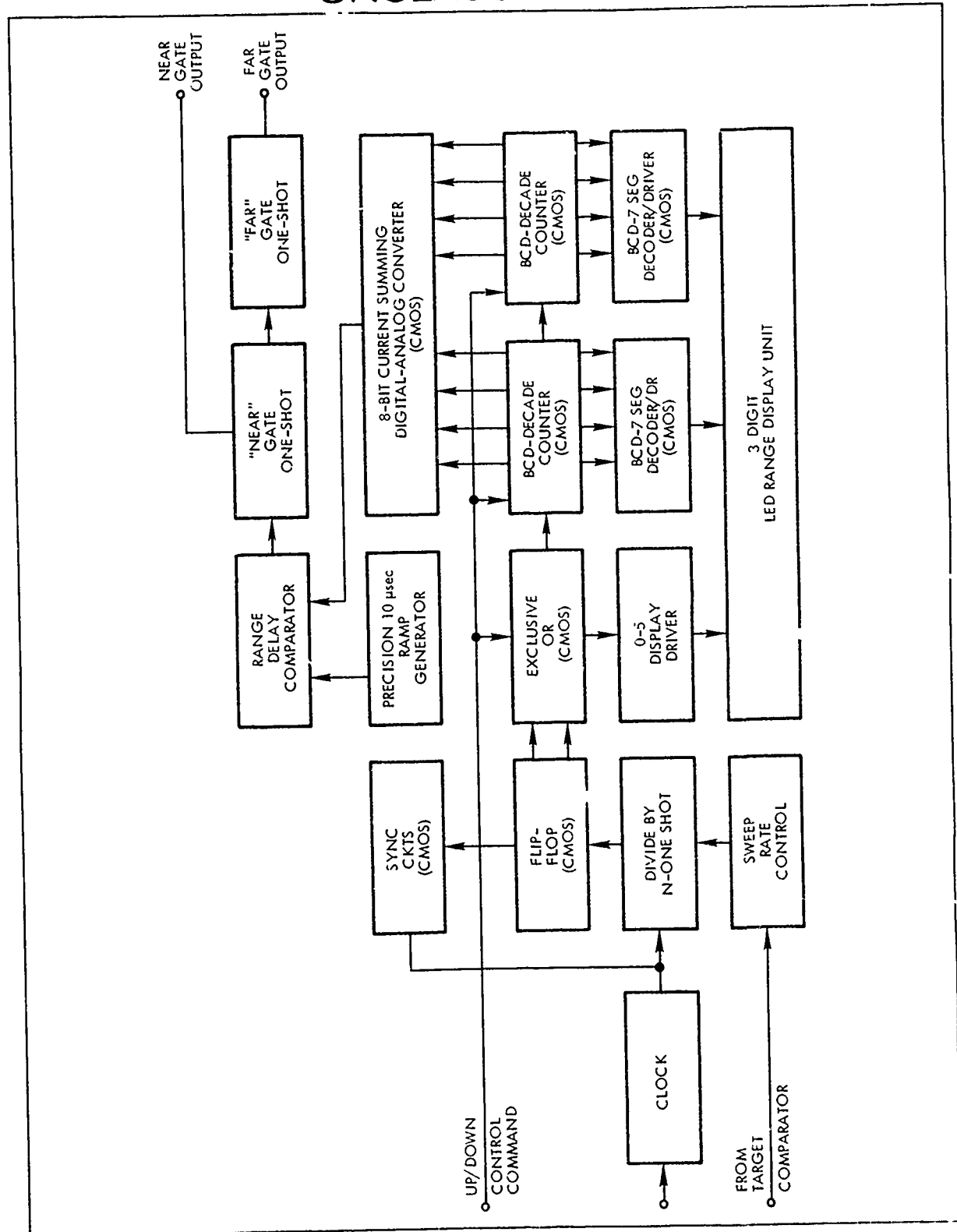


Figure 3.26 Automatic Range Sweep, Display and Timing

UNCLASSIFIED

(carried) to the 100's column counter and both counter BCD outputs applied to 7 segment decoder drivers which drive the 10's and 100's columns LED displays. Application of an unblinking level from the indicator LED driver unblinks the 0/5 display and the decoders for the other two digits, giving the target range. All counters, flip-flops, gates and decoders are CMOS to minimize power consumption.

As counting progresses the BCD outputs of the counters are converted from digital to analog form by means of conventional R-2R networks and current summing. Independent gain and offset adjustments on the summing amplifier permit calibration. The resultant staircase generated by the D/A converter is then applied to a precision high speed comparator and, each clock period, compared with the output of a 10 μ sec ramp. The summing amplifier calibration adjustments ensure voltage coincidence of the fast and slow ramps over the desired range. The result is a comparator output transition that steps out in range in 5M increments. This transition triggers 2 cascaded IC monostables to generate the pair of sequential 50 nsc range gates to drive the near and far gate sample-holds.

By this implementation, the range gate position is controlled by and synchronized with the range display count and when the target appears in the gate, the corresponding count read-out.

UNCLASSIFIED

3.7.3 Receiver AGC

To minimize the effects of "main-bang" transmit pulse tailing and atmospheric backscatter, the receiver gain is reduced by about 40 db initially and ramped up to maximum gain at a range of about 250 meters. The AGC slope is readily adjustable by means of a trim potentiometer to permit optimization during system calibration.

The AGC is implemented by applying the slow ramp (from D/A converter) to the AGC pin of the second MC1590 through a 10K potentiometer and summing the ramp with another fixed voltage. The ramp and receiver output from AGC are shown in Figure 3.27.

3.7.4 System Calibration, Advanced Model

The range error of the advanced model is a function of the timing errors, linearity of the fast 10 μ sec ramp and accuracy of the D/A conversion.

Calibration is achieved by varying the gain (slope) of the fast ramp and DC offset to give voltage coincidence with the slower ramp (D/A output) at the correct time. As gain and offset are adjusted, the time interval to the coincidence is measured with a precision time interval counter and correlated with the range readout. The count to the D/A is manually controlled in this case to permit making these measurements at several points between 50 M and 1000 M.

UNCLASSIFIED

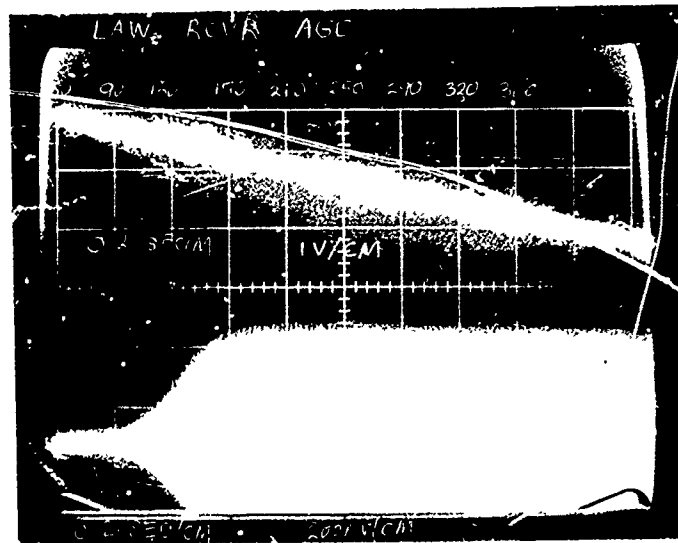


Figure 3.27 Top: Sweep Ramp; Bottom: Receiver Gain

UNCLASSIFIED

4. Design Requirements

The demonstration rangefinder described in Section 3 meets the performance criteria developed in Section 2. However, from the point of view of weight and cost, such a device would be unacceptable for large scale production. This section will consider the modifications necessary, in terms of material and production techniques, to reduce the weight and production costs of a similarly form factored rangefinder.

Since the system must continue to exhibit the ranging capability of the demonstration device, the manner in which any proposed changes affect this capability must be investigated. These considerations are important regarding modifications to the optics and to a lesser extent regarding the choice of material for the mechanical components of the device. These areas are discussed below. In addition, possible modifications to the electronics packaging are also discussed.

4.1 Optical Design

The overall design goal for each of the optical subsystems comprising the LAW Rangefinder is the attainment of adequate optical performance under constraints of cost, weight and size. Additional considerations involve availability and performance of optical components over the temperature range specified for the LAW device.

Conventional optical components provide adequate performance over the temperatures considered but generally involve costs and weights greater than desired. Because of this the use of plastic optical components in the receiver, transmitter and viewfinder has been investigated. Generally speaking, molded optical

UNCLASSIFIED

components are about half the weight of their glass counterparts, and in quantity are considerably less in cost. In addition, because of the molding process, the restriction to only spherical surfaces is no longer a practical consideration since aspheric lenses are readily produced in large quantities. Many, although not all, of the traditional difficulties encountered in the use of plastic optical components have been overcome in recent years. For example, haze and dimensional stability are controllable to the extent that they should not present problems for this application. Other areas, such as thermal dimensional changes and thermal refractive index changes must be either allowed within the tolerances of the system or means provided for compensation.

The following sections will detail the baseline optical schematic and the rationale employed in arriving at this configuration. In addition, the choice of material for the optical components will be considered and the use of these components in the rangefinder subsystems will be discussed.

4.1.1 Baseline Optical Configuration

The configuration of the receiver optics is the primary factor determining the overall size of the rangefinder. In addition to collecting area (which is heavily influenced by available transmitted power in conjunction with range requirements) the speed of the receiver as well as the choice of a refractive or a reflective system directly affect the resultant size. Initially, both refractive and reflective receivers were considered and trade-offs employed in arriving at the baseline configuration. This baseline optical configuration employs refractive optics and is illustrated schematically in Figure 4-1. The transmitter and receiver are arranged coaxially for maximum compactness. In addition, the receiver lens acts as the support spider for the transmitter reducing the number of parts needed and also eliminating further obscuration of the receiver optics

UNCLASSIFIED

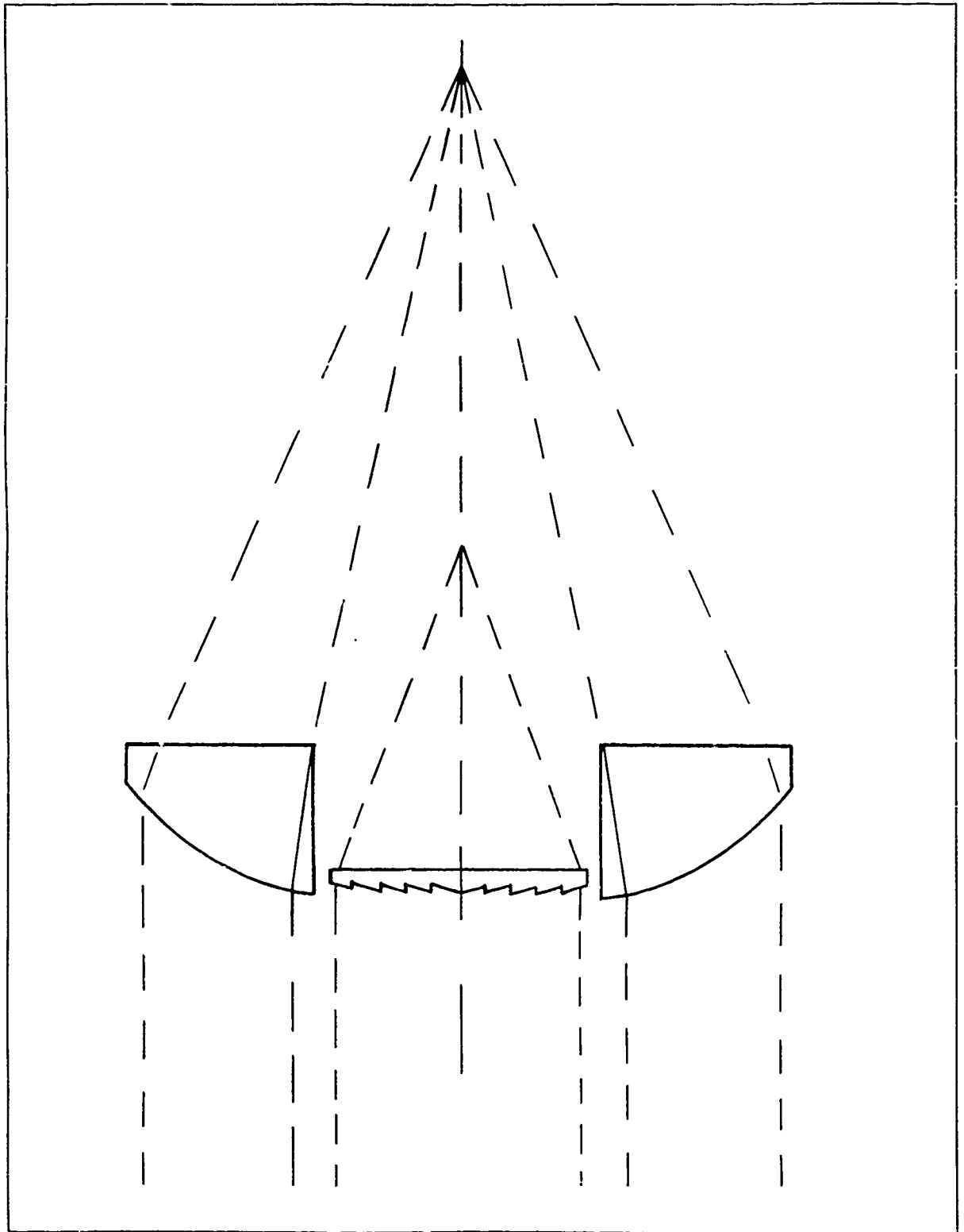


Figure 4.1 Baseline Optical Configuration

UNCLASSIFIED

which would otherwise result. This arrangement also enables the transmitted beam to avoid passing through the receiver lens and hence, reduces the possibility of scattered light reaching the detector. It is noteworthy that this was not a problem in the LAW demonstration device which utilized glass optics. However, the possibility that plastic optical components may scatter the transmitted light sufficiently to affect the receiver remains, and thus this arrangement is preferred.

A direct benefit of a refractive system, when compared to a reflective receiver, is the smaller volume which must be maintained free of obscuration between the detector and light collecting element. For a refractive system this unobscured volume is conical with the apex at the detector, whereas for a reflective system the volume required is cylindrical. Thus, in the refractive case, annular circuit boards may be placed in the region surrounding the conical light baffle.

The principal advantage of a reflective system is that the possibility exists of a slight reduction in weight. This may be realized since the collecting mirror would be lighter than an equivalent lens. However, there are several distinct disadvantages. Alignment problems are more critical with a reflective system and, unless the system is folded, the detector is back-to-back with the laser. This presents the possibility of electromagnetic interference effects. Folding the system is not advantageous since this introduces the need for an additional optical element and increases further the alignment sensitivity and cost.

4.1.2 Optical Component Material Selection

The important considerations regarding the selection of material for the optical components of the rangefinder are transmittance and refractive index in conjunction with cost and ease of component fabrication. In addition, it is necessary that the temperature variation of refractive index fall within the tolerance limits of the optical system.

UNCLASSIFIED

In order to simultaneously satisfy the requirements of adequate receiver collecting area and overall small range-finder length a relatively fast receiver system must be considered. To obtain the required resolution with conventional lenses while restricting the receiver optics to a single plano-convex element (necessary for cost considerations) a relatively thick element of high index flint glass is necessary. The weight of such an element is high. For the purpose of comparison, Table 4-1 presents some pertinent physical and optical properties of several readily available plastics suitable for use in optical components, along with values of selected properties of optical glasses. It is immediately apparent that a weight savings of over a factor of two is potentially available through the use of plastics as compared to glass.

A measure of the quality of surface finishes available as well as the amount of embedded colloidal sized particles is provided by the haze percentage of the material. The percentage refers to the amount of light lost due to scattering from surface imperfections as well as embedded particles. From Table 4-1 it is seen that the best plastics in this respect are acrylic and polycarbonate, with acrylic having a somewhat higher overall transmittance. The transmittance of acrylic, polycarbonate and polystyrene are given in Figure 4-2 as a function of wavelength for the purpose of comparison.

Additional important considerations are the value of the index of refraction, the precision within which it can consistently be obtained in the material and the variation of the refractive index with temperature. For the relatively fast (F/1.48) receiver system under consideration a high index is desirable. Acrylic has a somewhat lower index at the sodium D lines than the four remaining candidate materials, although due to its higher reciprocal relative dispersion (Abbe v value) this will drop less rapidly with increasing wavelength. For index value only, polycarbonate is probably superior to acrylic, although the lower index of acrylic can be compensated for by

UNCLASSIFIED

GENERAL OPTICAL SPECIFICATIONS FOR PLASTICS

	METHYL METHACRYLATE (ACRYLIC)	POLYSTYRENE (STYRENE)	POLYCARBONATE	STYRENE NITRILE COPOLYMER	STYRENE METHACRYLATE COPOLYMER	GLASS
Specific Gravity (Density)	1.19	1.04 to 1.08	1.2 to 1.3	1.05 to 1.08	1.14	2.4 to 3.4
Refractive Index (nD)	1.491	1.590	1.586	1.569	1.533	1.5 to 1.8
Abbe Value (V)	54 to 57.4	30.9	29.9	90%	91%	65-80
Luminous Transmittance (0.125" thickness)	92%	88%	89%	<5	<5	
Haze %	≤2	<5	<4	39.5°	40.7°	
Critical Angle (I _c)	42.2°	39.0°	39.07°	1.75	1.87	
Ratio of Minimum Radius to Thickness	2.02	1.70	270°F	215°F	190°F	
Deflection Temperature	210°F	209°F	Lexan	Tvfil	zerlon	
Trade Names	Lucite Plexiglass	Dylene Styron	Merlon	NAS		0.71
Coeff. of Thermal Expansion 10 ⁻⁵ /°C	5-9	6-8	7	6-8		
Max. Cont. Service Temp. °C	60-93	66-82	138-143	77-88		
Rockwell Hardness	M84-M105	M70-M85	M70-M118	M75-M90		
Heat Distortion 264 psc, °C	M97 typ	M90 typ	M70	91-104		
Warp (93/18/0) 23°F	66-99	80-99	135-145			
Impact Strength (Izod Notch)	.3	.2	.15			
dn/dt x 10 ⁻⁵ /°C	.3-.5	.35	12-17			
	8.5	12.0	14.2			

TABLE 4.1

UNCLASSIFIED

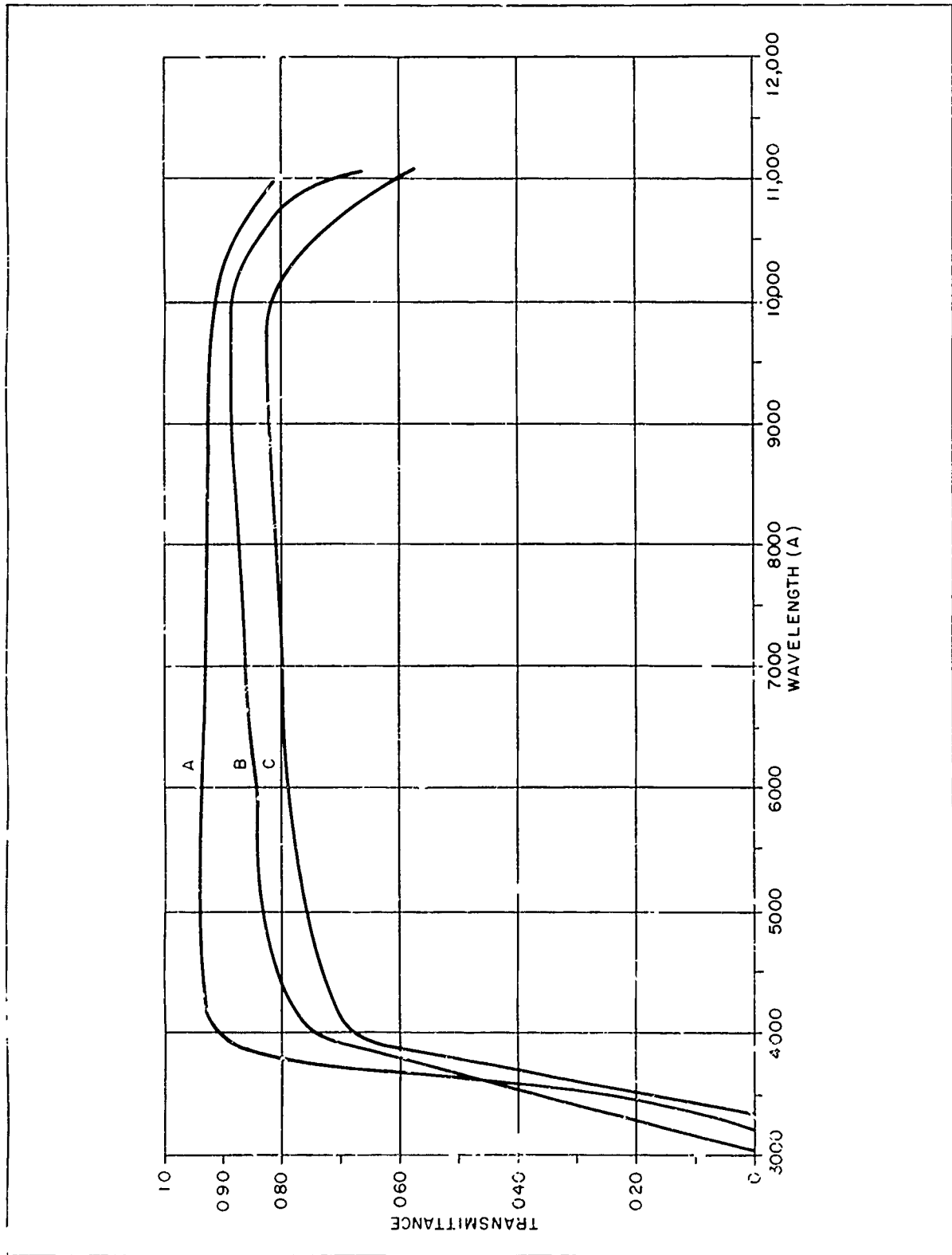


Figure 4.2 Transmittance of Acrylic (Curve A) and Polystyrene (Curve C) -0.25 inch thick. Transmittance of Polycarbonate (Curve B) -0.5 inch thick

UNCLASSIFIED

the use of an aspheric refracting surface for the lens. This entails very little additional cost when molded lenses are considered. In addition, the tolerances on the refractive index of acrylic lenses are readily maintained to within ± 0.001 . A plot of the refractive index of acrylic as a function of wavelength is presented in Figure 4-3.

The value of the refractive index is subject to change with temperature for both acrylic and polycarbonate. However, for the latter material the degree of change is significantly greater as indicated in Table 4-1.

A measure of the resistance of the material to abrasions is given by the hardness. Reference is again made to Table 4-1 for typical values for the plastics considered in this report. In general, plastics are much softer than glass and this has constituted one of the major drawbacks to the use of plastic as an optical material. The use of hard coatings on plastics is receiving increasing attention in an effort to overcome this deficiency. Of the plastics listed in Table 4-1, acrylic is superior insofar as hardness considerations are concerned.

In view of the above considerations acrylic is the optimum choice for a plastic lens material for the LAW Rangefinder.

4.1.3 Receiver Optics

The baseline receiver lens was designed to provide a collecting aperture of 2.432 inches with allowance for a central obscuration diameter of 1.300 inches. The resulting collecting area of the receiver is approximately 3.34 inches² (21.53cm²). The lens material is acrylic with the refractive index at 0.9 microns and 70°F taken as 1.4825. A prescription for the baseline lens is contained in Table 4-2.

A plano-aspheric element was considered a priori. The basic trade-off parameters involved in the choice of the

UNCLASSIFIED

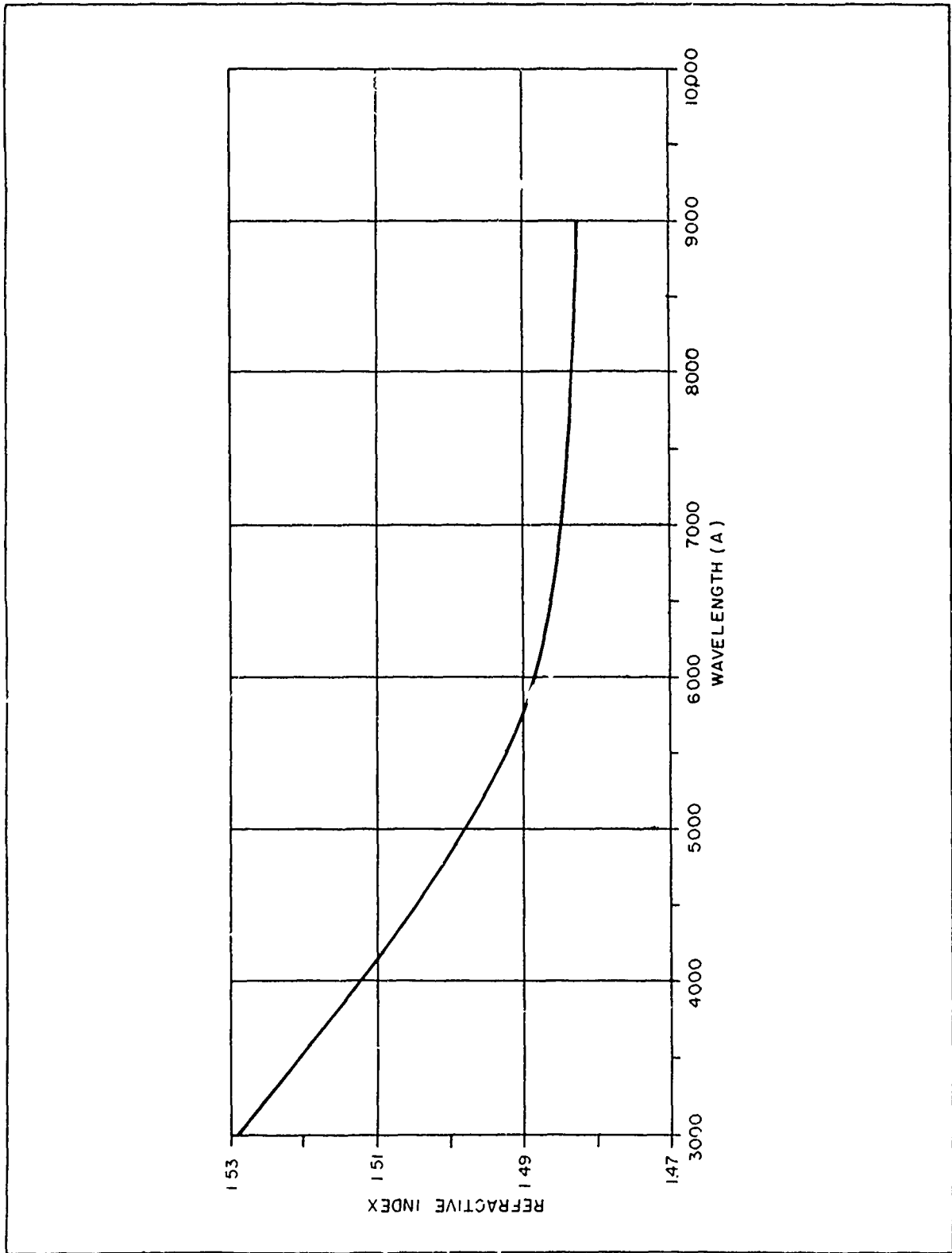


Figure 4.3 Refractive Index of Acrylic as a Function of Wavelength

UNCLASSIFIED

TABLE 4.2 RECEIVER LENS PRESCRIPTION

LENS TYPE	-	CONVEX ASPHERIC - PLANO SINGLET
FOCAL LENGTH	-	3.625 INCHES
F/#	-	1.48
PUPIL O.D.	-	2.437 INCHES
PUPIL BLOCKAGE DIAMETER	-	1.300 INCHES
COLLECTING AREA	-	3.34 IN ² (21.5CM ²)
DETECTOR DIAMETER	-	0.1 INCHES
APPROX. FIELD OF VIEW	-	1.4 ^o
LATUS RECTUM OF ELLIPSE	-	3.496 INCHES

ELEMENT	MATERIAL	THICK- NESS (INCHES)	SURFACE	ECCEN- TRICITY	POSITION (INCHES)	O.D. (INCHES)	I.D. (INCHES)
-	-	-	1	0.7669	0.000	2.437	1.300
RECEIVER LENS	ACRYLIC	0.65	-	-	-	-	-
-	-	-	2	PLANE	.65	2.341	1.171
-	AIR	3.193	-	-	-	-	-
DETECTOR	-	-	3	PLANE	3.843	-	-

UNCLASSIFIED

final design were the central and edge thicknesses of the lens. In general, the less the central thickness of the lens the less the thickness at the edge of the required clear aperture. The baseline lens has a central thickness of 0.65 inches and a thickness at the edge of the clear aperture of approximately 0.20 inches.

The distance from the planar (back) surface of the lens to the image plane is maintained at 3.193 inches. The front (convex) surface of the lens is an aspheric, but includes no higher order terms than those corresponding to a conic. For the baseline lens, this conic is an ellipse with an eccentricity of 0.7669. This value is the optimum for a lens which yields acceptable blur spot sizes for object points on-axis and $\pm 0.7^\circ$ off-axis. The blur spot diagrams for these points are shown in Figures 4-4 and 4-5 respectively. Also included in these figures is a circle corresponding to the proposed detector diameter (EG&G SGD-100A) of 0.1 inches.

These blur spot diagrams (and all succeeding blur spot diagrams in this section) were obtained by setting up a uniformly spaced grid, consisting of 180 rays, in the entrance pupil of the system and tracing these rays through the optical system to the image plane.

As mentioned previously, acrylic lenses are readily obtained with the refractive index controlled to within ± 0.001 . For worst case analysis however, the baseline receiver lens was toleranced for index errors of ± 0.0085 in order to determine the magnitude of the detector repositioning necessary to give an adequate blur spot. These distances were -0.060 inches for $\Delta n = 0.0085$ and $+0.063$ inches for $\Delta n = -0.0085$. Refocussing by these distances yields blur spots which are essentially identical to those shown in Figures 4-4 and 4-5.

The LAW receiver must operate at ambient temperatures which can range from -40°F to $+140^\circ\text{F}$. The baseline design is

UNCLASSIFIED

Scale Factor = 50,000

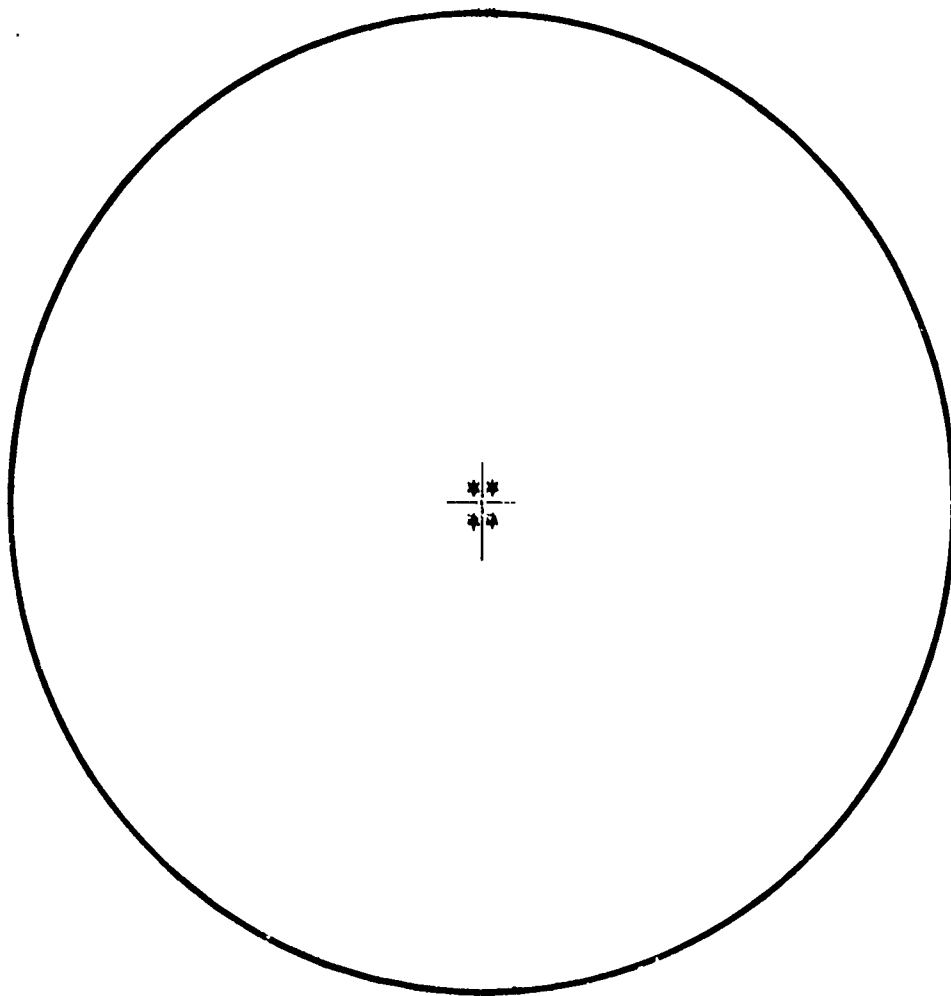


Figure 4.4 Blur Spot Diagram for a Point on Axis

UNCLASSIFIED

Scale Factor = 50.0000

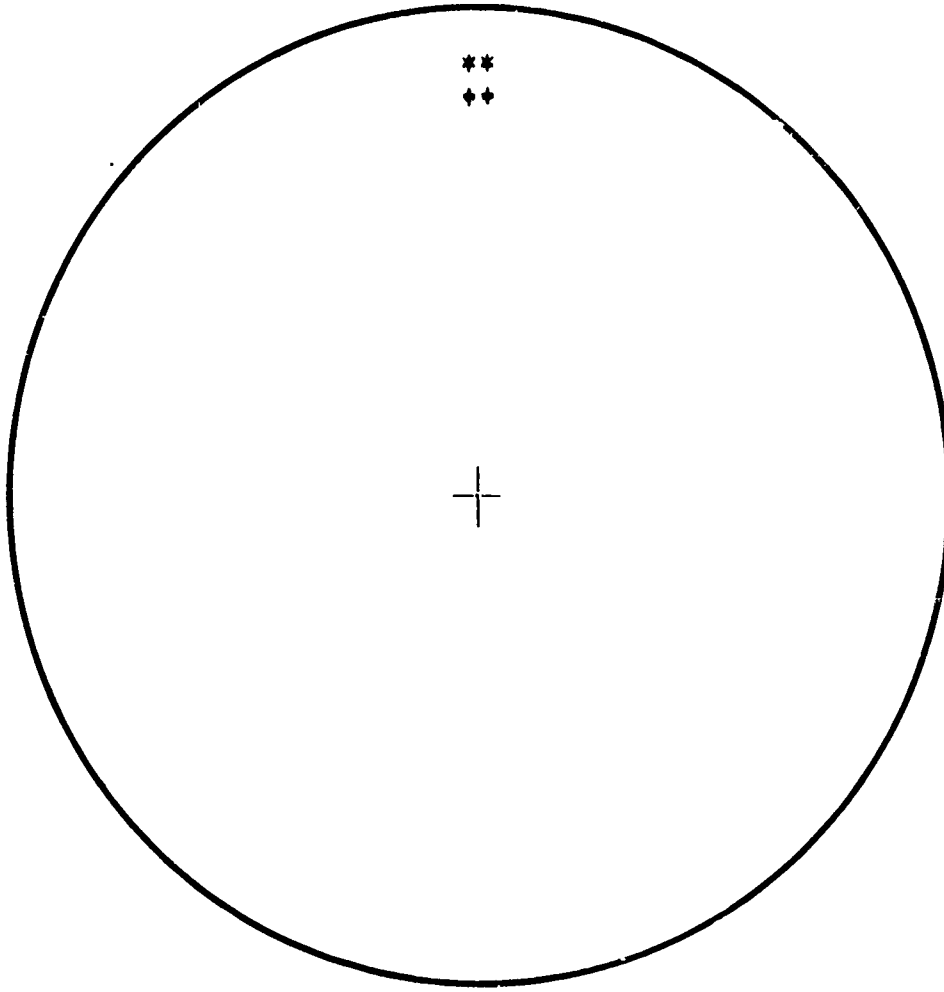


Figure 4.5 Blur Spot Diagram for a Point 0.7° Off Axis

UNCLASSIFIED

dimensionally and optically viable at 70°F. However, both dimensional and refractive index changes will occur over the above ambient temperature range. In addition, the position of the detector relative to the lens will change as a function of housing expansion and contraction. Consequently, it is necessary to tolerance the system for these changes. This was accomplished in two steps. Dimensional changes in the lens due to a temperature variation of +70°F (i.e., 70°F to 140°F) were introduced into the system. These consisted of the change in the lens thickness, the change in the inner and outer diameters and the change in curvature. The appropriate coefficient of thermal expansion is given in Table 4-1. In addition, the refractive index change corresponding to this temperature variation was also included as was the shift in detector position due to housing expansion. For the purpose of this calculation a thermal coefficient of expansion of $7 \times 10^{-5}/^{\circ}\text{C}$ was assumed for the housing material. This value is consistent with a housing material of polycarbonate plastic (cf. Table 4-1) or cyclopy KHP plastic. (The merits of each of these materials for the rangefinder mechanical components are discussed below.) The system was then evaluated for object points on-axis and 0.7° off-axis. As the second step the dimensional and optical changes in the above quantities were introduced for a temperature variation of -110°F (i.e., 70°F to -40°F) and the system evaluated in a similar fashion. Figures 4-6 and 4-7 contain blur spot diagrams for a point on-axis and 0.7° off-axis, respectively, for a temperature variation of -110°F. This temperature variation yielded the largest blur spot change of the two cases. As can be seen, there is a fairly significant defocussing of the incident radiation relative to the system at the design temperature (70°F). However, since the receiver is not an imaging system, it is only required that sufficient energy be deposited on the detector. Figure 4-7 indicates that this condition is still maintained even for the case of a transmitter-receiver field mismatch of $\pm 0.7^{\circ}$.

UNCLASSIFIED

Scale Factor = 50.0000

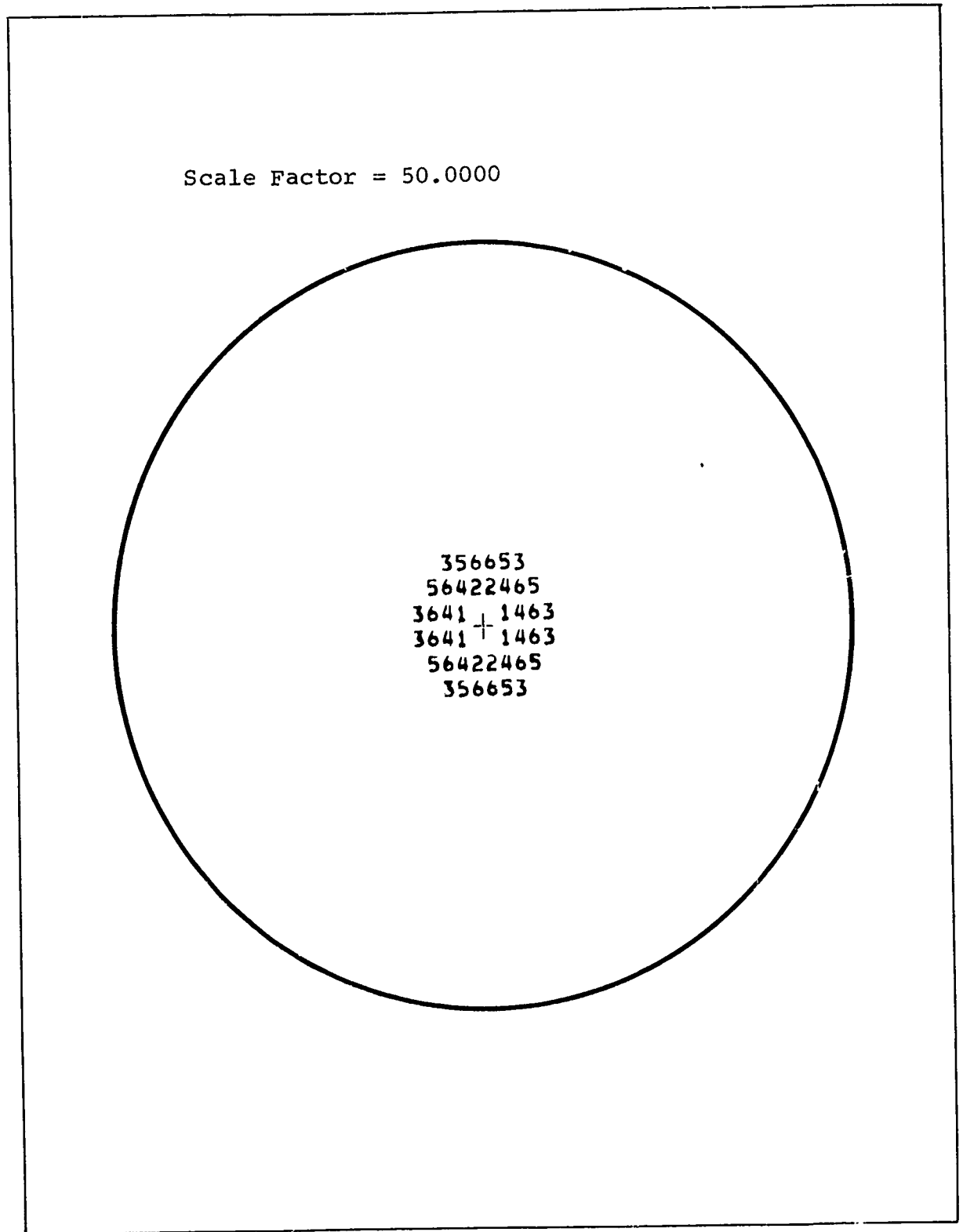


Figure 4.6 Blur Spot Diagram for On-Axis Point at -11°F

UNCLASSIFIED

Scale Factor = 50.0000

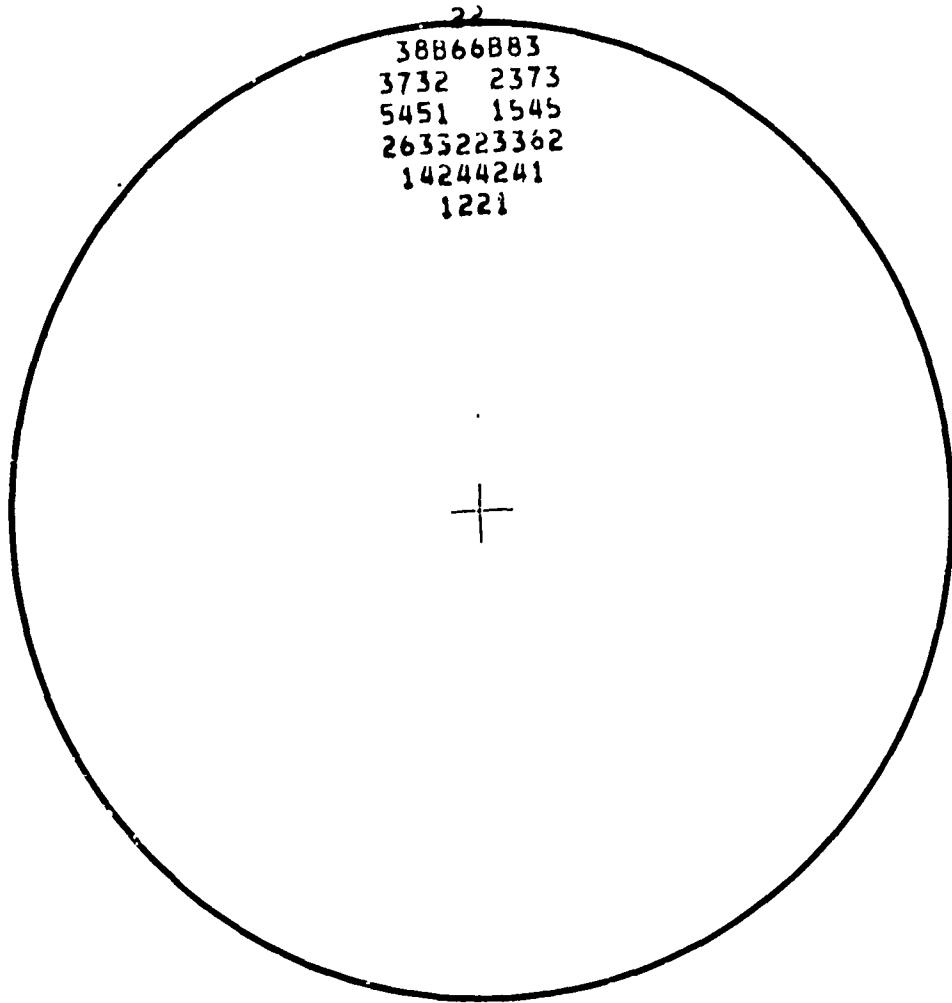


Figure 4.7 Blur Spot Diagram for a Point 0.7°
Off Axis at -110° F

UNCLASSIFIED

4.1.4 Transmitter Optics

The primary functions of the transmitter are to collect and collimate the radiation emitted by the laser diode to the extent necessary that adequate target irradiance is obtained. The degree of collimation is affected by the diode dimensions, lens focal length and lens aberrations. In general, the GaAs laser diodes employed do not operate in a single mode. This, in conjunction with diffraction effects at the junction, yields a divergent emitted beam. From typical manufacturers data, the angular extent of the emitted beam is such that about an F/1 system is needed for essentially complete collection of the radiation. However, the decrease in collection efficiency with increasing F-number is quite slow, at least up to F/1.40. Consequently, this represents an area wherein the use of transmitter optics which are slower than F/1 will provide attractive advantages while requiring only a small loss in collection efficiency.

The overall size of the transmitter unit is also of importance since the optical form factor is such that the transmitter obscures part of the receiver field. In view of this consideration, the transmitter clear aperture was set at a diameter of one inch.

For optimum performance, the transmitted beam should be confined to a total divergence of about 10 milliradians or less. This will yield adequate irradiance of typical targets at ranges to 500 meters. It is noteworthy however, that the demonstration rangefinder described in Section 2, exhibited good ranging capability with a transmitted beam divergence somewhat greater than 10 milliradians. Consequently, 10 milliradians need not represent a hard upper limit for this quantity. The maximum junction dimension of the laser used in the demonstration device is .016 inches. However, GaAs lasers of the required power are available with maximum junction dimensions of .009 inches.

UNCLASSIFIED

Column 2 of Table 4-3 gives the beam divergence, for various F-numbers, due to the size of the laser, with no contributions from aberrations. If a conventional singlet element is used to collimate the beam, further angular spread will result due to aberrations. These are given in columns 3 and 4 of Table 4-3 for spherical aberration and coma respectively. As can be seen the largest angular blur is due to spherical aberration. This precludes the use of a conventional singlet element as the transmitter lens. However, acrylic Fresnel lenses are available which are corrected for spherical aberration while maintaining compactness and lightweight. Such lenses, when employed as a collimator, can be used as fast as F/1 with essentially no deterioration in peripheral transmittance relative to slower configurations. The transmittance for an acrylic lens at 0.9 microns is in excess of 90%.

Table 4-3

F-Number	Divergence Due to Diode Size (mrad)	Spherical Angular Blur (mrad)	Coma Angular Blur (mrad)
1.00	+4.5	+34	+0.04
1.10	+4.1	+25	negligible
1.25	+3.6	+17	negligible
1.40	+3.2	+12	negligible

For the purpose of evaluation the effects of temperature variations on the collection efficiency and transmitted beam divergence a Fresnel lens can be treated as a thin lens with acceptable accuracy. The thin lens formula for a plano-convex lens is given by equation (4-1):

$$\frac{1}{F} = (N-1) \left(\frac{1}{R}\right) \quad (4-1)$$

where F is the focal length, N the index of refraction and R the radius of curvature of the convex side. Identifying R as the effective radius of curvature of the Fresnel lens, differentiating with respect to temperature, T, and rearranging yields

UNCLASSIFIED

$$\frac{1}{F} \frac{dF}{dT} = \frac{1}{R} \frac{dR}{dT} - \frac{1}{(N-1)} \frac{dN}{dT} \quad (4-2)$$

This defines the effective thermal coefficient of expansion for the focal length. The first term on the right of equation (4-2) is the thermal coefficient of expansion of the effective radius of curvature and dN/dT is the thermal change in refractive index. Both of these quantities are given in Table 4-1 for acrylic.

Equation (4-2) forms the basis for determining the thermal changes to be expected in collection efficiency and beam collimation for an acrylic Fresnel lens. The collection efficiency is directly dependent upon the F-number of the system. The variation in this quantity with temperature is given by:

$$\Delta (F/\#) = \frac{-(F/\#)}{(N-1)} (dN/dT) \Delta T \quad (4-3)$$

where equation (4-2) has been used and the coefficients of expansion of the lens diameter and effective radius of curvature have been assumed equal. Figure 4-8 contains a plot of the variation in F-numbers. As can be seen the slower the transmitter system, the greater the change with temperature. However, even for a F/1.40 system $\Delta F/\# \approx .015$ for $\Delta T = -110^\circ\text{F}$, which represents a small change in the collection efficiency of the system. Consequently, it can be concluded that thermal effects on the collection are small and the resulting loss in collected power is negligible even if a F/1.40 system is used.

Equation 4.2 can also be utilized in determining the effect of temperature on the transmitted beam collimation. As mentioned above, for a lens corrected for spherical aberration the collimation is most heavily influenced by the combination of F-number in conjunction with the laser size. Strictly speaking, this is only true at the design temperature. As the temperature is changed, the lens focal length will change according to equation

UNCLASSIFIED

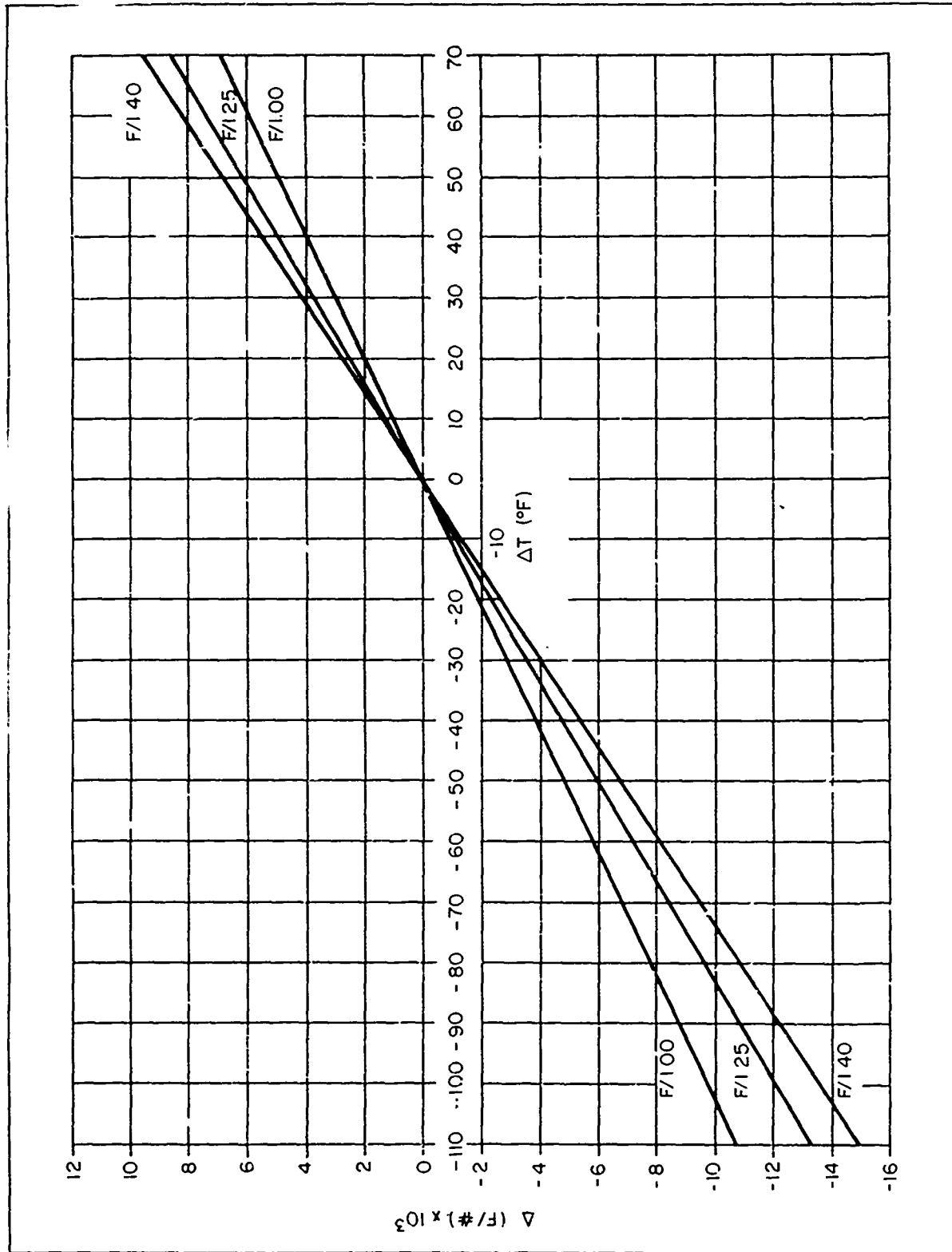


Figure 4.8 Change in Transmitter F-number with Temperature

UNCLASSIFIED

2 and the laser position will change due to dimensional changes in the transmitter housing. In general, the laser will not be situated in the focal plane and hence defocussing will occur increasing the angular divergence of the transmitted beam in the far field. With the assumption that a Fresnel lens is adequately described by thin lens formulae, this increase in divergence is given by:

$$\alpha = \pm \frac{D |s-F|}{2sF} \text{ radians} \quad (4-4)$$

where s is the laser position, F the focal length of the lens and D the diameter of the lens. The absolute value signs are used since only the divergence in the far field is considered. The quantity defined by equation (4-4) is added to the angular divergence given in column 2 of Table 4-3. Figure 4-9 contains a plot of this resultant beam divergence as a function of shift in temperature, ΔT , relative to 70°F^* . It is obvious from Figure 4-9 that a slower transmitter has advantages insofar as the thermally induced divergence is concerned. The dashed line in Figure 4-9 represents the beam divergence of the demonstration rangefinder described in Section 3. Thus, the beam divergence for an $F/1.25$ system can be maintained approximately as small as that of the demonstration rangefinder over most of the range of operational temperatures and the divergence of a $F/1.40$ system is less than that of the demonstration rangefinder over the full range of operational temperatures.

* A thermal coefficient of expansion for the housing material of $7 \times 10^{-5}/^\circ\text{C}$ was assumed for these calculations. This value is consistent with polycarbonate or cycloy KHP plastic as the housing material.

UNCLASSIFIED

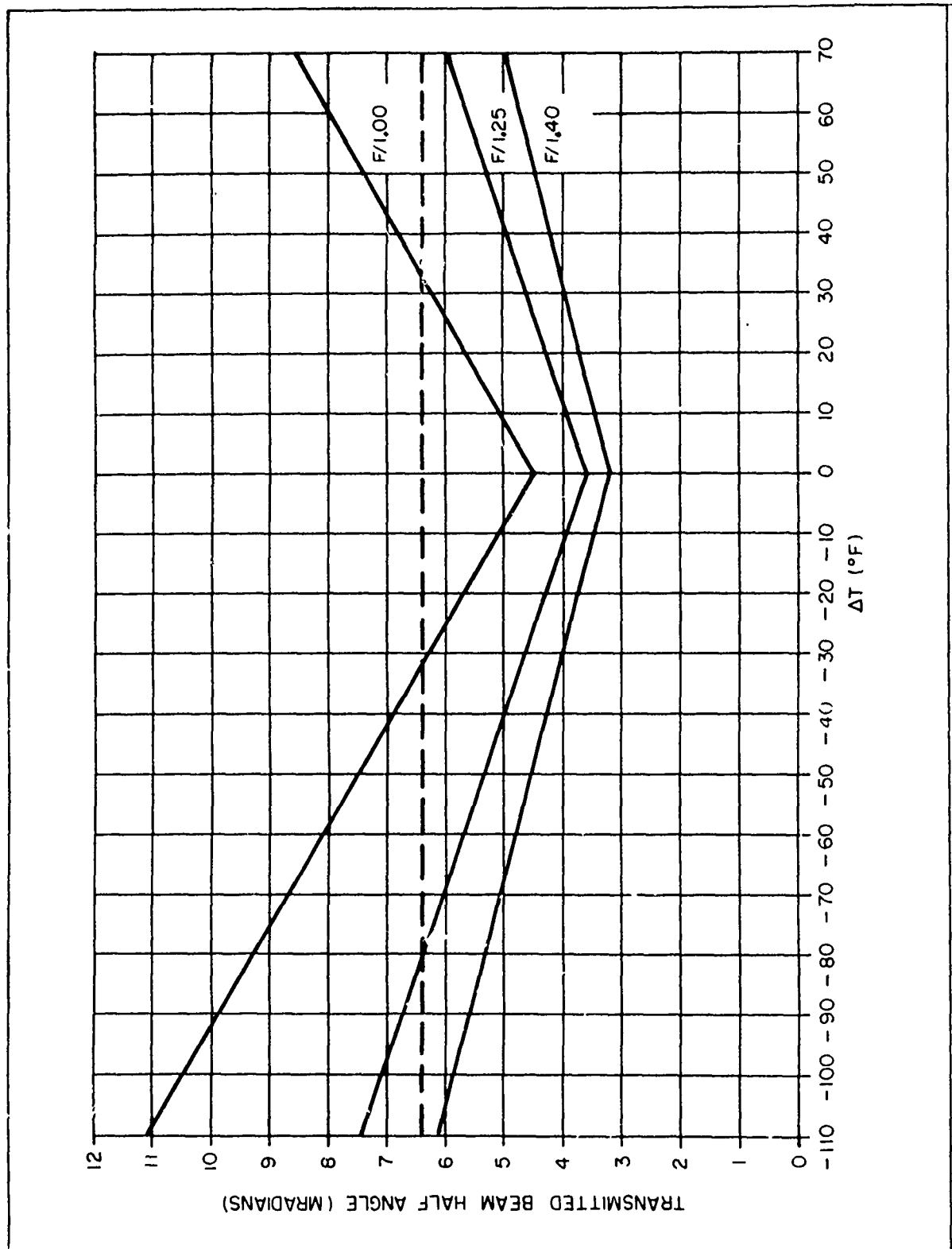


Figure 4.9 Transmitted Beam Divergence as a Function of Temperature Change

UNCLASSIFIED

4.1.5 Viewfinder Optics

Generally, the viewfinder must provide an erect image of the target as well as a means of accurately pointing the transmitted beam at the target. The field of view of the viewfinder must be larger than that of the transmitter. However, because of the relatively small divergence of the transmitted beam an accurate transmitter-viewfinder boresight must be maintained.

The viewfinder may or may not provide magnification. In the former case an erect image can be provided by a low power telescope mounted external to the rangefinder. Such a device provides a convenient means of utilizing a reticle for aiming purposes in conjunction with a relatively small size. If a unit power viewfinder is acceptable a further reduction in size is possible. A baseline design for such a viewfinder has been incorporated into a mock-model of the LAW Rangefinder. Basically it consists of a reticle, Fresnel lens and beamsplitter. The reticle is situated in the focal plane of the Fresnel lens and consists of a photographic transparency of the desired reticle pattern. When back illuminated the diverging light is collimated by the lens and projected onto the beam splitter. The beam splitter has a reflectivity of approximately fifty percent and hence, the collimated light is partially reflected toward the observer. The result is that the observer views the reticle pattern at infinity. Since the beamsplitter has a transmittance of approximately 0.25*, the target is simultaneously visible to the operator. Provision is made for boresighting the projected reticle pattern with the rangefinder transmitter by lateral movement of the reticle in the lens focal plane. Figure 4.10 contains an illustration of this viewfinder.

* Losses associated with thin film aluminum beam splitters can be quite high depending on transmittance, cf. Smith (1966).

UNCLASSIFIED

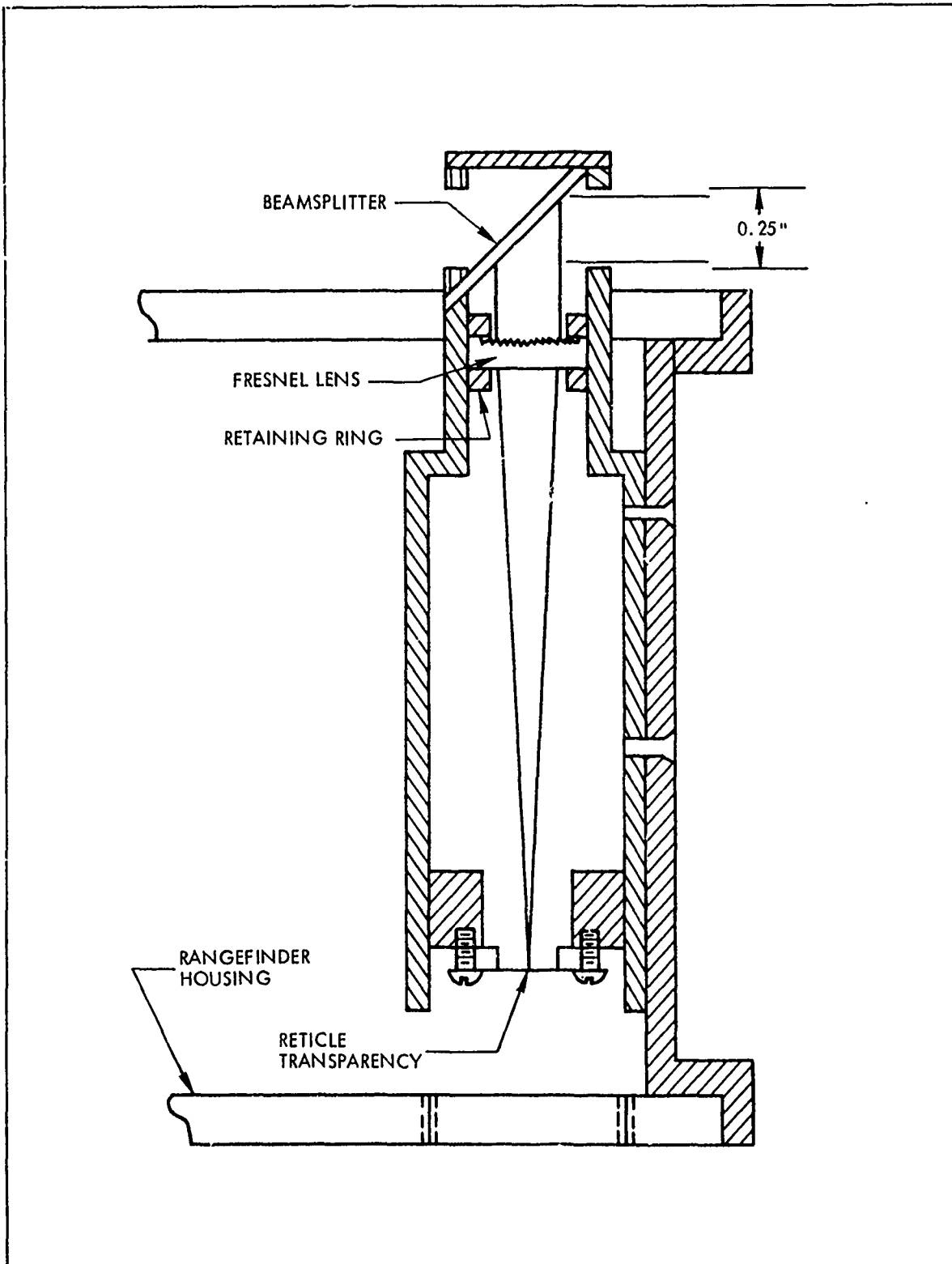


Figure 4.10 Unit Power Viewfinder

UNCLASSIFIED

Illumination of the reticle in the viewfinder shown in Figure 4.10 is provided by a tungsten lamp powered by a small battery. However, ambient light can be used via a fiber optic bundle. In principle the bundle can collect light from the focal plane of the receiver objective lens without interfering with the detector. This method is desirable for two reasons. First there is no additional protrusion from the rangefinder housing and secondly, since the ambient light is collected from the region of the target the necessary contrast is always insured. This arrangement is illustrated in Figure 4.12.

The transmitter-viewfinder boresight requirements are fairly stringent since the beam divergence for the transmitter can be as small as ± 3.2 mrad for a F/1.40 transmitter. Thus, the uncertainty in this boresight must be considerably less. Once an acceptable assembly boresight with the transmitter is attained at the design temperature, uniform heating or cooling of the rangefinder over the operational temperature range will not affect the alignment establishing the boresight. However, if the reticle is designed to indicate visually an angular diameter corresponding to the transmitted beam divergence, then defocusing will occur over the operational temperature range and this correspondence will not be maintained. This affect can be evaluated qualitatively by considering the viewfinder as a relatively slow collimator (F/8). From Figure 4.9 it can be established that the far field divergence for an acrylic collimator increases with decreasing F-number. Thus, the increase in the visual diameter of the projected reticle pattern will be less than that of the transmitter. The net result is that the transmitted beam will have a greater divergence than the visual indication provided by the viewfinder. As a consequence the operator is assured that a target within the visual diameter of the projected reticle is fully illuminated.

UNCLASSIFIED

A more important aspect of thermal defocusing in the viewfinder, however, is the possibility of a parallax error being introduced. This can occur even though the optical axes of the transmitter and viewfinder are mutually aligned since the viewfinder is characterized by a finite size aperture as opposed to an ideal pin hole. Thus, if the position of the virtual image, as seen by the operator, is not coincident with the position of the target, parallax may be present. The magnitude of the angular error, ϵ_p , introduced is given by:

$$\epsilon_p = \frac{D}{2} \left[\frac{s-F}{Fs} - \frac{1}{R} \right] \text{ radians} \quad (4-5)$$

where R is the range of the target, F is the focal length of the lens, S is the position of the reticle relative to the lens and D is the viewfinder aperture diameter. The quantities D, s, and F will vary with temperature as described previously. The resulting parallax error, ϵ_p , is plotted in Figure 4.11 as a function of $|\Delta T|$ relative to 70°F. For convenience, the effective range of the target is taken as infinity and the thermal coefficient of expansion governing the reticle position is taken as $7 \times 10^{-5}/^\circ\text{C}$, which is consistent with both polycarbonate or Cyclopedia KHP as the viewfinder housing material. From Figure 4.11, it is seen that for $|\Delta T| = 110^\circ\text{F}$ (corresponding to $T = -40^\circ\text{F}$) an aiming error of as much as 0.27 mrad is possible. Since the total error budget allowed for the superelevation uncertainty is ± 0.5 mrad, the superelevation setting mechanism must be such that this limit will not be exceeded with the contribution due to parallax included.

4.1.6 Superelevation Considerations

There are basically two methods whereby the correct superelevation of the LAW weapon may be obtained. These involve changing the relative angle between the rangefinder and the weapon, or alternatively maintaining a mutual boresight of the weapon and rangefinder and providing an elevation indicator in the viewfinder. In both approaches, the correct elevation would be set or indicated, respectively, simultaneously with the setting of the range gate. Thus, in the former method the cam or elevation screw providing the angular displacement of the rangefinder with respect to the weapon would be

UNCLASSIFIED

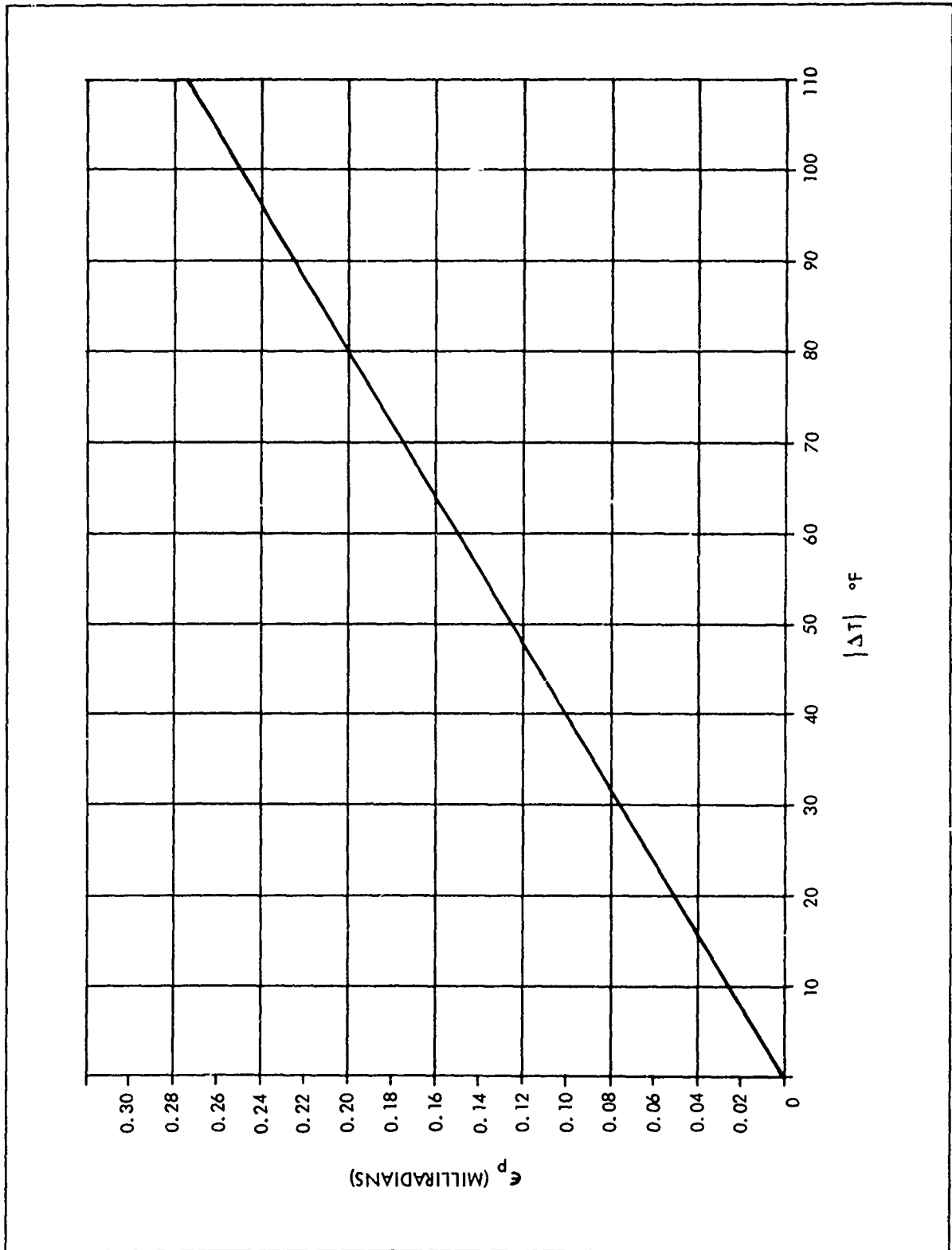


Figure 4.11 Parallax-Induced Angular Error as a Function of Change in Temperature

UNCLASSIFIED

mechanically linked to the range gate potentiometer. Hence, changing the position of the range gate would automatically change the relative angular orientation of the rangefinder and weapon. The appropriate change would be built into the mechanism and be dependent upon the type of round being used in the weapon.

The choice of method employed is heavily dependent upon the application. For the LAW weapon it was decided to use a relative angular displacement of the weapon and rangefinder for the demonstration of the superelevation mechanism. The main reason for this choice was the simplicity of the method, which was largely due to the position of the firing mechanism on the weapon. This is illustrated in Figure 4. 12. With the rangefinder mounted over the firing mechanism, the viewfinder is in a convenient place for the operator and in addition, only one hand is required to operate both the weapon trigger and the elevation thumbwheel. The thumbwheel is attached to an elevation screw which changes the relative angular orientation of the rangefinder and weapon. Thus, if the operator maintains the target centered in the viewfinder the weapon will be at the correct elevation. This method also has the advantage that the rangefinder need not be removed from the target at any time up to and including firing.

Tension was maintained on the thumbwheel by means of a piece of spring steel as indicated in Figure 4. 12. The elevation screw was supported by means of a tapped screw hole in the rear support. The threading of the elevation screw was chosen to yield a one-degree relative angular displacement per revolution for the four inch baseline which is also indicated in Figure 4. 12.

Any backlash in the screw mechanism will constitute the major source of error in the device, since a rotation of the elevation screw will move the range gate, yet not change the elevation until the backlash is taken out. This becomes more important if the combination of range potentiometer and elevation screw is such that a complete search of the range (and thus all superelevation angles) can be accomplished in one revolution of the thumbwheel. For the mock model superelevation device, backlash corresponding to approximately a 10.3 degree rotation of the thumbwheel will introduce an error of 0.5 mrad in the superelevation. This, however, represents the

UNCLASSIFIED

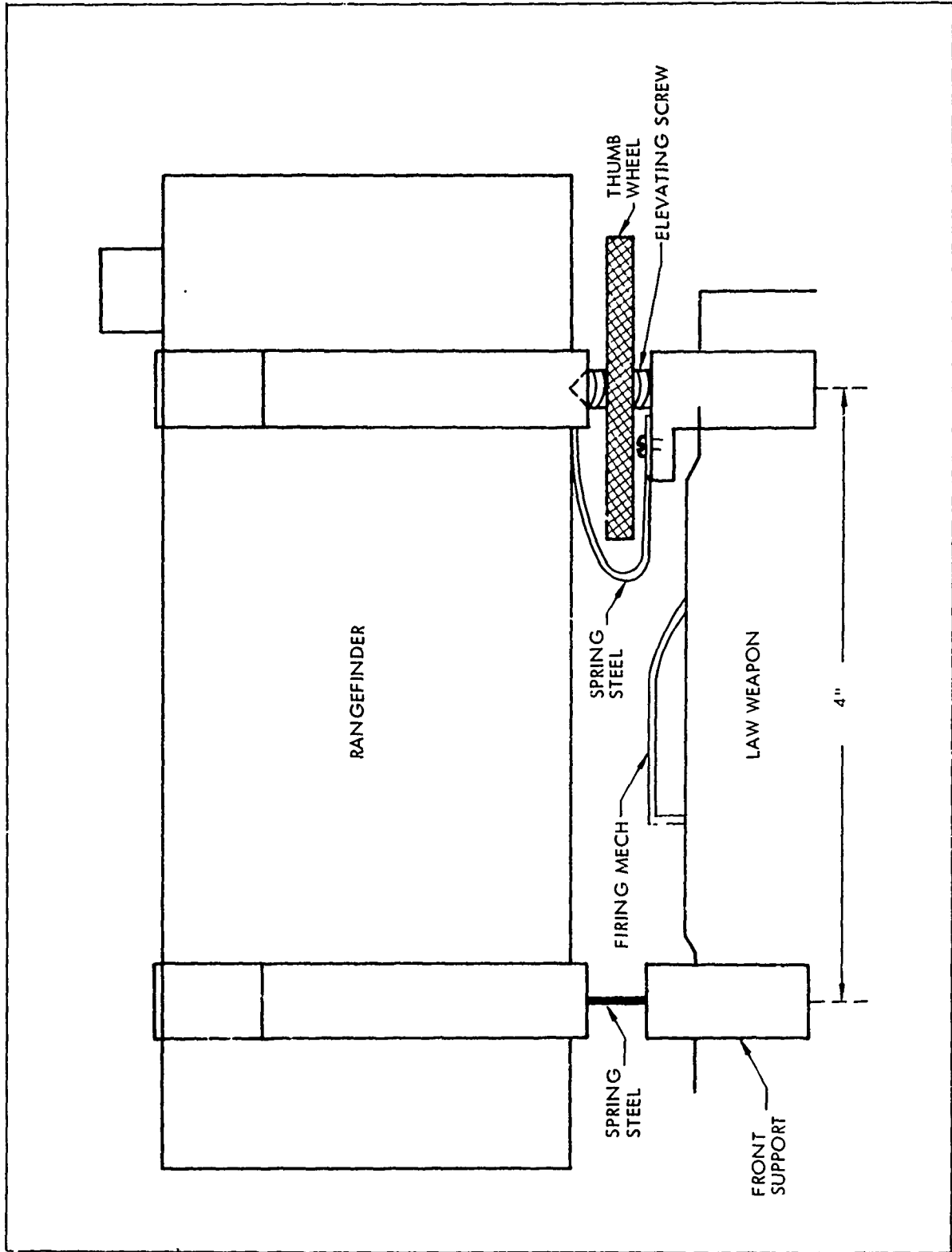


Figure 4.12 Superelevation Mechanism for LAW Weapon

UNCLASSIFIED

entire error budget. Since a viewfinder parallax error of as much as ± 0.27 mrad can exist at the low extreme of the operating temperature range, the backlash tolerable in the superelevation mechanism must be less. Requiring that the root of the sum of the squares of the uncertainties introduced by backlash and parallax be at most 0.5 mrad, yields an allowable backlash corresponding to a revolution of the thumbwheel of 8.5 degrees.

An alternative method of providing superelevation information involves providing an indicator in the focal plane of the viewfinder and the means of slaving the movement of the indicator to that of the range gate potentiometer. Such an indicator may take the form of a transparent tape with small sections of a contrasting color which would act as fiducial lines. The displacement of these lines from the center of the reticle would serve to define a new reticle center, which when placed on the target would automatically require that the weapon be at the correct elevation angle. In general the mechanism required for the implementation of this approach is more complicated than that fabricated for the LAW weapon. In addition, this method required that the weapon elevation be set at the time of firing and is such that no further range updates are possible since the rangefinder has been removed from the target.

4.2 Mechanical Considerations

The optical form factor and characteristics of the transmitter and receiver, as described in Section 4.1, establish the mechanical requirements of the system. Basically these requirements fall into two categories; materials choice and fabrication techniques. Each of these areas is discussed below.

4.2.1 Structural Materials

Initially polycarbonate plastic was chosen as the baseline material for the structural parts of the lightweight rangefinder. The reasons were primarily the low weight and very high impact strength. In addition, polycarbonate retains a high impact strength at low temperatures and is well matched, thermally, to the optical elements. The properties of polycarbonate also lend themselves well to molding applications, ultrasonic staking techniques, and the material is readily bonded using solvents, urethane

UNCLASSIFIED

adhesives or epoxies. However, the temperatures and pressures required for injection molding polycarbonate are relatively high, which, depending on the complexity of the piece being molded, may reflect in higher mold costs. Also the cost of the material is somewhat higher than other plastics available. Consequently, alternative materials have been examined which potentially would allow a lower parts cost while retaining, as far as possible, the desirable physical properties of polycarbonate. This then represents an area where desirable tradeoffs may be possible.

Two additional plastics have been considered. These are polyphenylene oxide copolymer and an alloy of polycarbonate and acrylonitrile-butadiene-styrene (ABS) copolymers. The trade names and manufacturers of these materials are respectively Noryl (General Electric Corp.) and Cycloy KHP (Mabon Division, Borg-Warner).

Cycloy KHP is characterized by physical properties which are similar, in many instances, to those of polycarbonate. The specific gravity and coefficient of thermal expansion are essentially the same for the two materials. Cycloy KHP has a high impact strength (although not as great as polycarbonate) and is well suited for injection molding, ultrasonic staking and bonding. In addition, Cycloy KHP molds at relatively modest temperatures and pressures and is somewhat less expensive compared to polycarbonate. For estimation purposes, material costs are generally specified as 3.5 cents per molded cubic inch for polycarbonate and approximately two cents per molded cubic inch for Cycloy KHP. Hence, the use of this material represents a potential cost reduction, but at the price of the reduced impact strength. This may become important at the low end of the operational temperature range. For example, at -40°F the impact strength of Cycloy KHP is given as 1.5 ft-lbs/in. (notch), whereas for polycarbonate the value is 2.5 ft-lbs/in. (notch). Both of these materials, however, are still characterized by a relatively high impact strength even at the low extreme of the temperature range.

The second material considered as a possible alternative to polycarbonate is Noryl. Although a high impact strength plastic, it is lower in this category than both polycarbonate and Cycloy KHP. In addition, the cost is somewhat greater than Cycloy KHP, although less than polycarbonate.

UNCLASSIFIED

Thus, Noryl would seem to be an inferior alternative to polycarbonate compared to Cyclopy KHP, and is included here only for the purpose of comparison.

The pertinent physical properties of polycarbonate have been included in Table 4. 1. Table 4. 4 lists some important physical properties of both Cyclopy KHP and Noryl.

TABLE 4. 4 PHYSICAL PROPERTIES OF CYCOLOY KHP AND NORYL

	<u>Cyclopy KHP</u>	<u>Noryl</u>
Specific Gravity	1.2	1.06
Deflection Temperature 264 psi	220°F	265°F
Coefficient of Thermal Expansion in./in./°F x 10 ⁵	3.7	3.3
Impact Strength (ft lbs/in) notch	10.5 (73°F)	5.0
Flammability	SE-1*	SE-1*
Water Absorption 24 hrs, 73°F	.24%	.066%
Mold Shrinkage (in/in)	.005 - .007	.005 - .007
Dielectric Strength V/mil	456	500

* self extinguishing - non dripping

UNCLASSIFIED

4.2.2 Fabrication Techniques

The optimum fabrication techniques, under constraints of cost, are heavily dependent upon considerations such as ability to dismantle an assembled rangefinder or to perform optical realignments after assembly. These considerations are in turn dependent upon whether the device is to be reused many times or have a limited service life. If the ability to dismantle the device after assembly is considered necessary, then many of the component mechanical parts will need to be threaded. Because of the good molding properties of Lexan and Cycloxy it is possible to produce relatively fine threaded parts of good quality. Also, where the design permits, cylindrical parts can often be produced from rod or tubing stock in an automatic-screw machine facility with a comparatively low cost in tooling and set-up time. Because the use of precision molded parts involve far fewer finishing operations compared to the use of metal for the same part, considerable advantages from the point of view of cost and weight are presented. For example, large scale production of a plastic version of the demonstration rangefinder discussed in Section 3, would provide a device lighter in weight than the metal version, and also of lower unit cost. The unit cost would be further reduced with minimum mechanical redesign which would retain the dismantling ability while reducing the overall parts number and making the remaining components design more amenable to molding.

A significant cost reduction for the rangefinder assembly can be attained by a mechanical redesign aimed at the elimination of all possible screw threads, and the combination of as many sub-assemblies of parts into one-piece functional units as possible. The economics of injection molding requires a high initial cost for tooling which results in a small unit cost only if a sufficient number of parts are produced. The desirability of eliminating the need for threaded parts becomes apparent when

UNCLASSIFIED

it is realized that tooling for threaded sections may result in an order of magnitude increase in cost relative to tooling for equivalent non-threaded parts. Figure 4.13 is a sketch of a rangefinder which is quite similar to the demonstration device in form factor but which contains significantly fewer mechanical parts and in which threaded sections have been eliminated. In this approach, the outer housing shell of the device will be extruded in one piece. The receiver lens, after insertion, can be attached either by bonding with a silicone adhesive-sealant or held in place by a rim section of plastic which is spin welded in place. Both approaches serve to hermetically seal the device at this end. Behind the receiver lens is a one piece molded light baffle assembly which after insertion is held in place by stakes ultrasonically inserted from the outside of the housing. The mechanical properties of the plastics are such that this method of attachment is attractive.

The transmitter housing would consist of two molded sections which are ultrasonically staked together in assembly after the laser-adjust ball is inserted between them. This would then leave the ball free to move for alignment purposes, but permanently captured in the transmitter housing. The laser would be inserted in the rear section of the ball and be attached by means of ultrasonically staked tabs. After alignment of the laser and the Fresnel lens, the laser-adjust ball itself will then be ultrasonically staked in the correct position.

As mentioned earlier, the receiver lens would act as the support spider for the transmitter housing. The method of attachment consists of bonding the transmitter housing in annular groove molded into the receiver lens using a silicone adhesive-sealant.

UNCLASSIFIED

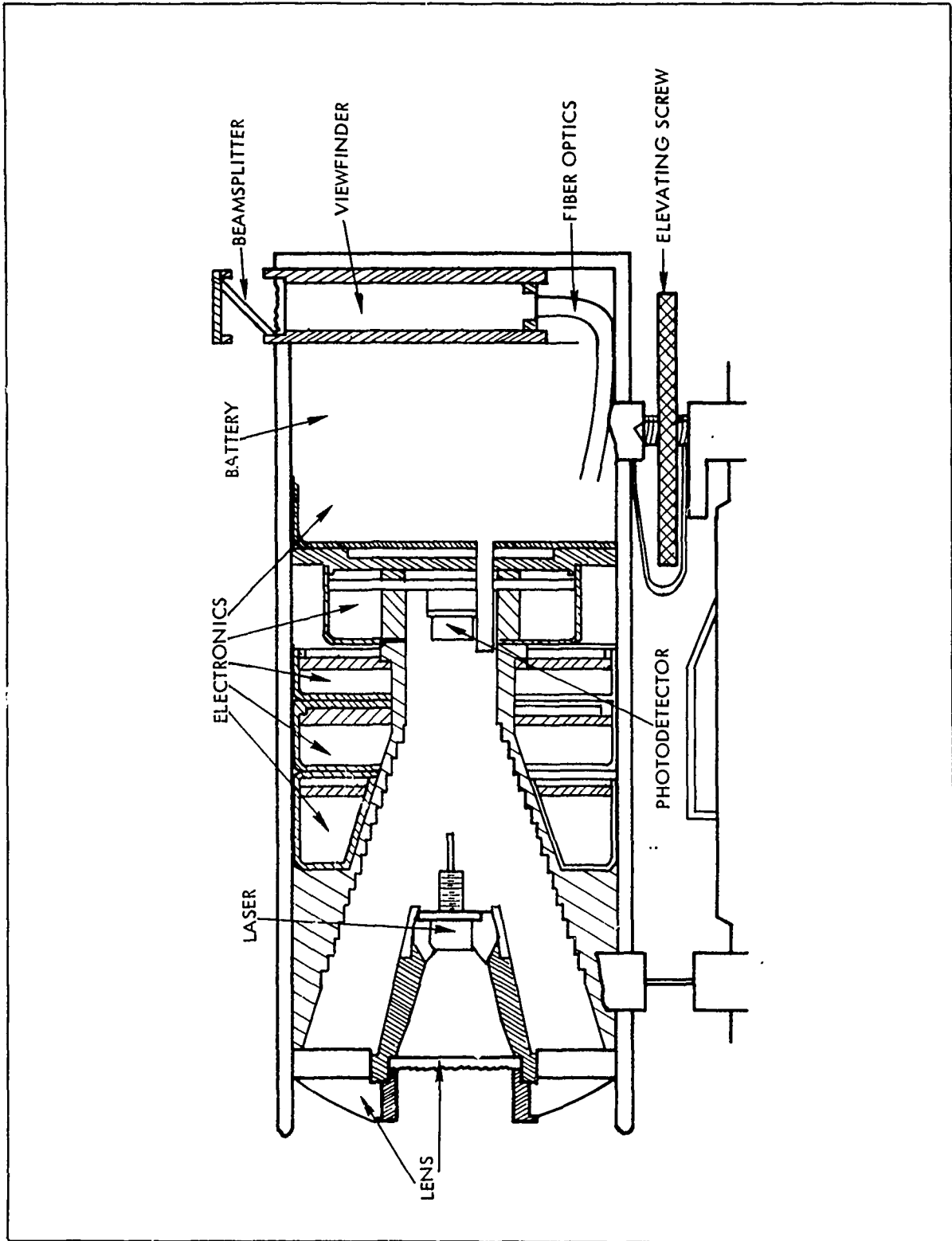


Figure 4. 13 Rangefinder with Unit Power Viewfinder and Superelevation Mechanism

UNCLASSIFIED

Where shielding of the electronics is necessary, the appropriate circuit boards would be contained in molded cans of a diameter equal to the inside diameter of the housing. These will then be held in place by ultrasonic staking through the housing. These parts will be metallized or plated to provide the required electromagnetic shielding.

For the purpose of comparison, Table 4.5 contains a summary of parameters and approximate values common to three types of rangefinders. These types are categorized as: 1) a reuseable rangefinder employing glass optics and metal structural parts, 2) a reuseable rangefinder constructed of plastic optical and structural components, and 3) a rangefinder designed for a limited service life, constructed of plastic and designed to minimize the number of component structural parts. For simplicity, all are considered to be of a general form factor similar to that of the demonstration rangefinder and have the same ranging capability.

Since the receiver is not an imaging device it is only necessary that reflected radiation be collected and directed onto the detector. Hence, if glass optical components are desired, pressed glass lenses should be adequate and thus provide considerable cost savings compared to ground and polished glass lenses. Alternatively, plastic lenses offer a significant weight savings as indicated in Table 4.5, although costs relative to pressed glass lenses should be comparable. The optics necessary for adequate ranging performance are the same for both the plastic reuseable and limited service rangefinders.

The use of plastic for the structural components of the rangefinder represents a weight reduction of over 50 percent for these components when the two reuseable types of rangefinders are compared. A further reduction is possible when the limited service life version is considered. This is mainly due to a structural redesign aimed at both weight and parts number reductions. Approximate values are given in Table 4.5.

A significant contribution to the overall weight of the rangefinder is made by the battery pack required. The battery weight listed in the first column of Table 4.5 is that of the particular pack used in the demonstration device. For a limited service device, this could be reduced considerably, if a thermal battery is acceptable. For the purpose of comparison, the

UNCLASSIFIED

TABLE 4.5 COMPARISON CHART FOR THREE POSSIBLE RANGEFINDERS

Rangefinder Parameter Type		Reuseable-Conventional Materials	Lightweight Reuseable	Lightweight-Limited Service
Optics	Lens Type	Receiver: Plano-Convex Singlet Transmitter: Positive Singlet	Receiver: Plano-Aspheric Singlet Transmitter: Fresnel Singlet	Receiver: Plano-Aspheric Singlet Transmitter: Fresnel Singlet
	Lens Material	SF1 Glass	Acrylic	Acrylic
	Filter Type	Wratten 87C	Wratten 87C	Wratten 87C
	Lens Fabrication	Pressed Glass	Precision Molding	Precision Molding
	Lens Weight	Receiver: 4.3 oz Transmitter: 0.4 oz	Receiver: 2 oz Transmitter: 0.15 oz	Receiver: 2 oz Transmitter: 0.15 oz
	Lens Cost per 100,000 Units Including Filter	\$3.50	\$3.50	\$3.50
Structural	Structural Material	Aluminum; Some Machining Required. Some Parts Can be Cast Aluminum	Injection Molded Lexan, or Cycloy KHP	Injection Molded and Extruded Lexan or Cycloy KHP
	Structural Assembly Method	Many Parts Threaded. Tapped Screwholes and Screws Required.	Many Parts Molded with Threads. Bonding where Possible.	Spin Welding, Ultrasonic Staking and Bonding.
	Structural Parts-Weight	17.6 oz	7.8 oz	6.5 oz
	Structural Parts-Cost per 100,000 Units	\$8.00	\$5.00	\$3.65
Electronics	Battery Weight	7.4 oz	7.4 oz	3.5 oz
	Electronics Weight	0.67 oz Average per Printed Circuit Board	0.67 oz Average per Printed Circuit Board	0.67 oz Average per Printed Circuit Board
	Electronics Assembly	Printed Circuit; Discrete Components	Printed Circuit; Discrete Components	Printed Circuit; Discrete Components
	Electronics Cost per 100,000 Units	\$21.00	\$21.00	\$21.00

UNCLASSIFIED

battery weight listed in Column 3 of Table 4.5 is that of a thermal battery suitable for this application.

In comparing the reuseable and limited service plastic range-finders, it is seen from Table 4.5 that components which allow the greatest weight reduction of the latter are primarily the battery pack and secondly the reduced parts number. These are also the items which yield a somewhat lower cost for the limited service device.

The values given in Table 4.5 indicate trends only since these values depend heavily upon specific details. Consequently, weights and costs indicated are approximate.

4.3 Electronics Packaging Considerations

The electronics for the demonstration laser rangefinder described in Section 3 have been packaged using conventional printed circuit board and prepackaged discrete component construction with the components soldered in place using 60-40 lead-tin solder. The choice of this technique was arrived at after careful consideration of several parameters - packaging density requirements, size, electrical performance, reliability, and cost. The alternative to this choice was a hybrid approach using a ceramic substrate with the conductive and resistive network screen printed and fired to the ceramic and with micro-electronic components attached by soldering or thermocompression bonding.

The first of the factors considered was that of size constraint; the amount of available space for the electronics package. This, in turn, determines the component density needed to package the function; density being defined as the number of components per square inch of board area. The normal layout criteria for construction with a printed circuit board fabrication technique is 8-10 components per square inch. When the volume constraints are such that the area available for the electronics package require a density greater than 8-10 components per square inch, a trade-off between costs and an alternative technique must be considered.

UNCLASSIFIED

The thick film hybrid approach, for example, allows for a much greater packaging density - normally, 25 or more components per square inch. The higher packaging density stems from the ability of a hybrid to attach a semiconductor chip or beam leaded device directly to the ceramic substrate instead of the use of a prepackaged device such as a flatpack. A beam leaded device for example consumes 0.0025 square inches of substrate area while a flatpack consumes 0.1100 square inches; a 20 to 1 advantage. If a flatpack is used on a hybrid, the area under the package can still contain screened-on resistors reducing the area loss by use of a prepackaged device. In either case the hybrid allows more components per square inch. Further, the hybrid can utilize passive chip components, which are physically smaller and require less packaging area. The printed circuit board cannot use these components because of board flexing and differences in the coefficients of expansion. However, the use of smaller, microelectronic components carry with them an approximate 30-40% premium in cost. This can have a net affect of increasing the total electronics cost by a factor of approximately 25%. Therefore, the importance of a careful review of the size, weight, and volume requirements is critical if one is to achieve the optimum packaging/cost relationship. In the case of the laser rangefinder, it was determined that adequate volume was available for a printed circuit, discrete component approach and that the density requirement did not justify the use of a hybrid thick film approach.

The second area for consideration was that of required circuit performance. In applications for high frequency circuitry where line lengths, shielding, and grounding parameters are critical, the hybrid approach is necessary for improvement in circuit performance. This factor is not a problem in the electronics package for the laser rangefinder and consequently does not influence the choice of packaging scheme.

UNCLASSIFIED

Similarly, reliability requirements can be met by either technique. The increased reliability attainable by use of a thick film hybrid approach through elimination and reduction in the number of soldered connections is not warranted and would not justify the increase in cost.

In summary, the printed circuit approach for this application, best fits the overall objectives of this system. It meets the size, density, reliability, and performance needs while minimizing the electronics cost.

4.4 Cost Considerations

Based on current cost data obtained from vendors for similar systems a production model cost estimate for quantity production cost was determined. The costs indicated here are current and do not reflect any state of art or learning curve adjustments which will certainly result in cost reductions in the production of GaAs lasers, integrated circuits and silicon diodes which are major cost items of this system. However, no adjustment for inflation effects which would also occur between the present and production at some later time has been made. These two factors tend to offset each other. Therefore, the cost indicated could be considered valid over the next few years. The following reflects the expected costs for a production quantity of 100,000 units of a limited service life rangefinder.

Considering that all plastic structural components as discussed previously will be used, estimates are for some 20 components including outside housing, transmitter structure, receiver cone, electronic housings, viewfinder housing, and fittings, etc. The total cost for structural components per unit is \$3.65.

The optical elements, including the receiver, transmitter, and viewfinder lenses, beam splitter filters and fiber optics, are estimated at \$3.50.

UNCLASSIFIED

The standard electronic components, considered as a group, including all resistors, capacitors, P.C. boards, wiring, etc., are priced at \$9.00 per unit.

The special electronic components which include the preamplifier and postamplifier I.C.'s, logic I.C.'s, transformer, SCR, etc., result in a cost of \$4.00 per unit.

The current price quoted for GaAs laser of the power required is \$8.75. However, in consideration of having a real contract for 100,000 in hand and consideration of the expected increase in usage in the near future, a more realistic price for this application at production time is projected at \$5.00.

Assuming the same approach for silicon photodiodes, which are currently priced at the order of \$6.00, a more realistic cost of \$3.00 per unit appears appropriate.

Consideration of the present production techniques available at Raytheon production facilities resulted in a cost for assembly per unit, for a 100,000 total buy, of \$25.85 and recurring and non-recurring cost of \$4.80 per unit.

These costs are summarized in Table 4.6. With the addition of \$14.70 to cover general administrative cost and fee the total sale price, per unit, for a 100,000 buy is estimated at \$73.50. In consideration of the many elements involved in arriving at such a cost at this time in the development, one should consider the result only to arrive at the order of magnitude of the cost expected. Realistically one can conclude that the unit cost, in large production quantities, would be between \$60.00 to \$100.00.

UNCLASSIFIED

TABLE 4.6 PRODUCTION COST BREAKDOWN FOR A LIMITED SERVICE RANGEFINDER

Material

1. Plastic Structural Components	3.65
2. Optical Elements	3.50
3. Standard Electronics Components Resistors, Capacitors, P. C. Boards, etc.	9.00
4. Laser, GaAs	5.00
5. Photo Diode	3.00
6. Special Electronic Components, I.C.'s Transformers, etc.	4.00
	<hr/>
Total Material	28.15
Assembly Labor	25.85
Recurring Support	1.45
Non-Recurring Support	3.35
G&A and Fee	<u>14.70</u>
TOTAL ESTIMATED SALES PRICE PER UNIT	\$73.50

4.5 Reliability Analysis

A preliminary reliability study was made on the advanced model of the LAW Laser Rangefinder. This was done to establish the baseline reliability characteristics of the design. A production model can be expected to achieve this reliability as the project develops. The final achievement of a low cost, reliable rangefinder depends on design simplification and exploitation of the operational characteristics of the devices in the use environment.

The laser rangefinder is designed for minimum maintenance loading. The preliminary reliability estimate is 940 accumulated hours of operation before a corrective maintenance action is required. Rechargeable batteries can be expected to be replaced periodically, estimated 12 to 15 months.

UNCLASSIFIED

Since rechargeable nickel cadmium batteries are used, an external plug will be provided so that recharging can be accomplished without requiring disassembly. Scheduled recharging of the batteries should avoid a trickle charge since this promotes oxide buildup between the cells, degrading battery life.

The lasing device, a Gallium Arsenide Stacked Diode Laser, is the gating item of the system's reliability. The estimated MTBF of this unit is 2,000 hours. The usual mode of failure of this unit results in degradation of output optical power. Calibration procedures can determine when unacceptable output levels have occurred.

A summary of the reliability prediction is tabulated below in Table 4.7. The right-hand column devotes the reference figure numbers in the text used for the analysis.

TABLE 4.7 RELIABILITY PREDICTION OF LAW LASER RANGEFINDER

Item	MTBF (hrs)	Reference
Receiver	5,350	Figures 3.3 and 3.4
Logic	6,750	Figures 3.7 and 3.24
Pulse Modulator, Transmitter	1,660	Figures 3.10, 3.11, 3.12 and 3.13
Power Supply	8,000	Figure 3.15
Total	940	

The prediction was made utilizing the prediction techniques and data found in RADC Reliability Handbook, Volume II (TR-67-108). The conditions used for this study are:

- MIL-STD quality grade parts were assumed
- The use environment will be that designated by the RADC Handbook as ground portable. This assumes:
 - Vibration - 2-60 Hz at 2-15g
 - Noise - 40-100 dB
 - Pressure - 30-15 Hg

UNCLASSIFIED

- Relative Humidity - 5-100 Percent
- Shock - 15-90g at 11 msec; 1500g at 0.5 msec
- The ambient temperature is 35°C
- No degradation in optics is expected throughout the usual life of the rangefinder

UNCLASSIFIED

5. HAZARD LEVEL DOCUMENTATION

This section contains a consideration of potential hazards represented by the LAW Demonstration Rangefinder to both operating personnel and personnel in the vicinity of the device. The specific potential hazards examined are eye hazards and electrical shock hazards. With proper use of the device it is believed that a low hazard level is presented in both of these areas, and particularly in the latter area. However, circumstances can be envisioned wherein an individual may conceivably suffer injury from the device. It is the purpose of this section to point out these circumstances and to suggest possible preventative measures. Generally speaking, injury thresholds have been obtained from the current literature. In cases where data are not available for a particular set of circumstances, or the hazard level represented by a particular situation is not well defined (e.g., semi-diffuse object at close range within the transmitter field), the suggested preventative measures have tended to be conservative with hopefully a large safety factor included.

5.1 Eye Hazard Documentation

The use of GaAs lasers in military and commercial applications is increasingly more common. Many of these applications require a highly collimated beam coupled with both high PRF and power. As such, they represent a potential hazard to unaware personnel in the vicinity of these devices. An evaluation of these potential hazards is necessary for at least two reasons. Primarily, operational guidelines must be established to prevent chorioretinal injury due to accidental exposure. Secondly, realistic damage thresholds are needed so that the use of these devices is not unnecessarily curtailed because of an overestimation of the hazards.

UNCLASSIFIED

There have been difficulties encountered in establishing realistic permissible exposures. In many cases, the necessary biological data have been lacking. In addition, by the very nature of injury thresholds they must be universally applicable. However, there are wide variations in the tolerances exhibited by individuals which forces estimates of permissible exposure levels to be conservative. This represents an area of current research and permissible exposure levels are being reappraised in the light of more recent data. The safety standards proposed by the American National Standards Institute, committee Z-136 (1972) (ANSI Z-136) have received much attention in the recent past. These represent significant increases in the maximum permissible exposure levels for certain cases, relative to many earlier standards.

Two aspects of the problem will be considered. First, eye damage mechanisms will be briefly reviewed with an emphasis on phenomena peculiar to near infrared wavelengths. Secondly, corneal and/or retinal irradiance levels are estimated for several situations likely to be encountered in the use of a laser rangefinder and compared to the appropriate permissible exposure values obtained from the literature.

5.1.1 Eye Damage Mechanisms

The most common damage mechanism in the eye due to near infrared radiation is thermal in nature. Thus, the parameters of interest in this process are tissue absorption as a function of wavelength, tissue heat conduction and dissipation, incident power and exposure times.

Radiation entering the eye and incident upon the retina has been transmitted in succession through the cornea aqueous humor, crystalline lens and vitreous humor. In order to lend perspective to the retinal damage problem, the damage mechanism in each of these regions is briefly considered below.

UNCLASSIFIED

Although the cornea is still quite transparent in the region from 0.75 to 1.3 microns, Michaelson (1972) cites studies wherein minimum regressive corneal damage was brought about by a dose of $7.6 \text{ watt sec/cm}^2$ for wavelengths between 0.88 and 1.1 microns. At longer wavelengths the same response was produced by a smaller dose consistent with increased corneal absorption in that wavelength region.

The iris is highly pigmented and characterized by a high absorptance in the near infrared. Because of decreased efficiency of heat dissipation in the iris it is more susceptible to damage than the cornea on an absolute basis. However, because of absorption in the cornea and aqueous humor the corneal dose required to cause damage in the iris is greater than that necessary to produce corneal damage.

The lens of the eye is suspended behind the iris and is somewhat isolated from blood vessels which could assist in heat dissipation. Although the lens is quite transparent in the near infrared, there is evidence to suggest that cataract development in the lens is associated with temperature increases due to absorption by the iris.

Generally speaking, damage thresholds in each of the regions mentioned above are significantly higher than thresholds associated with retinal damage. In addition, radiated power levels of the rangefinder are such that retinal damage represents the major eye hazard. Consequently, only damage mechanisms in this region of the eye will be considered.

Significant absorption of near infrared radiation occurs in the retina. A small fraction of radiation is absorbed in the rods and cones with the majority absorbed in the pigment epithelium and choroid. The former is a thin layer containing a high concentration of melanin granules of approximately 10 microns thick. Because of the high absorptance of the melanin granules the greatest temperature rise is experienced here.

UNCLASSIFIED

In addition, there exist damage mechanisms other than thermal which can occur at the retina. For q-switched laser pulses the rapid absorption of energy and resultant rapid heating can cause acoustic waves which contribute to the damage. For very short pulses non-linear optical effects such as stimulated Brillouin scattering can play a role in the damage process. However, the peak power associated with the LAW Laser Rangefinder is orders of magnitude below that necessary for the latter effects to occur. Also the pulse widths are generally much longer than those associated with q-switched lasers. Consequently only thermal effects will be considered as the retinal damage mechanism. In addition, because of the relatively long thermal time constant of the retina (approximately 0.1 sec) compared to the laser PRF (approximately one pulse every millisecond) the rangefinder will be considered as a CW device of the equivalent average power.

It should also be noted that the degree of retinal disability is characterized by the size of the burn, the extent to which the underlying choroid is involved, and the part of the retina suffering the burn. In addition, the affected part of the retina may be larger than the image size because of involuntary eye movements which have the effect of causing the image to fall on different parts of the retina.

5.1.2 Exposure Criteria

Spectral transmittance data available in the literature for the eye is characterized by a significant spread in values for most wavelengths. This is due in part, to the inclusion or exclusion of forward scattered light in various studies. Retinal absorption is also a function of wavelength which generally decreases as one moves from the visible to the near infrared. The product of the transmission of the ocular medium, τ , and the retinal absorption, α , at a given wavelength represents a retinal absorbed dose relative to a corneal dose.

UNCLASSIFIED

A plot of $\alpha\zeta$, after Shiney and Fresier (1973), is shown in Figure 5.1 as a function of wavelength.

An important parameter in the retinal damage process is the image size. Heat is much more readily conducted away from the irradiated area for image sizes 10μ to 50μ in diameter than for larger images. For a given retinal irradiance confined to a small image spot it is estimated that thermal equilibrium is attained within milliseconds, whereas for larger images significantly greater time is required and higher temperatures obtained. This is reflected in retinal irradiance thresholds for injury which vary in excess of two orders of magnitude for image from 25μ to 1000μ in diameter, at least for exposure times between 0.1 and 10 seconds.

For the case where an extended source subtends an angle greater than about 20 min of arc the retinal image size can be determined with little error using geometric methods. The GaAs laser used in the LAW Demonstration Rangefinder consists of two junctions, each .016 inches long by 8×10^{-5} inches wide. The device is constructed such that the junctions are parallel with the long sides separated by .004 inches. Due to diffraction and the multi-mode nature of the emitted light, radiation is emitted into a cone of solid angle approximately 0.66 steradian. The laser is situated in the focal plane of a one inch diameter, F/1.25 collimating lens. This yields a situation wherein, visually, the long side of the junction subtends an angle of about 12.8 milliradians, and the junction separation subtends an angle of approximately 3.2 milliradians. If a focal length of 1.7cm is assumed for the eye, the resulting dimensions of the retinal image are 218 microns for the long side, 54 microns for the junction separation, and 1 micron for the junction width. These image dimensions would be constant and independent of range if there were no vignetting by the collimating lens rim. However, the angle subtended by the lens is equal to that subtended by the long side of the junction lens at about two meters. Thereafter, with

UNCLASSIFIED

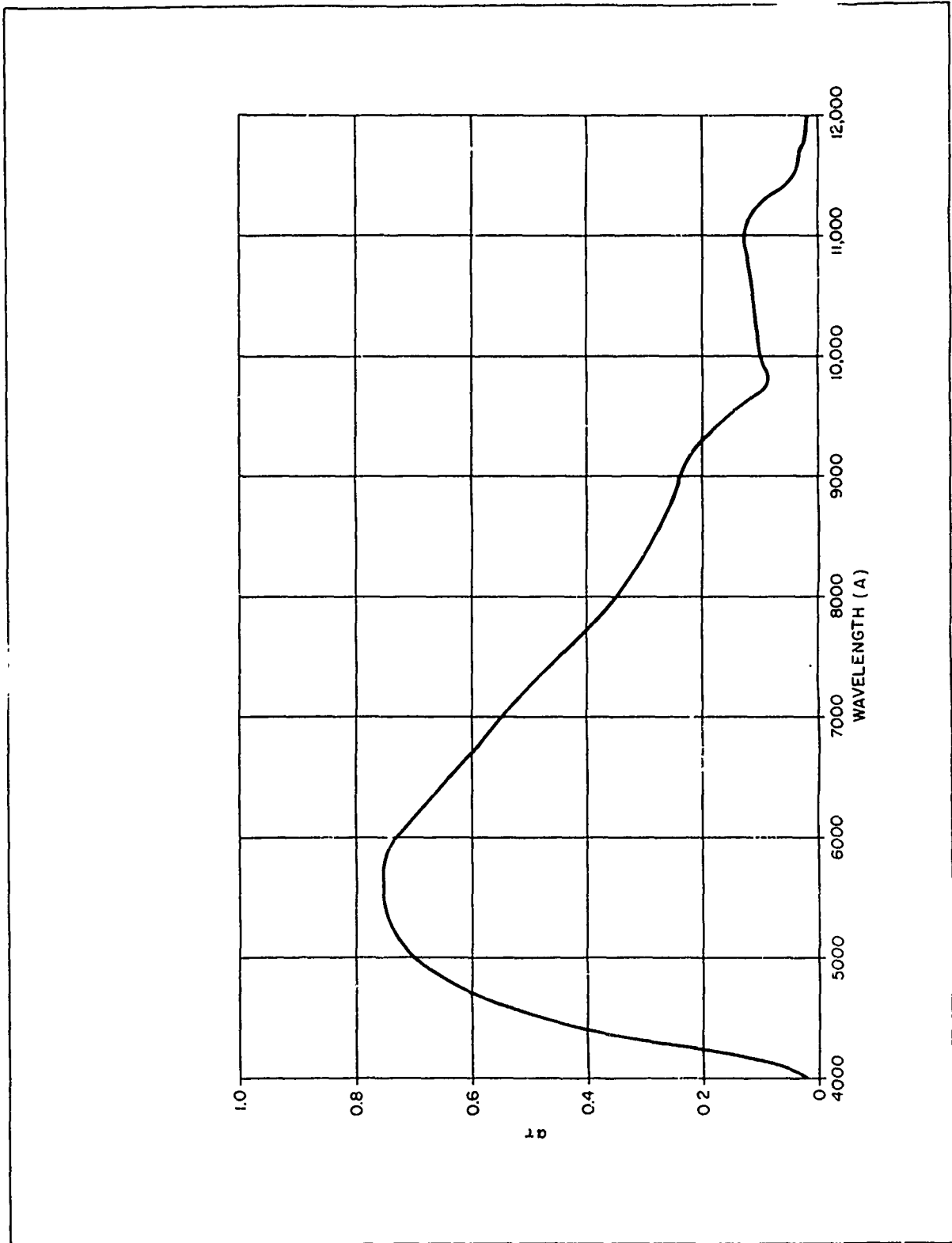


Figure 5.1 Wavelength as a Function of the Product of the Transmission of the Ocular Medium and the Retinal Absorption

UNCLASSIFIED

increased range less of that dimension of the laser can be seen. The net result is that the retinal image size decreases. At approximately eight meters the angular diameter of the lens is equal to the separation of the junctions. Consequently, for greater ranges only part of one junction will be visible at a time.

There is evidence which suggests that if the retinal images of two sources are displaced by less than 100 microns, a significant overlap of the thermal profiles exists. Consequently, for the purposes here, the retinal image area will be considered as the total area enclosed by the image of the two junctions. As a further simplification the area will be specified in terms of the diameter of a circle of the same area. Figure 5.2 is a plot of this effective retinal image diameter as a function of range for the laser used in the demonstration rangefinder.

For the case where the source subtends an angle greater than about 20 min of arc, the absorbed retinal image irradiance H_R , can be related to the source radiance, N_S , again using geometrical methods. The corneal irradiance, H_C , is given by:

$$H_C = N_S \Omega \quad (5.1)$$

where Ω is the solid angle subtended by the source at the eye. Thus the power incident upon the retina, P_R , for an ocular medium transmission, τ , is:

$$P_R = \tau H_C A_C = \tau \Omega A_C N_S \quad (5.2)$$

where A_C is the pupil area. Consequently, the absorbed retinal irradiance is:

$$H_R = \frac{\alpha \tau A_C N_S}{f^2} \quad (5.3)$$

where f is the eye focal length and α is the retinal absorption at the wavelength in question.

UNCLASSIFIED

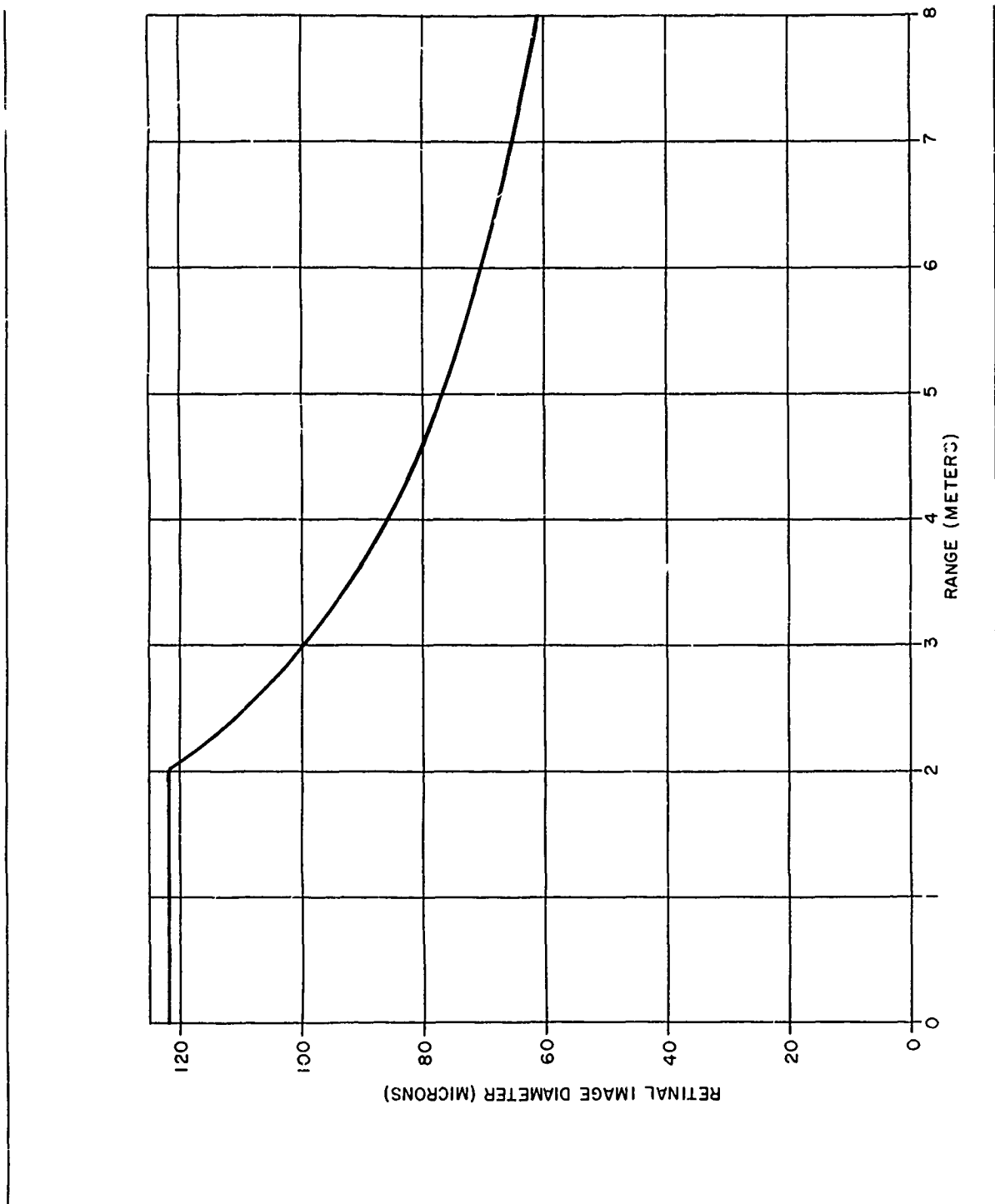


Figure 5.2 Retinal Image Diameter (including thermal overlap) of Equivalent Circular Image Area for a Two Junction Diode Collimated by an F/1.25 System, as a Function of Range

UNCLASSIFIED

Because the thermal damage mechanism is a rate process, the exposure time must be considered in conjunction with the image size, in order to determine damage threshold values for H_r . Two exposure times are commonly used for the purpose of hazard evaluation. These are exposures within the blink reflex (approximately 0.15 sec) and long time exposures (e.g., staring into the beam). Furthermore, it is customary to assume an eye pupil diameter of 7mm, which corresponds to a relatively large aperture. Figure 5.3 contains a plot of the maximum permissible retinal irradiance as a function of image size for an exposure time of 0.15 seconds. The image is assumed circular; however, it is noteworthy that the maximum absorbed retinal irradiance for rectangular images of equivalent areas differ only slightly. These data are from Shiney and Freasier (1973).

When the angular diameter of the source at the eye is less than about 10 min of arc, the retinal absorbed irradiances predicted by equation 5.3 are significantly higher than the actual values. This decrease in the actual retinal irradiance is the result of diffraction at the pupil, aberration in the eye, and scattering within the ocular medium. In addition, the decrease is a function of pupil size and the angular diameter of the source. Gubisch (1967) has presented relative retinal image irradiance profiles for disk sources subtending various small angles (<20 min of arc). However, according to Shiney and Freasier (1973), objects subtending angles less than approximately 1 minute of arc have corresponding retinal image irradiance profiles which cease to show any change. Thus, the convention has been to evaluate the potential hazard presented by intra-beam viewing of a laser (in cases where it is represented effectively as a point source) in terms of the resulting corneal irradiance. Table 5.1 contains limits for corneal irradiance associated with intra-beam laser viewing as recommended by various organizations. As can readily be seen, there is a significant spread in values. It should also be noted that these

UNCLASSIFIED

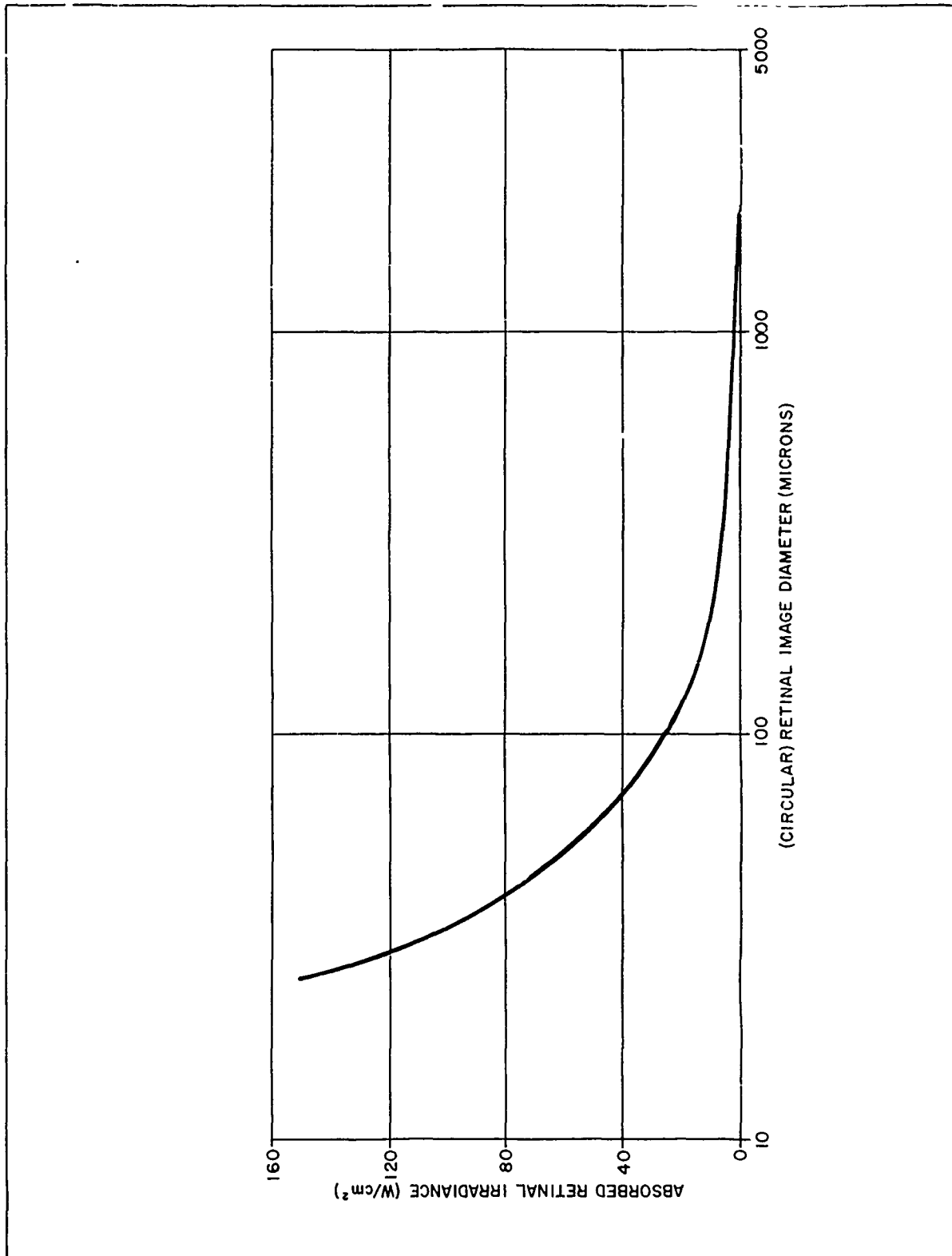


Figure 5.3 Maximum Permissible Absorbed Retinal Irradiance (w/cm²) as a Function of Retinal Image Diameter for 0.15 dc Exposure

UNCLASSIFIED

values assume a 7 millimeter diameter pupil, which based on purely geometrical considerations implies an irradiance gain, H_r/H_c , in excess of 10^5 if an image of 10 microns diameter resulted.

Table 5.1

Source	Wavelength Region (mm)	Duration	Corneal Irradiance (w/cm ²)
Laser Systems Code of Practice (1969)		Continuous	10^{-6}
U.S. Dept. of Navy NAVMED P-5052-35 (1969)	400-1400	Continuous	10^{-6}
U.S. Dept. of Army* TB MED279 (1969)	400-1400	Continuous	10^{-6}
U.S. Dept. of Air Force AFM 161-8 (1971)	1,064	10-500nsec	1.3×10^{-2}
ANSI Z-136 (Proposed 1972)	900	>100 sec	2.44×10^{-4}

*This has recently been revised to a corneal irradiance of 2.5×10^{-4} watts/cm².

5.1.3 Caution and Hazard Viewing Distances

Distances for which retinal damage can be effected for exposure times within the blink reflex are designated as hazardous viewing distances. The GaAs laser used in the LAW Demonstration Rangefinder is characterized by a peak power of 40 watts with a PRF of 1.0KHz and a 70nsec pulse width. Thus, the average power per junction is 1.4 milliwatts. The laser radiation is emitted into 0.66 steradians and the junction dimensions have been given above. Consequently, the average radiance of the device is approximately $257 \text{ watts/cm}^2 \text{ ster.}$

UNCLASSIFIED

From Figure 5.1 $\alpha \zeta = 0.24$ at 0.9 microns. Assuming a 7 millimeter diameter pupil and a focal length of 1.7cm for the eye, equation 5.3 yields a value of 8.1 watts/cm² as the absorbed retinal irradiance. From Figure 5.2, the maximum equivalent image diameter is 122 microns. Referring to Figure 5.3 the maximum permissible retinal irradiance absorbed within the blink reflex is approximately 20 watts/cm² for an image diameter of 122 microns.

For the case wherein long term intra-beam viewing of the laser radiation is considered, the beam irradiance along the optical axis can be determined as a function of range, r , with sufficient accuracy, from:

$$H_c(r) = \pi N_s \sin^2 \theta(r) \quad (4)$$

where $\theta(r)$ is the angle subtended by the lens radius at the range r . From Table 1, the ANSI Z-136 maximum permissible corneal irradiation for exposure times in excess of 100 seconds and for a 7 millimeter diameter pupil is 2.4×10^{-4} watts/cm². This yields from equation (4) a caution distance of approximately 23 meters.

5.1.4 Recommendations

The caution and hazardous viewing distances discussed above do not represent sharp lines of demarcation between safe and unsafe viewing conditions. For example, although the laser radiance is not great enough to cause retinal damage within the blink reflex even for very small viewing distances, damage can result for somewhat longer exposures. In addition, the blink reflex may not provide the usual safeguard for an accidental exposure because the radiation is not visible, and thus such exposures may involve greater exposure times. It is therefore recommended that personnel be cautioned regarding entering the beam within the range where both junctions can be seen simultaneously (approximately 8 meters). Similarly staring into

UNCLASSIFIED

the beam should be avoided for ranges less than 3 meters.

Reflections from objects at close range represent a potentially hazardous condition if the specular component is high and directed back toward the operator. In general, most objects exhibit both diffuse and specular reflective characteristics, the relative percentage depending upon the material and surface conditions among other things. Since this is a very difficult area to quantify generally, it is recommended that objects within the field of the transmitted beam be avoided if within a distance of eight meters.

5.2 Electrical Shock Hazard Evaluation

Except for the laser modulator, the system operates at low voltages and low current levels, the order 10 to 12 volts and 100 ma. which presents no hazard at all.

The modulator is a discharge capacitor type and charges to a maximum voltage of 100 volts which produces a maximum current of 75 amperes in the laser transmitter circuit. This circuitry, located at the center section of the configuration, has short leads, less than one inch, and is insulated from the mounting which is plastic and a non-conductor. The outside housing and all other structures is plastic and non-conductive also.

In consideration of the above it can be safely said that no electrical shock hazard exists.

UNCLASSIFIED

6. Summary and Conclusions

Theoretical considerations, undertaken at the commencement of this study, have indicated the feasibility of a rangefinding system which utilizes a relatively low power GaAs laser and yields ranging capability in excess of 500 meters. The initial aspects of the study were concerned with signal processing techniques which would afford this ranging capability while utilizing optical and electric components commensurate with a small, portable system. The signal processing method chosen as the result of this study involves received pulse integration yielding a signal-to-noise ratio enhancement proportional to the square root of the number of pulses integrated.

The manner in which various optical and electronic parameters affect the ranging capability of the system have also been determined. This has enabled trade-offs among these parameters to be realized. A specific set of these parameters was used as the basis of a demonstration rangefinder. The demonstration rangefinder was designed, fabricated and field tested. Test data indicate that the performance of the device is in good agreement with theoretical predictions. Extended targets have been ranged in excess of 900 meters. The device is completely contained in a cylindrical package of 2.75 inches diameter and approximately 8 inches long.

The demonstration rangefinder incorporates a manual range sweep with an LED range acquisition indicator. Target range is read directly from the ranging potentiometer. A second ranging device was fabricated which featured an automatic range gate sweep with target range readout by means of

UNCLASSIFIED

a three digit LED display. This device, deliverable to Frankford Arsenal, utilizes a dual range gate - range interpolation processing technique. Inherent within this approach is the ability of the device to track a moving target. Tracking of targets with speeds of up to 180 miles per hour is within the capabilities of this device.

The demonstration rangefinder served as a baseline for a study of the feasibility of utilizing lighter and less expensive optical and mechanical components in a production model. It has been concluded that acrylic optical components will not seriously degrade the ranging capability of the device over an operational temperature range of -40°F to $+140^{\circ}\text{F}$. The major changes required by the plastic optical components are a slightly thicker receiver lens and a reduction in the speed of the transmitter system. This latter aspect is necessary to maintain the transmitted beam collimation below that of the demonstration model over the full operational temperature range. This results in a slightly reduced collection efficiency for the transmitter.

Mechanical components of the rangefinder can be injection molded in a polycarbonate or cyclopy KHP plastics, yielding good thermal and impact strength characteristics at a significant reduction in weight. Cost reductions relative to cast or machined metal parts will be realized by a mechanical redesign eliminating the necessity of screw threaded components and by reducing the parts count.

A design for a unit power viewfinder, to be used with the rangefinder has been generated and a mock model fabricated. The device consists of an illuminated reticle, acrylic Fresnel lens, and beam splitter. The major advantage of such a device is its small size.

UNCLASSIFIED

Methods of acquiring correct weapon super-elevation have been investigated. The optimum method is dependent upon the rangefinder application. For the LAW weapon it was concluded that the simplest approach would employ a thumbwheel and elevation screw mechanically linked to the ranging potentiometer. This arrangement is such that a varying angular displacement of the rangefinder and weapon resulted as the range was swept by the range gate. A model illustrating the principles involved was fabricated.

The hazard level presented by the rangefinder has been investigated. It has been concluded that the potential for accidental retinal damage is low with minimal preventative measures. In addition it has been concluded that the hazard level represented by electrical shock is low.

UNCLASSIFIED

7. References

ANSI (1972)

"The Safe Use of Lasers, Proposed Standard Z-136"
American National Standards Institute New York.

Gubisch, R. W. (1967)

Optical Performance of the Human Eye, Journal of the
Optical Society of America, 57 (3), 407-415

Laser Systems Code of Practice (1969)

Ministry of Technology
Safety Services Organization
Kent, England

Michaelson, S. (1972)

Human Exposure to Nonionizing Radiant Energy -
Potential Hazards and Safety Standards
Proceedings of the IEEE, 60 (4), 389-421

Sliney, D. H. and B. C. Freasier (1973)

Evaluation of Optical Radiation Hazards Applied
Optics, 2 (1), 1-24

TB MED 279 (1969)

"Control of Hazards to Health from Laser Radiation
TB MED 279, NAVMED P-5052-35"
U. S. Department of Army, U. S. Department of Navy
Washington, D. C.

Smith, Warren J. (1966)

Modern Optical Engineering, McGraw Hill, New York.